Mechanics of Adenovirus: role of core proteins and environmental conditions in virion uncoating

A thesis submitted in partial fulfillment of the requirements for the degree of Doctor of Philosophy

Natalia Martín González

Departamento de Física de la Materia Condensada

UNIVERSIDAD AUTÓNOMA DE MADRID

Thesis Supervisors:

Pedro José de Pablo Gómez

Carmen San Martín Pastrana

January 2021

A todas las personas que admiro,

en especial a ti, Carlota

AGRADECIMIENTOS

Es difícil redactar las palabras que pondrán fin a esta larga etapa, aunque es mucho más duro describir en tan pocas líneas la inmensa gratitud que siento hacía todas las personas que me han ayudado a hacer esto posible.

En primer lugar, quiero agradecer a mis directores de esta tesis, Pedro y Carmen, sin su estimable ayuda, ánimo, sugerencias y directrices, que me han empujado y animado para llegar al final, esto no habría podido realizarse.

A Pedro, por brindarme la oportunidad de emprender esta aventura. Quiero agradecerte especialmente el apoyo y la confianza que pusiste en mi para iniciarme en la comunicación científica a través de los inolvidables momentos y charlas que he impartido, teniendo la oportunidad de compartir con la gente el amor por la ciencia que tú siempre me has transmitido. Espero de corazón que estés orgulloso de mi trabajo que también es tuyo. Gracias por abrirme el camino para iniciarme como científica.

A Carmen, quiero agradecer especialmente ese punto de vista biológico desde su respaldo como física, de ella he aprendido virología, y es para mí un ejemplo de cómo la multidisciplinariedad es tan importante en la investigación científica.

No quiero dejar sin mencionar el ánimo que en todo momento me demostraron mis compañeros de laboratorio, tanto las personas de la facultad de Ciencias, como a mis compañeros del Centro Nacional de Biotecnología ya que sin sus expresiones de aliento, que en todo momento me demostraron, y con sus ideas en la realización de esta tesis, sus sugerencias, y en muchos aspectos sus reflexiones y puntos de vista me hicieron pensar y aclarar muchas ideas que en unos principios podía tener confusas o insuficientemente maduradas. Gracias a todos ellos.

Las personas que fueron doctorándose en mi inicio me enseñaron la historia del laboratorio del que he formado parte, a Héctor, Bruno, Ana, Alba, Marina, Aida y a Álvaro quería dedicarles un pequeño recuerdo. A Álvaro en especial ya que no solo me inició en el mundo del AFM y del Adenovirus, si no que resultó ser mi mentor en muchos aspectos. Te agradezco todo tu esfuerzo y dedicación. Con Manuel, he compartido mucho, gran biólogo con el que he vivido grandes aventuras científicas por el globo, he aprendido mucho de ti. Gracias. A Paco, que me enseñó que la inquietud científica no tiene fin. A los que por afinidad en microscopía he tenido la suerte de compartir el doctorado os deseo lo mejor en vuestros caminos: Yolanda y Eva, gracias por vuestra disposición y ayuda. Aitor, ha sido un placer cruzarme contigo en el camino. En especial, Diego y Mariano, con los que compartí muchos momentos de la tesis y me han enseñado lo que es la vida en UHV, gracias por lo vivido dentro y fuera del laboratorio. A Cristina, Iván, Eduardo, Julio y Chema menciono y valoro cuantos momentos me han ayudado y aconsejado con sus opiniones, experiencia y bastos conocimientos en mi quehacer diario de investigación. Gracias a Alejandro, Pablo y Rafa, por todo lo que me habéis enseñado, ha sido un placer trabajar codo con codo con vosotros.

A los técnicos: Nacho, Jose María, Santiago y José Luis quiero dedicarles un pequeño recuerdo y agradecimiento por todas las atenciones que tuvieron conmigo, también imprescindibles en la realización de este trabajo.

I am glad that I could participate in a talk and collaborate with the group of Urs Greber, a great adenovirus expert at the University of Zurich. Alfonso and Urs, thanks for the nice conversations and the knowledge sharing.

Gracias por el apoyo incondicional de mi grupo del CNB. Gabriela, tu ayuda ha resultado esencial para mi desarrollo en el laboratorio en todo momento. A Merche, que la vida nos haya juntado en este laboratorio ha resultado muy enriquecedor para mi crecimiento. Mara gracias por tu disposición. Por último,

Marta y Jose, a los que les debo mucho. Ellos constituyen un pilar importante y son mi pequeña familia científica.

Son muchas las personas que brindándome su amistad han contribuido a mi desarrollo. Les agradezco de corazón todos los momentos que han compartido conmigo y que me acompañarán toda la vida.

Otro pilar en este largo camino ha sido Juan, que siempre me ha respaldado dándome la confianza que necesitaba. Constantemente preocupado por aconsejarme y animarme ha contribuido a que fuese capaz de sobrellevar los imprevistos que este final de etapa conlleva. Gracias por compartir conmigo este *viaje sin final* y enseñarme lo maravilloso de tu persona.

Por último, doy las gracias a toda mi familia: a mi padre que siempre me apoyó en mi toma de decisiones y en mis estudios brindándome su confianza y compañía cuando más lo he necesitado, a mi madre sin la cual no hubiese podido emprender la carrera universitaria y por supuesto esta tesis, ya que el apoyo, entrega y esfuerzo que siempre me ha brindado han resultado parte esencial de lo que ahora soy. A Mario, por haberse convertido en mi referente académico a lo largo de los años ofreciéndome apoyo y seguridad en mi vocación científica. A mis abuelos, Mari Carmen y Jesús, a los que agradezco el haberme orientado siempre en mi desarrollo educativo y profesional, habiéndose preocupado en todo momento por mi bienestar y futuro. A Luilli y a la yaya, por haberme llenado de cariño durante todos estos años, siendo un ejemplo de fortaleza y esperanza en el que me he cobijado en los momentos más duros de este trabajo. Por último, a mi hermana pequeña Carlota que ha colaborado activamente en esta tesis y en todos los aspectos de mi vida. Junto a ella he compartido muchas locuras, la más bonita ha sido sin duda Moka. Nunca podré devolverle toda la alegría que me ha regalado.

A todos, Gracias de corazón.

Contents

SUMMARY

This thesis is focused on the characterization of human adenovirus using mainly atomic force microscopy (AFM) in liquid milieu. Adenovirus is a non-enveloped icosahedral virus, formed by a protein capsid constituted by hexons and pentons. The genome is packed together with viral-encoded proteins inside the virus cavity. In particular, I have studied the changes in rigidity, brittleness and mechanical stability of different adenoviral particles. First, I have studied the penton release process, a key step for adenoviral disassembly (Chapter 4). Second, I studied the changes under conditions that play an important role during viral uncoating (Chapter 5). Third, I have studied the absence of two important core proteins from a biophysical perspective (Chapters 6 and 7). Finally, I have determined the effect of a virucide based on alcohol and divalent cations against Adenovirus (Chapter 8).

The thesis is divided in eight chapters and two appendixes. **Chapter 1** introduces human adenovirus, external structure, core, and its organization. Furthermore, I introduce the main technique used, AFM, its basics, and its application in biological samples. In **Chapter 2**, I describe the objectives of the presented thesis. In **Chapter 3**, I emphasize the materials and methods employed, mostly in the adenovirus characterization with AFM and how I measure its mechanical properties and disassembly process.

In **Chapter 4**, I study the dynamics of penton release by mimicking the power strokes in the cell with cyclic loading. Furthermore, a combination between the experiments, survival analysis and a theoretical model, reveals aging phenomena in virus capsids for the first time. **Chapter 5** discusses the effect that acidification has on the mechanics and genome accessibility of Human Adenovirus particles and their influence in biophysics of the core.

In **Chapter 6** I characterize a human adenovirus mutant lacking the major core protein (protein VII). Ad5-VII- mutant offered a clear opportunity to investigate the role of protein VII in the physical properties, mechanical stability and genome organization of virus particles. In the same way, in **Chapter 7**, I characterize a mutant lacking core protein V and study its mechanical properties and stability. Chapters 5, 6 and 7 provide new information about the organization of the human adenovirus core and how it changes in response to biological or chemical changes.

In **Chapter 8** I investigate the virucidal activity of alcohol and zinc salt combinations against adenovirus and aim at understanding their action mechanism. I show that a formulation containing 40% ethanol and 0.1% zinc sulfate has a significant virucidal activity against human adenovirus. I observe by AFM that the particle morphology is strongly altered by the ethanol/zinc formulation. Finally, I observe changes in the mechanical properties of virions in the presence of formulations.

Overall, this thesis helps to understand the human adenovirus core organization and its influence in uncoating through a biophysical point of view. Moreover, I propose an approach to characterize the dsDNA released from the capsid and to provide novel information about the role of the core proteins. Finally, the characterization of penton release allows us to understand its dynamics and influence in guaranteeing semidisrupted virus particles for successful genome translocation into the nucleus.

RESUMEN

Esta tesis se centra en la caracterización del núcleo del adenovirus humano utilizando principalmente la microscopía de fuerzas atómicas (AFM) en medio líquido. El adenovirus es un virus icosaédrico no envuelto, formado por una cápside proteica constituida por hexones y pentones. En su interior, el genoma está empaquetado con proteínas codificadas por el virus. En particular, he estudiado los cambios en la rigidez, fragilidad y estabilidad mecánica de diferentes partículas adenovirales. Por un lado, he estudiado el proceso de liberación de los pentones, un paso clave para el desensanblaje del adenovirus (Capítulo 4), además, he explorado los cambios mecánicos en condiciones que juegan un papel importante durante el desensamblaje del virus (Capítulo 5). Finalmente, he investigado los efectos de la ausencia de dos proteínas del núcleo del adenovirus bajo una perspectiva biofísica (Capítulos 6 y 7). Finalmente, he determinado el efecto de un virucida basado en alcohol y cationes divalentes contra el adenovirus (Capítulo 8).

La memoria está dividida en ocho capítulos y dos apéndices. El **Capítulo 1** introduce el adenovirus humano, su estructura externa, el núcleo y la organización del genoma. Además, introducimos la principal técnica utilizada en este trabajo, el AFM, sus fundamentos, y su aplicación en muestras biológicas. En el **Capítulo 2**, describo los objetivos de la tesis presentada. En el **Capítulo 3**, enfatizo en los materiales y métodos utilizados, sobre todo en la caracterización de Adenovirus con AFM y en cómo medimos sus propiedades mecánicas y el desensamblaje viral.

En el **Capítulo 4**, estudio la dinámica de escape del pentón imitando los golpes debidos a la aglomeración molecular en la célula con deformaciones mecánicas cíclicas a baja fuerza. Además, la combinación de estos experimentos con

análisis de supervivencia (Weibull) ha permitido establecer cómo el envejecimiento estructural del virus ayuda a conseguir virus semidestruidos listos para la transmisión genómica en el núcleo. En el **Capítulo 5** se discute el efecto que la acidificación tiene en la mecánica y la accesibilidad del genoma del adenovirus humano y su influencia en el estado del núcleo vírico.

En el **Capítulo 6** he trabajado con un mutante que carece de la principal proteína del núcleo del Adenovirus Humano (la proteína VII). Ad5-VII- ofreció una clara oportunidad de investigar el papel de esta proteína en las propiedades físicas, la estabilidad mecánica y la organización del genoma. De la misma manera, en el **Capítulo 7**, he trabajado con otro mutante que carece de la proteína V del núcleo. Los capítulos 5,6 y 7 proporcionan nueva información sobre la organización del núcleo del adenovirus humano y los cambios en el estado de condensación del núcleo.

En el **Capítulo 8** investigo la actividad virucida de las combinaciones de alcohol y sulfato de zinc contra el adenovirus y me propongo comprender su mecanismo de acción. Demuestro que una formulación que contiene 40% de etanol y 0,1% de sulfato de zinc tiene una importante actividad virucida contra el adenovirus humano. Observo por AFM que la morfología de las partículas está fuertemente alterada por la formulación de etanol/zinc. Finalmente, he observado cambios en las propiedades mecánicas de los viriones en presencia de las formulaciones.

En general, esta tesis de Física Virológica pretende entender la organización del núcleo del Adenovirus Humano y su influencia en el desensamblaje viral a través de un punto de vista de la biofísica. Además, diseñamos una forma de caracterizar el genoma liberado de la cápside del adenovirus y proporcionar información novedosa sobre el papel de las proteínas del núcleo. Por otro lado,

la caracterización de la liberación de pentón nos permite entender su dinámica para descubrir su influencia en la traslocación de su DNA en el núcleo.

CHAPTER 1

General introduction

CHAPTER 1: General introduction

Interdisciplinarity is a combination of approaches of different sciences, which are interlinked in different specific ways. This combination results more appropriate and necessary to solve problems that reach beyond the limits of a certain knowledge or scientific field.

Single molecule biophysics is the cross-disciplinary science necessary to solve biological problems from a physical perspective by studying nanoscale molecular aggregates. Biological molecules have been traditionally studied with bulk techniques in which a large number of molecules are measured and analyzed simultaneously. These methods and their results are referred to as "macroscopic" or “volumetric”. These experiments provide population averages of the characteristics of each individual molecule. The properties obtained by averaging offer an idealized view where the molecules have a slow and well-defined dynamic. But at the level of the individual molecule, the image is very different since its instantaneous dynamics is fast and sometimes stochastic, being far from the average population behavior. At this level of detail, the macroscopic image fails and a microscopic description is needed.

For instance, the process of genome release from virus capsids has been previously studied in experiments where, either with chemical or thermal stress, millions of viral particles are simultaneously disassembled. The information obtained is the average of multiple events that are assumed identical. However, the disassembly is a stochastic and asynchronous process and the information obtained is just about the initial and final states. Moreover, most of viral infections in a eukaryotic cell are initiated by few particles, thus studying the viruses at an individual level is important.

The possibility of applying nanometric techniques, such as Atomic Force Microscopy (AFM), of the manipulation of individual virus particles, allow investigating the link between the structure and the physicochemical properties of a virus particle and its functions[1]. AFM allows to study the dynamics and the disassembly process of viruses in conditions close to those of their natural environment and to analyze this process at a single particle level. This knowledge is very important in order to adapt viruses as tools in biomedicine, as genetic vectors, vaccines, or nanomaterials[2,3].

Despite being commonly known to be pathogens, viruses have multiple applications in the field of nanotechnology and biotechnology. The importance of their study lies in many cases in their potential use as nanocontainers, nanoreactors, biomaterials or vectors[4,5].

1.1 Adenovirus

Adenoviruses (AdVs) were first discovered in 1953 from adenoid human tissue[6], and since then they have been found in all types of vertebrates, from fish to humans. They are currently grouped in five genera [7]. Mastadenoviruses infect mammals and are the best characterized genus in which human Adenovirus (HAdV) is included. Aviadenoviruses infect birds. So far only a single member of the Ichtadenovirus genus has been reported, isolated from a fish (white sturgeon). The other two genera have broader host ranges. Atadenoviruses have been found in reptiles, ruminants, and birds, and Siadenoviruses in amphibians, birds, and reptiles.

In humans, more than 100 different AdV types have been reported. They are classified in seven groups based on genome similarity from A to G[8]. They cause mainly respiratory, gastrointestinal and ocular diseases, but infections are

controlled normally by the host immune system in immunocompetent patients. However, AdV causes high morbidity in immunosuppressed individuals[9]. The best characterized adenovirus system is human adenovirus type 5 (Ad5) which is also used as gene delivery vector for gene therapy and vaccines against cancer and other diseases[10–12].

1.1.1 Human Adenovirus genome

Human adenovirus genomes are linear double-stranded DNA (dsDNA) molecules approximately 36 kilobase pairs (kbp) long. The transcription units are divided into early, intermediate, and late depending on their activation before, during or after the replication of the genome respectively (**Figure 1.1**)[13,14]. The early transcription units are E1A, E1B, E2, E3 and E4. Their functions include the regulation of the expression of other proteins and the replication of viral DNA. The intermediate transcription units encode proteins such as IX, IVa2 and L4-22k/33k and these will activate the transcription of the late phase proteins regulated by the common major late promoter (MLP). Units L1 to L5 are transcribed at a late phase, encoding the structural proteins. Apart from the encoding regions the adenovirus also transcribes RNA called Virus Associated RNA (VA RNA) that helps prevent innate immunity from suppressing viral protein expression[15].

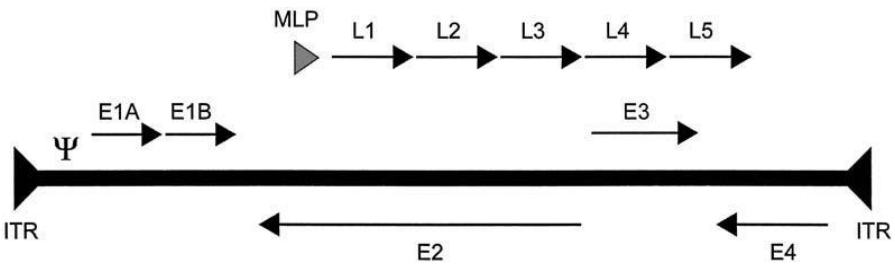

Figure 1.1. Scheme of the transcription unit distribution in the Ad5 genome. The central line corresponds to the adenoviral genome. ITRS (left and right), packaging sequence, early transcription units and major late transcription units are shown. Arrows represent the transcription direction. Scheme adapted from [13].

Finally, the AdV genome contains two elements necessary for encapsidation and replication. One is the Inverted Terminal Repeats (ITR) present at both ends of the DNA molecule that act as a starting point for genome replication[16]. The other is the packaging signal Ψ located adjacent to the left ITR. The packaging signal is essential for the incorporation of DNA into the capsid[17].

1.1.2 Human Adenovirus structure

Human Adenoviruses have non-enveloped large icosahedral capsids of 95 nm vertex-to-vertex diameter. Ad5 has a mass of $150 \cdot 10^6$ Daltons with a triangulation number *pseudo*T=25 and presents a complex protein composition. Its capsid is made of two major coat proteins called hexon and penton. These two proteins are the main building blocks of the capsid and are made of trimers of polypeptide II and pentamers of polypeptide III respectively. The capsid also contains minor coat proteins (IIIa, VI and VIII) situated on the inner side surface and protein IX on the outside. The core is composed of the dsDNA genome bound to viral proteins. The core proteins present in Ad5 are V, VII and X (also known as μ). The core also contains two copies of the terminal protein (TP) and the adenoviral protease (AVP) bound to the genome.

The Ad5 structure solved by cryo-EM at 3.2 $\dot{A}$ resolution provides information about the position of major, minor coat proteins IIIa, VIII, VI and IX (**Figure 1.2a**)[18] and for the first time core protein VII.

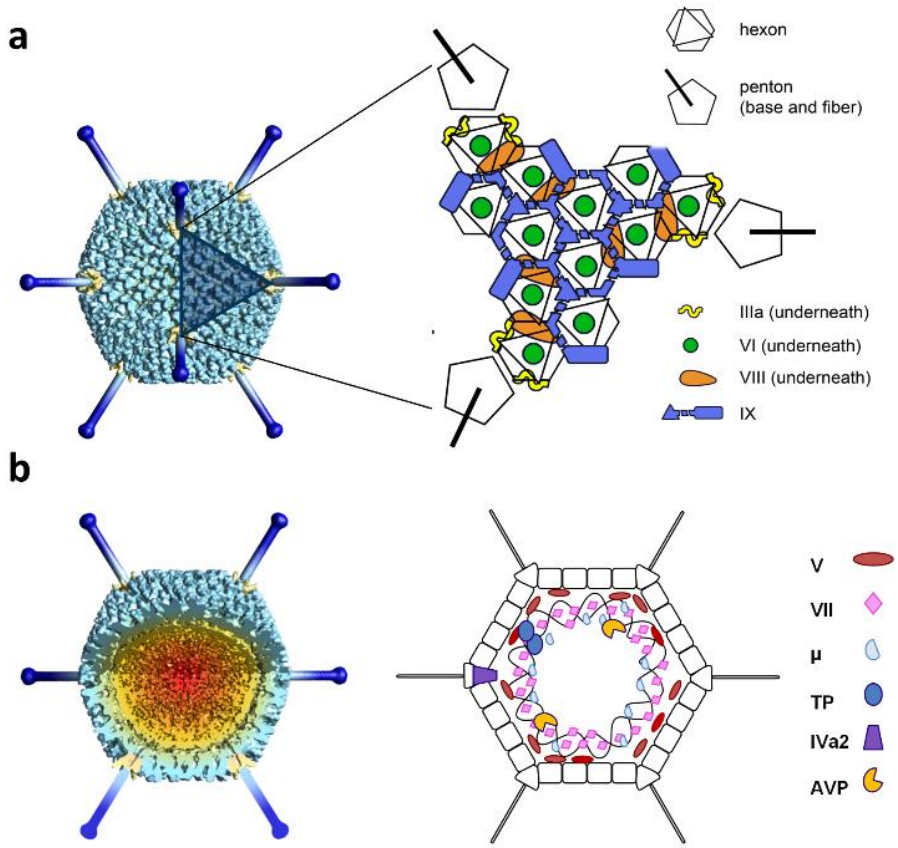

Figure 1.2. Adenovirus structure and components. (a) Cryo-EM map of the virion and schematic representation of the location of major and minor coat proteins in a triangular facet of the capsid. (b) Non-icosahedral components of the virion. Schematic representation of the tentative positions of the genome and core proteins. Scheme adapted from [19].

1.1.2.1 Major coat proteins

Hexon is the main building block of the capsid and constitutes the 60% of the total capsid protein mass. There are 720 copies of the polypeptide II monomer conforming 240 hexon trimers. Each monomer of Ad5 is composed of 952 amino acids (aa) and folds as two eight-stranded β-barrels providing two kinds of interactions with neighbouring capsomers[20]. According to their location in the facet, the 12 hexon trimers are divided into pertipentonal hexons associated with the pentons termed group of six (GOS) (5 hexons and 1

penton)and 9 hexons termed group of nine (GONs) situated in the center of the facet[21].

Pentons form each of the 12 vertices in the icosahedral capsid and are composed of 571 aa. Each penton is formed by the pentameric penton base and the trimeric fiber arranged in a non-covalent complex. Each penton base consists of five copies of polypeptide III[22]. The fiber is composed of three copies of polypeptide IV and forms a ~35 nm long fiber[23]. The N-terminal tails the penton attachment sites[24]. The rest of the fiber is flexible and the C-terminal is the globular knob (also named head) that is responsible for the initial attachment to the adenovirus receptor at the host cell membrane.

1.1.2.2 Minor coat proteins

Apart from the major coat proteins of the Ad5 virus capsid, there are minor coat proteins. Their location is shown in **Figure 1.2a, right**.

Protein IIIa is located underneath each vertex in five copies (585 aa). The N-terminal domain connects the GOS structure, contributing to anchor the penton with the surrounding hexons.

Protein VI (250 aa) is cleaved upon maturation by the adenoviral protease[25]. Protein VI plays an important role in virus entry and endosomal escape, as it alters the curvature of the endosomal membrane, promoting adenovirus escape to the cytosol[26].

Protein VIII (227 aa) is also cleaved upon maturation and now is the less characterized minor coat protein. It interacts with IIIa under the peripentonal hexons, collaborating in the GOS-GON union.

Protein IX (140 aa) is the only minor coat protein situated in the outer part of the capsid, acting as a cementing protein.

1.1.2.3 Core

The adenovirus capsid encloses the non-icosahedral core composed of a linear dsDNA molecule bound to viral proteins that constitute over 50% of the core molecular weight: 500-800 copies of protein VII (22kDa, 198 aa), 100-300 copies of protein μ (9kDa, 80 aa) and 150 copies of protein V (41 kDa, 366 aa)[27,28]. Also, in the core, there are two copies of the terminal protein (TP) and the protease involved in maturation (AVP). The TP is involved in the initiation of genome replication, while AVP processes minor coat proteins IIIa, VI and VIII, the TP, the packaging protein L1 52-55 kDa and the core proteins VII and μ (**Figure 1.2b**). This proteolytic maturation is essential to produce a metastable particle that protects the genome from aggressive conditions while permitting its correct delivery in new host cells. Little is known about the core organization since it does not follow the icosahedral symmetry, limiting its analysis by cryo-EM. Previous studies showed that cores released from Ad5 particles contain proteins VII, V and μ and appear as thick fibres of 150-300 $\dot{A}$ in diameter. However, only polypeptide VII remains associated with viral DNA after high ionic strength treatment of these cores[29].

Protein VII is a histone-like protein and the most abundant in the AdV core. It is rich in ariginine amino acids (23%)[30] that confer a positive charge and is the mature form of polypeptide VII after cleavage by the protease. This protein is thought to be responsible for wrapping and condensing the viral DNA[31]. Previous studies have shown that the association of VII with the viral genome forms a complex similar to the nucleosomes in the cell, termed adenosome, with a 10 nm beads on string structure(Mirza and Weber 1982; Giberson, Davidson, and Parks 2012).

Protein V is a core protein only present in mastadenoviruses. Protein V bridges the genome and the capsid by interacting with the penton base and protein VI[34]. Although protein V is a core protein, it has been observed, after the suppression of the V gene from the Ad5 genome, that V is not essential for adenovirus replication and assembly[35].

Protein μ is the smallest core protein in Ad5. It exists in a precursor form that AVP cleaves. Previous studies suggested that protein μ condenses the genome by a bridging action between strands of dsDNA[36].

1.1.3 Human Adenovirus infection cycle

The infection pathway of Ad5 starts at the plasma membrane where the virus recognizes a primary receptor CAR (coxsackie and adenovirus receptor) (**Figure 1.3, step 1**)[37]. For a correct internalization, the penton base interacts with an integrin ($\alpha v\beta 5$)[38]. Thanks to the flexible nature of the fiber the RGD motif (arginine-glycine-asparagine)of the penton base interacts with the integrin and induced a conformational change after interaction with integrin at the host cell membrane, triggering integrin-mediated endocytosis (**Figure 1.3, step 2**)[39,40]. After cell binding, the virus starts a stepwise disassembly starting by losing the fibers and presumably the penton base due to the mechanical interactions during internalization. In the endosome the pentons are released together with some internal components including protein VI (**Figure 1.3, step 3**) that needs to be exposed and causes disruption of the endosomal membrane, delivering the virus into the cytoplasm[41,42]. The protein VI exposition is a crucial step for a correct infection. Immature adenoviral particles fail to expose the pVI (precursor protein) during entry, become trapped in the endosome, and therefore are not infectious[43,44]. After escape from the endosome, intracellular trafficking of the remaining shell is mediated

by the interaction of hexon/penton base with motor-proteins that carry the particle along microtubules towards to the nucleus (**Figure 1.3, step 4**)[45]. Once at the nuclear pore complex (NPC) the viral DNA and associated protein VII are extruded through the nuclear pore where the genome is inserted in the nucleus, replicated, and transcribed (**Figure 1.3, step 5**).

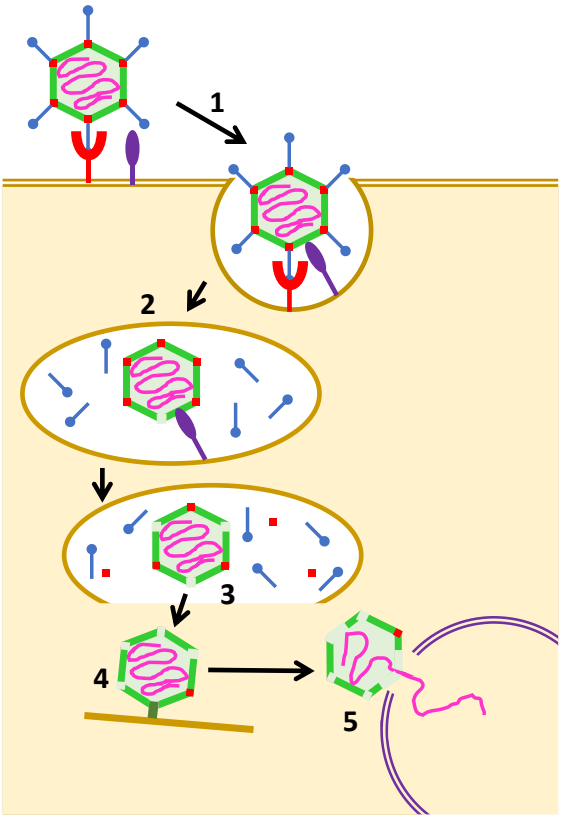

Figure 1.3. Scheme of Human Adenovirus infection. Adenovirus pathway simplified in five steps: 1. Cell binding, 2. Internalization via endocytosis, 3. Endosomal escape, 4. Capsid transportation through microtubules and 5. Genome translocation at the nuclear pore.

1.2 Atomic Force Microscopy applied to biological samples

Atomic Force Microscopy (AFM) belongs to the family of SPM (Scanning Probe Microscopies) that use a probe to measure physical properties at a nanoscale level over a surface. It was designed by G. Binning, C.F. Quate and C. Gerber in

1986[46], inspired by the Scanning Tunneling Microscope (STM). STM is based on establishing a tunnelling current between a tip and a sample. It is typically operated with a feedback system that keeps this current constant by applying the adequated voltages to the piezo, whose mapping provides the corresponding topography image. Since STM measures current, the sample and the tip must be conductors, and there was a great interest in the development of another proximity microscope in which these conditions are not required for avoiding the modification of biological samples[47]. This is how the AFM started, presenting also an advantage additional to the STM, since it allows the observation of samples in liquid medium, that is, in a physiological state for biological samples. The way AFM operates is based on the interaction forces that exist between the tip, located at the end of a cantilever and the sample.

1.2.1 Atomic Force Microscopy components and imaging in jumping mode

Atomic Force Microscope consists basically in a sharp tip located at the end of a flexible cantilever. The cantilever scans the surface in the XY plane. The deflection of the cantilever caused by the interaction of the tip and the sample is detected by a photodiode that registers the reflection of a laser beam placed at the end of the cantilever. For imaging purposes, the feedback algorithm of the computer manages the high voltage of the electronics to adapt the z-piezo in order to keep the photodiode signal constant at a certain value fixed by the user. This voltage is converted into nm to provide the vertical dimension of the topography (**Figure 1.4**).

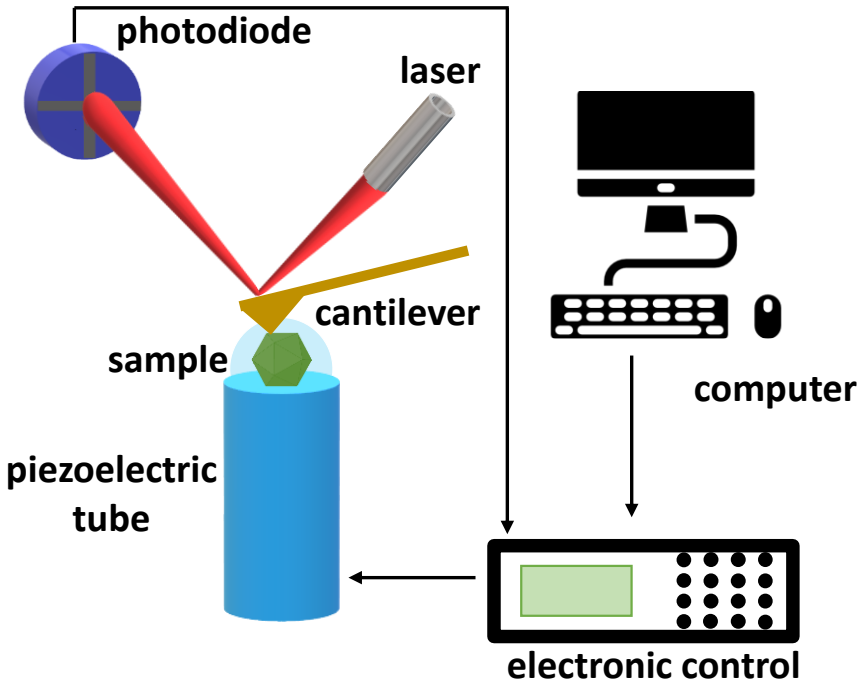

Figure 1.4. Representation of the AFM components.

The topography of the sample can be obtained in several ways. The three more standard methods are contact mode, dynamic mode and jumping mode. All the measurements of this thesis have been done using jumping plus mode (JM)[48], with a system from Nanotec Electrónica from Madrid, Spain which is controlled by the WSxM software[49]. Using this mode, the feedback employed to correct the position of the tip is the normal force registered by the photodiode. In this way, the damage that the tip may cause to the sample is attenuated because this mode minimizes the lateral dragging force between the tip and the sample. **Figure 1.5** shows the steps followed by the microcantilever in JM. JM operates by performing a force *vs.* Z-piezo distance curve (FZC) at each point of the XY plane: the microcantilever approaches the sample and deflects until a certain force is detected, called set point (1), and then retracts (2). Once the cantilever is moved away, it moves laterally (3) and the cycle starts again.

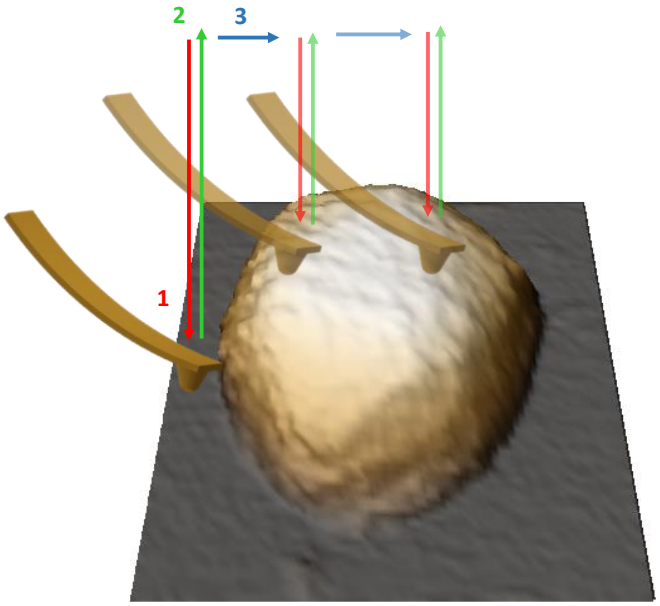

Figure 1.5. Operating representation of Jumping Mode. In this mode, the tip approaches the surface at one point (1: red arrow) until the deflection of the cantilever reaches a value determined by the user. The cantilever, then, withdraws (2: green arrow) and moves laterally to the next point (3: blue arrow).

1.2.2 Tip and sample interaction

The interaction forces between the tip and the sample can be described by an intermolecular potential of Lennard-Jones V(z) type. This potential is composed of attractive and repulsive interactions and depends on the separation distance z between both, which is described by the equation:

$$V(z) = -4\varepsilon\left[\left(\frac{\sigma}{z}\right)^{6} - \left(\frac{\sigma}{z}\right)^{12}\right] \quad (1.1)$$

were ε is the potential well, σ is the position of the potential and z is the intermolecular distance or in the case of the AFM, the tip-sample distance [50] The first term of the equation is attractive and comes from the van der Waals interactions that we will describe later in this section, while the second term

comes from repulsive forces between two atoms. The curve that describes this interaction potential can be seen in **Figure 1.6**.

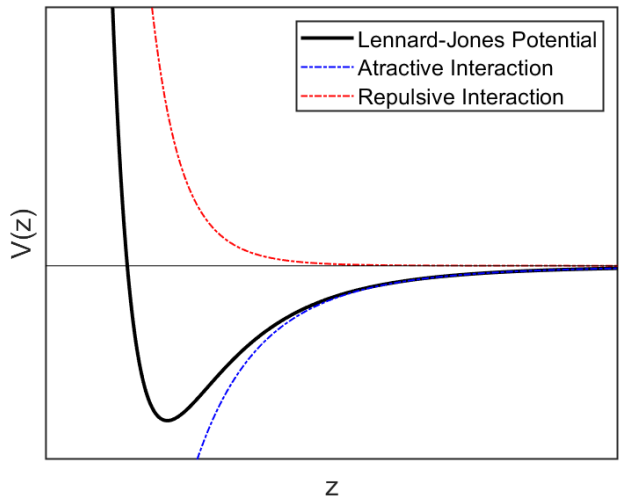

Figure 1.6. Lenard-Jones interaction potential. Intermolecular interaction potential V(z) in black as a function of the distance z that results from the attractive (blue) and repulsive (red) interactions.

The forces present when operating an AFM in liquid conditions are divided into long-range (more than 10 nm of distance between the tip and the sample) and short-range forces and basically are:

- **Van der Waals force:** It is a long-range attractive force that comes from both fluctuations in the moments of the electric dipoles of the atoms as well as their polarization. They are attractive forces and are always present regardless of the chemical composition of the surface or medium[51] The range of these forces are in liquids between 1-2 nm[52,53] when compared with vacuum conditions in which the range is from 10 to 15 nm.

- **Coulomb electrostatic force:** It is a long-range attractive or repulsive force that is caused by the presence of charges on the tip and/or sample (surface). In liquid conditions, these forces play an important

role due to the importance of the concentration of electrolytes in the solution that causes mainly repulsive interactions between the tip and the sample. These electrolytes interact with the surface causing a surface charge. The electrostatic double layer (EDL) formed in the vicinity of the surface is due to the charged nature of the surface and the electrolytes in the solution. This layer is called the Debye length (λ_D) that screens the surface charges and depends on the charge and the concentration of the electrolytes in solution. By probing the electrostatic interactions of the sample with the AFM tip, it was possible to determine the electrostatic charge of different viral particles[54].

- **Contact force:** It is a short-range repulsive force that occurs due to the mechanical contact between the tip and the surface. This contact produces a deformation of the particles with respect to their original shape.
- **Chemical interaction force:** When atoms are very near to each other, forces of chemical interaction emerge, which causes atoms to be linked together to form molecules. These forces are manifested when electronic atom clouds of the tip and the sample are superposed. They occur at sub-nanometric distances (0.1 - 0.2 nm).
- **Hydration forces**: they are short-range repulsive forces (~0.5 nm) that are attributed to the removal of the water molecules from the surfaces.

1.2.3 Spatial resolution In Atomic Force Microscopy

In AFM, three types of resolution need to be considered: instrumental, lateral and vertical. Apart from the instrumental, the resolution is mainly determined by the cantilever and the tip.

The **lateral resolution** depends on the size of the tip, the interactions and the separation between the tip and the sample (García, 2002). In **Figure 1.7** the lateral resolution effect is shown. The lateral resolution between two objects using a tip with a radius R, is defined as

$$l = \sqrt{2R}\left(\sqrt{\delta z} + \sqrt{\delta z + \Delta h}\right) \quad (1.2)$$

where δz is the vertical resolution and Δh is the height difference between the two objects[55].

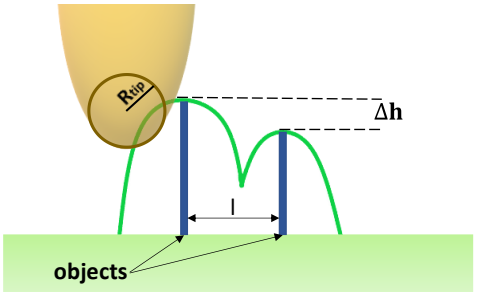

Figure 1.7. Scheme of the lateral resolution effect. Limitation of lateral resolution is determined by δz that depends on the tip radius the distance l and the height difference between two objects. Adapted from the thesis of Dra. Aida Llauró-Portell.

The **vertical resolution** is limited by the noise from the detection system and the thermal noise from the cantilever as

$$\delta z = \sqrt{\delta z^2_{thermal\ noise} + \delta z^2_{detection}} \quad (1.3)$$

In general, the thermal noise of the cantilever is usually the biggest source of noise in the AFM, and in our case, the deflection of the cantilever is measured with a photodetection system, so the expression of the thermal noise depends on k_B (Boltzmann constant), the temperature, and the spring constant of the cantilever. For the cantilevers used in this work (k_c=0.05 N/m) the thermal noise at the AFM working temperature (room temperature, 292 K) is

$$\delta z_{thermal\ noise} = \sqrt{\frac{4k_BT}{3k_c}} = \sqrt{\frac{4 \times 1.38 \times 10^{-23} \times 292}{3 \times 0.05}} = 0.328\ nm \quad (1.4)$$

Since the AFM uses a tip as a probe to scan the surface, the image is affected by a dilation effect[56], which is the geometrical convolution between the tip and the sample. In this way, the object to be studied appears wider than its actual size as shown in **Figure 1.8**.

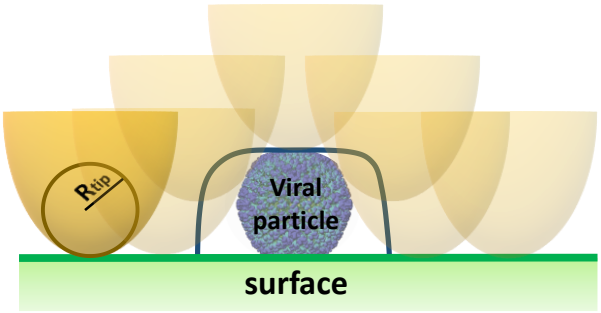

Figure 1.8. Scheme of dilation effect of a viral particle. The illustration represents the dilation effect of a viral particle with an AFM tip. The blue line is the acquired image of the virus particle.

1.2.4 Cantilever election

Cantilever election is a key decision in an AFM experiment. Nowadays, several companies manufacture AFM cantilevers with different characteristics. The shape and the composition determine the rigidity of a microcantilever. Different cantilever shapes can be found such as triangular (TR), rectangular (RC) or pyramidal (PR). The cantilever composition can be very different, the hardest ones are usually made of silicon (Si) and the softer ones are of silicon nitride. The force constant can vary from the softest 0.01 N/m to the hardest 100 N/m as for the frequency resonance that can be between 5 kHz to 1MHz.

Depending on the sample and the imaging mode the cantilever should present different characteristics. For instance, working in liquids requires using soft cantilevers while for dynamic modes normally a stiffer cantilever is used. In this thesis, we have used RC800PSA microcantilevers from Olympus. Their characteristics are silicon nitride of rectangular shape cantilevers with nominal

spring constant of 0.05 N/m. It is recommended to calibrate the cantilevers as the nominal spring constant may differ from one cantilever to another. Here, we have used the Sader method to calibrate[57]. This method allows us to obtain the spring constant given by this formula:

$$k_c = 0.1906 \times \rho \times b^2 \times L \times Q \times \Gamma_i(\omega_0) \times \omega_0^2 \quad (1.5)$$

were ρ is the fluid density, b and L are the width and length of the cantilever, respectively. Q and ω_0 are the quality factor and the natural resonance frequency and finally Γ_i is the imaginary component of the hydrodynamic function.

If we consider the cantilever as a linear harmonic oscillator, its deformation (Δd) can be described by Hooke´s law as $F = -k_c \cdot \Delta d$. Considering this approximation, we can convert the voltage detected in the photodiode into units of force (nN) by applying the following equation:

$$F(nN) = k_c \left(\frac{nN}{nm}\right) \times deflection(V) \times sensivity \left(\frac{nm}{V}\right) \quad (1.6)$$

To obtain the conversion to units of force (Newtons, N), we need to know the sensitivity of the photodiode and the elastic constant of the cantilever, in nm/V and nN/nm, respectively. The cantilever is previously calibrated using Sader´s method (see above) and the sensitivity value is given by the relation between the voltage detected by the photodiode and the deflection in nanometers of the cantilever. To obtain the spring constant of the cantilever (k_c) the cantilever is deformed on a hard surface compared to the cantilever stiffness.

1.3 AFM to study Human Adenovirus

Studying viruses results necessary to understand how viral infection occurs. Furthermore, viruses present interesting characteristics that can be applied in medicine, nanotechnology and biotechnology. Adenoviruses structure is intensively investigated by using Cryo-EM[18] and other techniques. However, applying single molecule techniques such as AFM not only resolve the structure of AdV capsid at a nanometer scale in native conditions but also allows us to derive viral particle mechanics and patterns of disassembly processes in real time. Ad5 has been extensively studied. Its first AFM characterization was performed in 2011 in air conditions[58]. The development of AFM in liquid conditions permits to scrutinize viruses in physiological conditions closer to their natural environment. Previous studies by Ortega-Esteban characterized different assembly states of human adenovirus: the mature[59] and the immature particles ts1[60].

The first mechanical study provided evidence of internal pressure in Ad5 despite the presence of the core proteins. Moreover, this study reported that the internal pressure changes upon maturation of Ad5 virus[36]. The nature of the internal pressure is due to an increase in the electrostatic repulsion in the minichromosome (DNA + core proteins) which alters the interactions of the core proteins with the DNA.
Therefore, despite part of the genome charge is neutralized by proteins, the estimated internal pressure is ~30 atmospheres.

Other studies showed that the core condensation state increases upon maturation by inducing mechanical fatigue of Ad5[61]. This approach allowed, for the first time, to monitor the disassembly of Ad5 in real time. By measuring the topographical height evolution, it was found that while the capsid of immature particles was cleanly peeled out to release an almost intact core, the mature particles were completely collapsed. This data indicated that the

genome remains more condensed in immature particles due to the presence of precursor core proteins. Besides, with this mechanical fatigue method, it was possible to measure the penton stability of the viral particles. In this study, it was found a higher probability to release pentons in mature particles than in immature particles, however, the dynamic of penton release was not investigated.

Finally, they further investigated the genome diffusion by using a combination of AFM with fluorescence microscopy that enables the mechanical unpacking of the virus genome, and the simultaneous surveillance of the nucleic acids release[62]. These results showed that the mature Ad5 core expands faster and it is more accessible than the immature one, thus corroborating that the genome is less condensed in the mature Ad5 viral particle.

Altogether, these studies provided important inputs in physical virology showing a core rearrangement during maturation. Nevertheless, several basic questions of Ad5 remain unknown. In this thesis we will address the specific function of two core proteins, the core protein V and VII. Moreover, we will study the viral response to chemical cues like the ones in the cell, and the dynamics of penton release.

c

CHAPTER 2

OBJECTIVES

CHAPTER 2: Objectives

Based on the background given in the introduction, this doctoral thesis has the purpose of understanding the Ad5 uncoating dynamics under mechanical and chemical cues, as well as the core structure using AFM as the principal technic. Ad5 results a good candidate as a vector for gene therapy. Therefore, its comprehension of basic structure and functionality is fundamental for studies in several fields such as biomedicine.

This thesis was developed thanks to the collaboration between the group of Pedro Jose de Pablo Gomez (Universidad Autónoma de Madrid-UAM) and the group of Carmen San Martín (Centro Nacional de Biotecnología-CNB). Moreover, the different projects were carried out thanks to the collaboration with other departments, universities, and research institutions. This synergy is essential for developing a multidisciplinary doctoral thesis

The specific objectives of this thesis are:

1. To study the dynamics of penton release of Ad5 from an experimental physical point of view. Likewise, to develop a theoretical model to be applied in these experiments and establish the interplay with the infection process of Ad5.
2. To investigate the influence of the acidification process that Ad5 must undergo in the uncoating process.
3. To explore the structural role of the core proteins VII and V of Ad5 and their function in genome release.
4. To determine the virucidal action mechanism of alcohol and divalent cations based formulations against human adenovirus.

CHAPTER 3

Materials and methods

CHAPTER 3: Materials and methods

In this chapter, I will introduce the virus samples and the first steps of this thesis employing AFM with Human Adenovirus. Furthermore, I will explain the importance of the surface election and the methodology to obtain information about Ad5 in the field of physical virology.

3.1 Production and purification of adenovirus samples

This section describes the different adenoviral samples used in this thesis.

For the control Ad5 wildtype, we have used the constructs Ad5GL[63] (Chapter 4 and 5) and Ad5/attP[59] (Chapter 6,7 and 8). These viral particles are structurally wildtype in their structural protein but their genome contains some deletions for genes involved in replicative cycle control (E1 region) and host immune system evasion (E3 region)[64]. Ad5/attP also expresses green fluorescent protein (GFP) to facilitate tracking of virus amplification kinetics and titration. Ad5GL carries the GFP (G) and the firefly luciferase genes (L). The wild type human adenovirus type 2 (HAdV2) is used in virucidal standard efficacy tests in Chapter 8.

Genome-less capsids were obtained with the delayed-packing mutant Ad5/FC31, which is an E1, E3-deleted construct carrying GFP and the FC31 attB and attP sequences flanking the adenovirus packaging signal Ψ. These insertions hinder genome packaging, leading to the generation of an excess of empty particles. Here we use the Ad5/FC31-L3 particles, which are completely sealed[65].

Ad5/attP, Ad5GL and Ad5/FC31 were propagated at 37°C in HEK293 cells. Infected cells were harvested at 36 hours post infection (hpi) for Ad5/attP and

Ad5GL, and 56 hpi for Ad5/FC31. Viral particles were purified by equilibrium centrifugation in double CsCl gradients, desalted on a Bio-Rad 10 DC column, and stored in 20 mM HEPES, pH 7.8, 150 mM NaCl (HBS) plus 10% glycerol at -80 °C, as previously described[65].

In Chapter 6, a mutant that lacks core protein VII was used provided by Dr. Patrick Hearing, from Stony Brook University. The parent virus Ad5-VII-loxP contains loxP sites flanking the protein VII open reading frame and was generated and propagated as described[66]. Particles lacking protein VII (Ad5-VII$^-$) were produced using the Cre66 cell line, a cell line expressing Cre recombinase derived from HEK-293 cells. The cells were maintained in Dulbecco's modified Eagle's medium supplemented with 10% HyClone Fetalclone III serum, penicillin, streptomycin, and 0.25 mg/ml of Geneticin (Life Technologies). Cre66 cells (6×10^8 total cells) were infected with 200 CsCl-purified Ad5-VII-loxP virus particles/cell for 1 h at 37^{o}C. Cells were harvested for 3 days, and Ad5-VII$^-$ particles were purified as described for Ad5-wt and empty capsids.

In Chapter 7, we have used a mutant in which core protein V is absent (Ad5—ΔV, provided by Dr. Urs Greber, of Zurich university). In brief, protein V was deleted from the genome by recombineering from the pKSB2 bacmid, which contains the entire Ad5-wt300 genome (a specific Ad5 variant)[67,68]. The resulting virus was expanded in 911 cells at 37 °C and harvested 5 days post infection. Supernatant and cellular fractions were separated through centrifugation. Particles within the supernatant were PEG precipitated overnight at 4 °C[43,69]. Cell pellets were lysed through three freeze-thaw cycles and stored at -80 °C. Particles were purified over two cesium chloride gradients[43,69]. Virus bands were extracted with a syringe and dyalized on a Slide-A-Lyzer Dialysis Cassette (ThermoScientific) against dialysis buffer (150

mM NaCl, 1 mM MgCl2, 10 mM Tris/HCl pH 8.1) finally supplemented with 10% glycerol for long term storage at -80 °C.

3.2 Human Adenovirus adsorption

To study viruses with AFM they must be adsorbed on a surface. These surfaces should allow the interaction with the virus. This immobilization should be minimized to be able to measure mechanical properties of intact viral particles but should be strong enough for remaining stable under the scanning of the tip. Immobilization is reached through physical interactions such as electrostatic and polar forces, but it can be achieved also thanks to the functionalization of the surface[70]. The most used surfaces to study biological samples are muscovite mica, highly oriented pyrolytic graphite (HOPG) and functionalized glass.

In this subsection I have studied the adsorption of Ad5 particles in HBS (20 mM Hepes, 150 mM NaCl, pH 7.8) to these three surfaces.

First, any surface that is going to serve as a supporting substrate for imaging with AFM should be as clean as possible. In this sense, mica and HOPG represent an advantage since they can easily be cleaved to reveal a fresh and atomically flat surface. On the contrary, glass coverslips need to be washed with KOH and ethanol and afterwards functionalized with Hexamethyldisilazane (HMDS). Initially, we tried to use HOPG. Due to its high hydrophobicity, it is widely used to adsorb proteins. In the case of Ad5 resulted in a partially damage population as shown in **Figure 3.1, left**. Although some of the viral particles seem intact, this surface does not represent a good option. The presence of disassembled particles in HOPG could be due to the excessive virus-surface interaction due to hydrophobicity. We hypothesize that the external structure of Ad5 may be populated by proteins with high hydrophobic of alpha-helices[71].

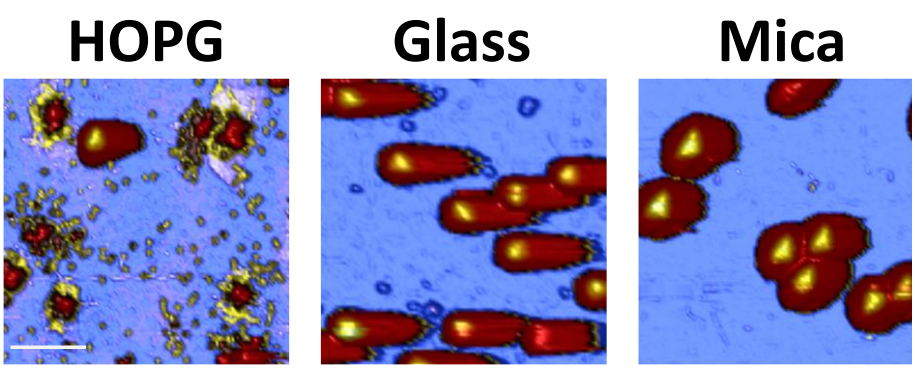

Figure 3.1. Human adenovirus particles adsorbed on different substrates. AFM topographies of Ad5 in HOPG, silanized glass and mica. The scale bar corresponds to 200nm.

Glass coverslips were used after a silanization treatment that confers a hydrophobic behavior that governs the interaction with the biological sample[72]. Using silane-coated glasses we can distinguish an intact population of viral particles (**Figure 3.1, center** and **Figure 3.2**) that present views along the three types of symmetry axes in the icosahedron as shown in **Figure 3.2, third row**. This surface represents a good option to study particles oriented following the different symmetries of the adenovirus capsid. A previous work showed different mechanical responses of Ad5 depending on the adsorption symmetry[73].

At last, we tried mica. Mica becomes negatively charged when it is immersed in water. Under these conditions the forces that govern the adsorption of viral particles to the mica are the electrostatic and Van der Waals forces. As previously reported in[54], there are several non-enveloped viruses that are negatively charged in the outer part of the capsid including Ad5. To adsorb Ad5 on mica is necessary then, the presence of 2+ cations in the solution that will reduce the Debye length and allow the virus particles to be attached. Ad5 in HBS with 5 mM $NiCl_2$ (Ni-HBS) firmly attaches to the mica substrate and presents an enough population of intact particles (**Figure 3.1, right**), with high stability to perform AFM experiments. This methodology also allows the

dsDNA (negatively charged) to interact with the mica as shown in Chapters 5 and 6. In this thesis, we have worked as previously reported in [61] with muscovite mica in the presence of divalent cations (5mM $NiCl_2$)[74].

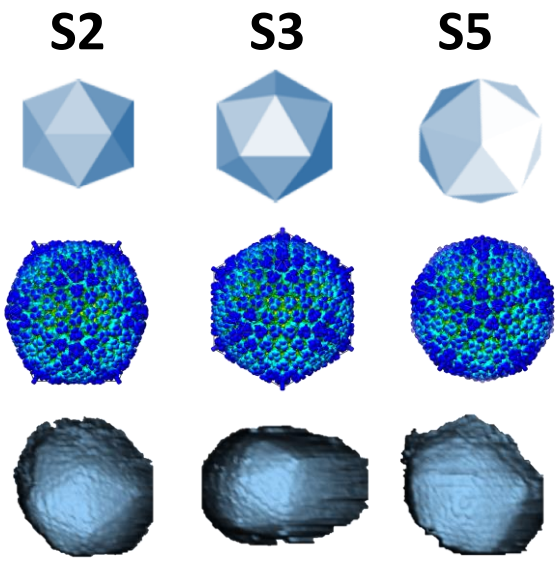

Figure 3.2. Different symmetries of Adenovirus. The first row shows a representation of the different symmetries (two-fold (S2), three-fold (S3) and five-fold (S5)) of an icosahedron. The second row shows the different symmetries of the Cryo-EM map of Ad5 (EMD-7034). The third row shows AFM topographical images (300 nm^2) of the three orientations of Ad5 on silane coated glass.

3.3 Sample preparation

For all the AFM experiments carried out in this thesis, virus samples were dialyzed against HBS at 4°C to remove the glycerol added for storage. They were then frozen in single-use, 5 µl aliquots and stored at -20°C. Stock particle concentrations varied from $1x10^{11}$ virus particles (vp)/ml to $11x10^{12}$ vp/ml for all the samples tested. For AFM measurements, single-use aliquots were thawed, diluted in 20 µl of Ni-HBS, and adsorbed onto freshly cleaved mica for 20 minutes at 4°C. After five washes with Ni-HBS, 200 µl of buffer were deposited on the mica surface to avoid desiccation. The AFM tip was prewetted with 30 µl of Ni-HBS so the total volume was about 260 µl.

3.4 Direct visualization by AFM of Human Adenovirus

To visualize individual viral particles by AFM in JM thousands Force vs Z-piezo distance curves (FZCs)at low force are required. When imaging biological samples, it is important that the sample is not deformed by the tip, so that the displacement of the piezoelectric in the z-axis should reflect the topography of the sample at that point. The performance and recording of FZCs in the x, y plane composes a three-dimensional image of the studied particle that allows to identify its topography. This approach allows determining the integrity and orientation of the particle (**Figure 3.3a**). In our case Ad5 adsorbed on mica showed only 3-fold symmetry. Under these conditions, an initial topographical height measurement of an 80 Ad5 particles random population (**Figure 3.3b**) showed a value of 85.9 ± 0.2 nm(average ± SEM). This value is consistent with the nominal diameter of Ad5 and indicates that none of them underwent substantial deformations after adsorption. The deformation of the viral particle with the substrate is 4.5%. from its nominal diameter (90 nm) Therefore can disregard the alteration of the particle structure[61,75,76].

Comparison of images obtained along time allows following the temporal evolution of a particle in a mechanical fatigue experiment (explained in Section 3.6). Similarly, the comparison of images before and after different physical interventions allows the study of the effect caused on that individual particle by these physical queues. For example, it is possible to perform a mechanical indentation experiment (explained in Section 3.5) on the particle and by performing a new image check the effect that such mechanical aggression has had on the particle. If the particle has shown an elastic behavior the previous and subsequent images will be normally the same, but if this has not been the case the subsequent image will show changes on the topography that may correspond to a loss of integrity or a displacement of the particle.

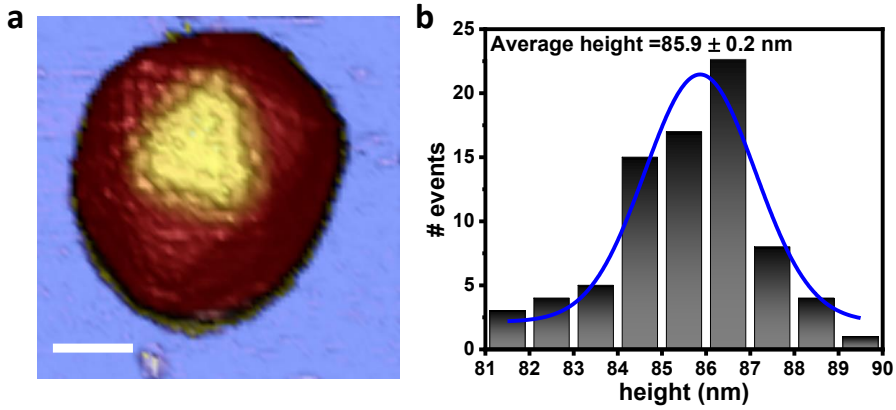

Figure 3.3. Ad5 adsorbed on mica and height distribution on the three-fold symmetry. (a) Single viral particle of Ad5 adsorbed on mica at three-fold symmetry. Scale bar corresponds to 45 nm. (b) Height distribution data presented in histograms for Ad5. Mean data and standard deviation (SD) are obtained by fitting a Gaussian distribution to the histogram (blue line). The value is present in the legend of the graph.

3.5 Mechanical properties of viral particles

Initially, the AFM was designed to visualize non-conductive samples, but the AFM also enables manipulating them and obtain quantitative information about the mechanical response of any sample. The AFM allows to obtain force vs. Z-piezo curves (FZCs). These curves provide physical information about the sample and allow obtaining parameters such as elasticity, brittleness, surface charge density[77] and cohesion energy, among others. This capacity is the reason why this experimental technique has become an essential part of a wide variety of research fields, from biology to materials engineering[78].

In physical virology, the deformation of particles has been studied under the continuum elasticity theory of thin elastic shells[79]. This theory predicts that the force depends linearly on the deformation up to indentations of the order of capsid thickness[80–82]. In this case, the particle and the cantilever are represented as two spring constants in serie. **Figure 3.4a** shows an example of two FZ curves, one made on a non-deformable mica surface and the other on

a deformable viral capsid, in which a linear behavior can be seen as long as the particle is not broken. In this situation, the indentation experiment allows to directly measure the elastic constant of the system. This information and the value of the elastic constant of the cantilever (previously calibrated) allow to calculate the elastic constant of the virus particle, and therefore its mechanical stiffness (**Figure 3.4b**). The force-indentation curve (FIC) provides information about the brittleness from the critical indentation, the rigidity from the elastic constant and the strength from the breaking force[1].

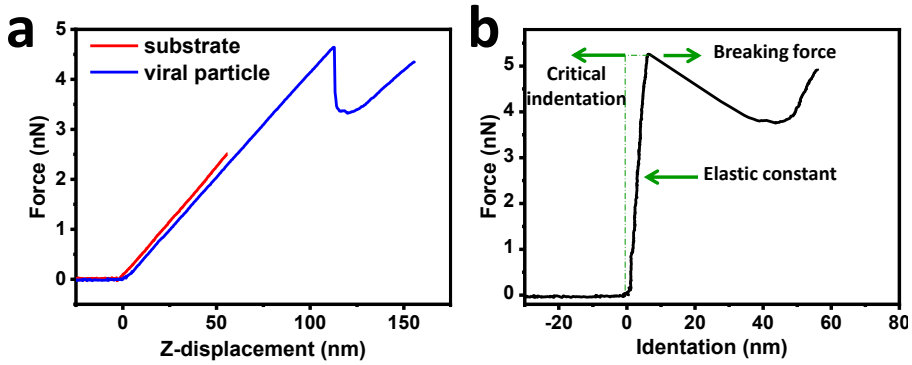

Figure 3.4. Nanoindentation experiment on a single Ad5 particle. (a)Force versus distance (FZ) curve performed on the substrate (blue line) and on the viral particle (red line). (b) Force versus indentation curve (FIC) of the viral particle. Mechanical parameters can be derived from the curve such as spring constant, critical indentation, and breaking force.

In this thesis, all the single indentation assays were performed with the same procedure and parameters for providing comparable information. All the particles were imaged before and after performing a FIC in the centre of the particle facet (**Figure 3.5**). We avoid measuring particles presenting defects such as penton vacancies. The Z piezo approached to the top of the particle at a loading rate of 150 nm/s in which we had the contribution of the cantilever and the viral particle. In order to subtract the contribution of the cantilever, to obtain the viral particle mechanics, we performed two FZs curves at a loading rate of 100 nm/s in the substrate before and after each experiment.

Two FZs allow to detect if the tip was contaminated in order to better control the experiment. Once we have the two curves (**Figure 3.4a**) we subtract the contribution of the bending of the cantilever and calculate the spring constant of the particle from the slope of the linear behaviour of the curve (**Figure 3.4b**). The linear part of the curve is sometimes preceded by a short-range non-linear behaviour due to electrostatic, van der Waals and hydration forces[83]. Therefore, we fit the curve avoiding this part.

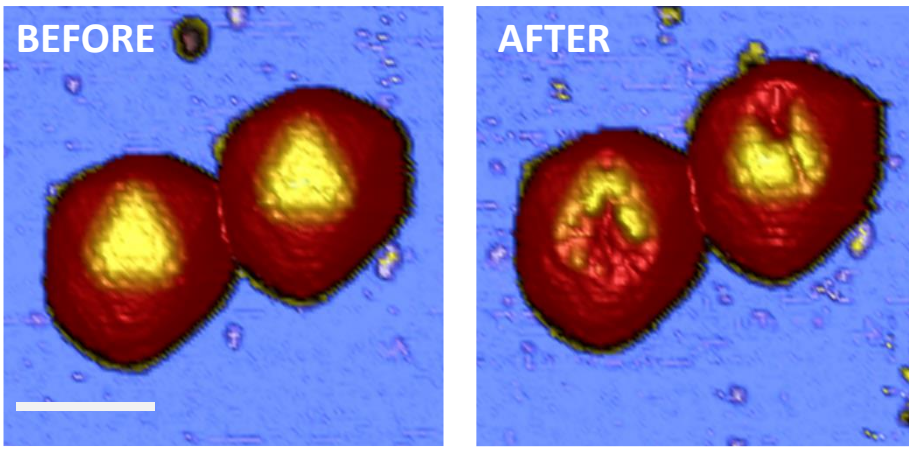

Figure 3.5 AFM Ad5 topographical images in an indentation assay. Topography images of two adenovirus particles before (left) and after (right) performing an indentation experiment. Scale bar corresponds to 100 nm.

3.6 Mechanical fatigue experiments in Human Adenovirus

AFM working in Jumping Mode Plus allows acquiring images while at the same time apply forces of100 pN s that are well below the breaking force of the viral particle. Therefore, by applying this low imaging force we can monitor the stepwise disruption of the viral particle and its intermediate disassembly states.

The procedure of mechanical fatigue experiments consisted of imaging a single viral particle in a field of 300 nm^2 at 128x128 pixels. The force can be estimated as follows:

$$Applied\ force(nN) = setpoint(V) \times k_{cantilever} \times calibration(nm/V)$$

To control the calibration/sensitivity of the system we performed a FZC on the substrate after each recorded image.

In this thesis, mechanical fatigue experiments were carried out to compare the disassembly process between different AdV mutants (Chapters 6 and 7) and to extract information about penton release dynamics (Chapter 4). Moreover, thanks to this technic it is possible to obtain information about the height, area and volume evolution along the disassembly process. To do so all the images of the particle disassembly process were aligned. Furthermore, information about dsDNA release can be obtained from these experiments.

3.7 Complementary techniques

Apart from the AFM as the principal technique of this thesis, the powerful collaboration with my co-director Carmen San Martin allowed me to access to fluorescence and electron microscopy assays with the help of Marta Pérez Illana and Mercedes Hernando Pérez. In this Section, I will briefly introduce these techniques and the specific objectives for the different projects of this thesis.

3.7.1 Fluorescence spectroscopy

Fluorescence spectroscopy was used to determine the thermal stability of Ad5 subjected to different pH conditions (Chapter 5) and the thermal stability of a mutant lacking protein VII (Chapter 6) (Ad5-VII-).

To determine the accessibility of the virus genome to the medium, extrinsic fluorescence spectra were obtained from samples subjected to different pH conditions, in the presence of an intercalating dye. Stock virus samples (~10^{12} vp/ml) were diluted to 5×10^{9} vp/ml of Ad5GL and Ad5-VII- in a final volume of 800 µl of and further incubated during 1 hour at 4°C at 300 rpm shaking. A volume of 8.8 µl of YOYO-1 diluted 1:100 in Milli-Q water from the initial stock (Thermo Fisher Scientific, stock composition: 1 mM YOYO-1 in DMSO) was added to the virus sample and equilibrated for 5 min at 30°C before data acquisition. Fluorescence emission spectra were obtained employing a Horiba FluoroLog spectrophotometer equipped with a Peltier temperature control device and continuous shaking. The dye was excited at 490 nm wavelength, and fluorescence emission was monitored from 500 to 580 nm using an excitation slit of 2 nm and an emission slit of 5 nm, integration time 2s and 950 V voltage. Maximal emission intensity occurred at 509 nm. The temperature in the sample cell was increased from 30 to 70°C, with readings every 2°C after holding for 0.5 min for equilibration. Each run took approximately one hour and a half to be completed. The fractional change in fluorescence (normalized fluorescence, F_n (T)), was calculated according to the following equation:

$$F_n\,(T) = \frac{F_{exp} - F_i(T)}{F_f(T) - F_i\,(T)}$$

Where T indicates the independent variable temperature (°C) and F_{exp} refers to the raw fluorescence signal in counts per second (c.p.s) at each

temperature. F_i and F_f represent the linear extrapolates, at this temperature, of pre-transition and post-transition base lines, respectively.

The half transition temperatures ($T_{0.5}$) were calculated from the fitting of the averaged fluorescence change fraction (F_n) as a function of temperature (T) to a Boltzmann sigmoid (Origin software package) according to this equation:

$$F_n(T) = F_{max} + \frac{F_0 - F_{max}}{1 + \exp\left(\frac{T - T_{0.5}}{dT}\right)}$$

Where $F_0 \cong 0$, $F_{max} \cong 1$ and dT = steepness of the curve.

3.7.2 Transmission electron microscopy

To visually assess particle disruption in thermostability assays at different pH values (Chapter 5) we used transmission electron microscopy (TEM). Furthermore, we investigate particle disruption after virucidal treatment (Chapter 8) using this technic. In TEM, a beam of electrons is transmitted through a specimen to form an image.

In Chapter 5, stock virus samples (~10^{12} vp/ml) were diluted to a concentration of 5x10^{10} vp/ml in HBS at different pH values and incubated for 1 hour at 4°C and 300 rpm shaking. 12 µl aliquots were loaded on a Mastercycle Neux (Eppendorf) thermocycler to simulate the temperature ramp in the extrinsic fluorescence assays. At the desired temperature point, samples were cooled down on ice and adsorbed onto glow-discharged, collodion/carbon-coated electron microscopy (EM) grids, washed with Milli-Q H_2O drops and negatively stained with 2% uranyl acetate. Grids were imaged in a JEOL JEM 1011 transmission electron microscope with a Gatan ES1000Ww camera.

In Chapter 8, 5 µL of a HAdV5/attP preparation containing 1×10^{12} viral particles ml^{-1} previous dialyzed against HBS during 1 hour at 4ºC. The virus sample was diluted in HBS with and without 5 mM $NiCl_2$ and incubated on glow discharged collodion/carbon coated grids for 5 min, blotted and incubated with 45 µL of formulation for different times and conditions. Grids were washed with HBS (500 µL), stained with 2% (w/v) uranyl acetate for 30 sec and examined in a JEOL JEM 1230 transmission electron microscope at 100 kV.

3.7.3 Cryo-Electron microscopy

To investigate the differences in Ad5 core structure when compared with a mutant lacking core protein VII (Chapter 6), we compared cryo-EM icosahedral averaged maps for the Ad5-wt and Ad5-VII- particles.

Virus samples were vitrified in liquid ethane and imaged in a 200 kV Talos Arctica microscope (FEI) equipped with a Falcon II detector. Image processing was carried out with standard cryo-EM software packages. More information can be found in[84].

CHAPTER 4

Long range cooperative disassembly revealed by aging during adenovirus uncoating

CHAPTER 4: Long range cooperative disassembly revealed by aging during adenovirus uncoating

4.1 Introduction

Upon entry into the host cell, eukaryotic viruses undergo a controlled genome uncoating process [85] which usually requires capsid disassembly following a timely precise process. In icosahedral viruses, protein subunits (capsomers) arrange in 20 triangular facets delimited by 12 fivefold vertices forming a structure of hexamers and pentamers[86]. Pentamers are located at each one of the twelve vertices surrounded by five hexamers. Therefore, pentons can be understood as the disclinations needed for achieving the curvature of a closed cavity using a planar hexagonal lattice[87]. Due to the geometrical constraints of the pentons within the icosahedral capsid, they are subjected to built-in mechanical stress [88–90]. In fact, some experimental findings report pentons as the weakest capsomers of icosahedral viruses under thermal or chemical stress[45,91]. In adenovirus, penton release is a necessary step for uncoating and infectivity [45,69]. As mentioned in Chapter 1, in the first step of infection a protruding fiber is attached to the penton base to mediate binding to the cell membrane protein CAR[92,93]. For a successful infection, the adenovirus particle releases protein VI to escape into the cytosol. This process requires capsid opening by penton loss [61,94]. Ad5 uncoating has been mimicked *in vitro* by physicochemical cues such as heat, inducing partial disruption and disassembly of the capsid shell [94]. The cyclic mechanical loading induced by AFM stylus also supplies energy to the system, allowing it to simultaneously trigger and monitor the disassembly of individual Ad5 particles in real time [61]. Pentons of the facet oriented upwards in mica-adsorbed particles escape sequentially, and afterwards the shell cracks open allowing genome release[95].

In this Chapter, we explore the dynamics of Ad5 penton release by combining single particle AFM imaging experiments with theoretical modelling based on survival analysis. This last was performed thanks to the collaboration with Rafael Delgado Buscalioni group. Pablo Ibañez developed the theoretical model and analysed the Weibull fitting of the experimental data.

4.2 Results

4.2.1 Establishing the force range for controlled Ad5 penton release under mechanical fatigue

AFM imaging at low force (~70 pN) allows us to select individual virus particles adsorbed on the mica surface in a 3-fold orientation and presenting three intact pentons[76]. For each selected capsid, we acquired a series of AFM images inducing cyclic mechanical stress with forces between 100 and 250 pN (**Figure 4.1, left**). We note that the applied force should be large enough to remove pentons during one experimental session (~5 hours) and small enough to avoid sudden uncontrollable large cracks on the viral particles. We found that the lower threshold is 100 pN, close to the limit force value allowing us to obtain AFM images of viruses (~70 pN)[48].

The experimental procedure consists of performing a sequence of AFM images of the virus particle using a prefixed imaging force F. Pentons are gradually lost, as more images are taken, neatly showing that pentons are the most fragile structures of the capsid. This in agreement with previous experiments where capsids were subjected to heat stress[28,94] and with the existence of built-in stress at the vertices[90]. In each experiment, we recorded the image number (N_i) at which we observed the escape of the first (N_1), second (N_2) and third (N_3) penton (**Figure 4.1**).

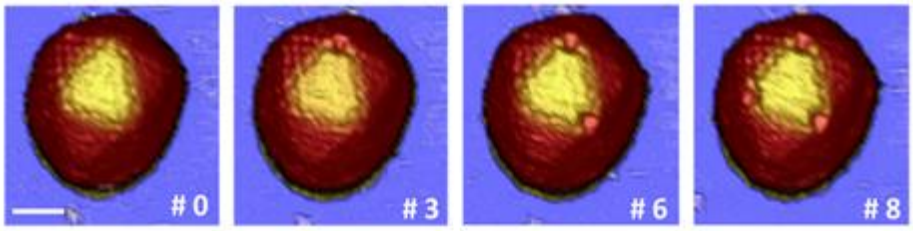

Figure 4.1. Ad5-wt penton release by mechanical fatigue. Individual frames of one Ad5 particle at 150 pN. Scale bar corresponds to 60 nm.

Further imaging beyond the dissociation of the 3rd penton revealed how penton-less capsids undergo further disassembly through cracking and crumbling[61] (**Figure 4.2**). In the experiments, we opted to use the applied force F as the relevant parameter, instead of increasing the imaging rate, which is also known to accelerate capsid disassembly[48]. The imaging rate was fixed to ~10 ms per pixel (128 x 128 pixels) which is long enough to guarantee the mechanical relaxation of the capsid after obtaining the topographical data of each pixel[96]. In this time other relevant experimental parameters such as the vertical distance travelled by the cantilever at each pixel (jump off) and the sampling rate (jump sample) (see Chapter 1)[48] are included. This timing is important as it ensures that each indentation is independent from the previous one, or equivalently, that *the capsid does not accumulate any stress over successive AFM strokes.* In mathematical terms, this lack of memory of the previous stroke is called Markovian hypothesis and will be later used (and validated) within the theoretical framework for the escape process.

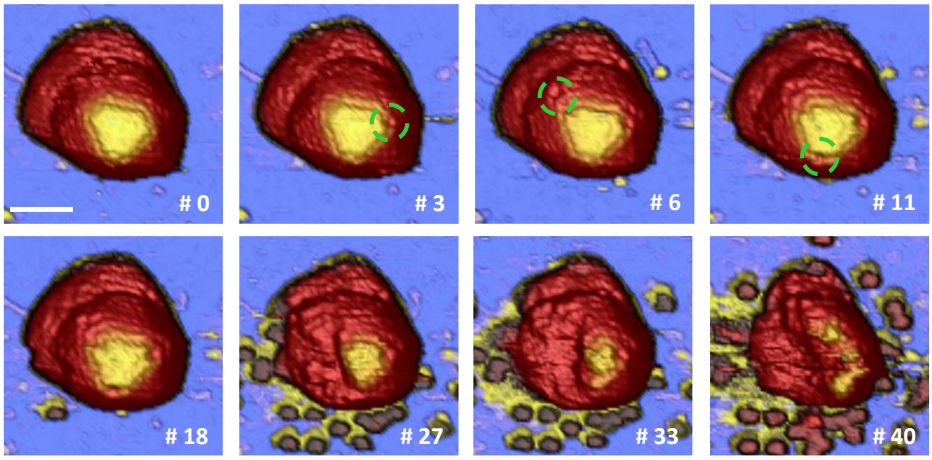

Figure 4.2. Ad5-wt disruption by mechanical fatigue at 150 pN of applied force. Selected individual frames along the disassembly process of a single adenovirus. Scale bar corresponds to 50 nm. Green circles indicate the loss of a penton.

4.2.2 Penton survival analysis provides evidence of aging

To investigate the statistics of penton escapes, we first collected all the penton failure timepoints (measured in frame number) in the same set of data {N}= {N_1, N_2, N_3} irrespective of the chronological order of escape. We then construct the histograms for the number of escape events observed at each image N and integrate (**Figure 4.3**) to obtain the cumulative probability P(N) for penton rupture (**Figure 4.4**). P(N) is thus the probability that some penton is lost after taking N images at a given force F or equivalently, the fraction of released pentons from the total sample at a given frame.

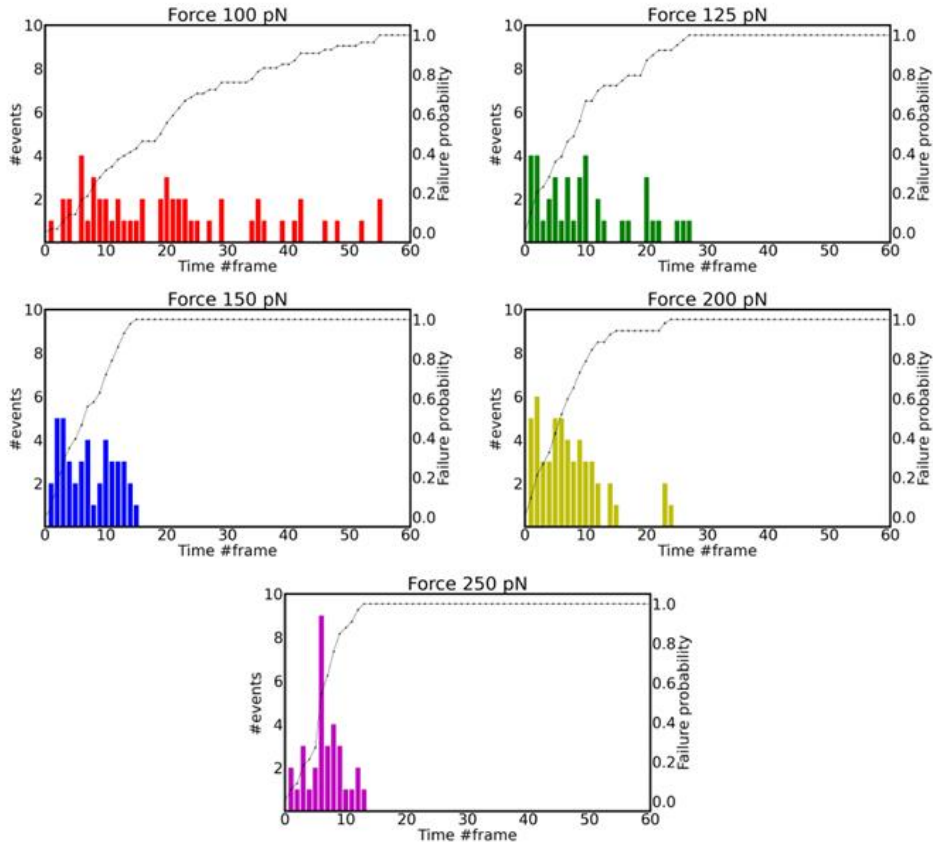

Figure 4.3. Histograms of penton loss events for the five forces studied. Experimental histograms of penton loss events for each frame and their cumulative probability (black lines) for 100, 125, 150, 200 and 250 pN.

As shown in **Figure 4.4**, P(N) significantly deviates from a Poissonian distribution, meaning that the penton failure rate is not constant, but instead varies over time (i.e. over the frame number, N). To get more insight we fitted P(N) with a Weibull distribution[97,98] which, in survival analysis, is a standard way to model processes with time-dependent failure rate. As the variable N is an integer, we use the discrete version of the Weibull distribution whose cumulative probability is

$$P(N) = 1 - \exp\left[-((N+1)/< N_p >)^{\beta}\right] \quad (4.1)$$

Here <N_p> represents the average lifetime of a penton in terms of number of images. Note that the failure rate varies with N as $\frac{d\left(log\left(1-P(N)\right)\right)}{dN} = \frac{\beta}{\langle N_p \rangle} \cdot \left(\frac{N}{\langle N_p \rangle}\right)^{\beta-1}$, being determined by <$N_p$> and the so-called shape parameter β. Importantly, β determines how the failure rate varies over time. Specifically, β= 1 corresponds to a constant failure rate and in this case, the Weibull distribution becomes equivalent to a Poissonian distribution. By contrast, β>1 is indicative of aging: the failure rate increases over time (i.e. with N).

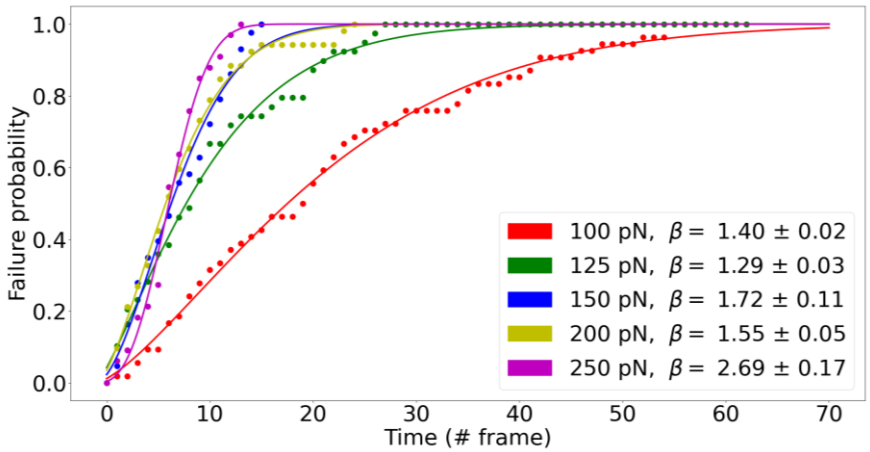

Figure 4.4. **Penton release analysis and Weibull fitting.** Penton release distribution at the five different forces studied. Dots represent the experimental data fitted by a discrete Weibull distribution (lines). The parameter calculated for the distribution (right bottom inset) corresponds to the exponent β.

Experimental penton escape probabilities (**Figure 4.3** and **Figure 4.4**) are found to be in excellent agreement with aging, i.e. with Weibull distributions having β>1. We found β≈1.5 for the range 100 pN < F < 200 pN, while for F=250 pN it increases up to β≈2.5, which indicates a fast aging. In fact, the increase in failure-rate with time is even faster than predicted by the Weibull test as we did not consider that the probability of finding a survival penton decreases after another penton(s) is gone. For instance, after one of the three accessible pentons is lost, the probability of hitting one of the remaining pentons decreases by a factor $\frac{2}{3}$ and this contributes to a spurious decrease in the Weibull

analysis of the failure-rate. As an aside, during the AFM experiments, we observe that when applying forces higher than 150 pN, the experimental probability curves start to overlap (**Figure 4.4**), preventing the use of higher forces. This experimental resolution limit in force agrees with our theoretical prediction for having a probability higher than 95 % of penton release during the acquisition of the first image (**Figure 4.5**).

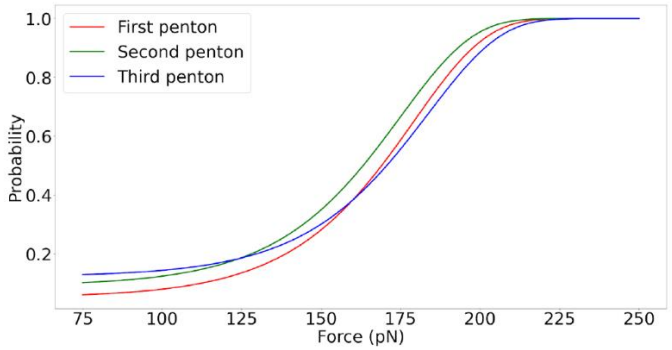

Figure 4.5 Force saturation effect for the three pentons. The theoretical probability P(n = 1) of encountering one penton escape event after taking one image, for different values of the indentation force F (see Eq (4.5) of main text and Eq. (23) of Appendix 1.). Note that the probability jumps steeply above 150pN. The saturation force, corresponding to P > 0:95, is predicted to be around 200pN.

The increase of the penton release rate along the experiment is a landmark of aging, which might arise either from an accumulation of capsid stress during each pixel acquisition or from the fact that we did not take into account the chronological order of penton escape in the analysis. It is important to elucidate between both causes because the first one (stress accumulation) would be against the Markovian hypothesis. To analyze this point we removed the memory stored in the chronological chain of escape events by resetting the time-counter each time an escape event takes place. This allows us to study each penton escape event independently. To this end, for each applied force, we gather three types of "time-interval" data: $\{n_1\}=\{N_1\}$, $\{n_2\}=\{N_2-N_1\}$ and $\{n_3\}=\{N_3-N_2\}$, which correspond to the survival times for the first, second and third penton, respectively. Notably, Weibull tests based on n_i with i= {1,2,3}, revealed

that the resulting probabilities $P_i(n)$ correspond to exponentials (i.e. β≈1.0, **Table 4.1**). The escape of a single penton is thus a Poissonian (memory-less) process and confirms the validity of the "Markovian hypothesis", i.e. the tapping process does not introduce stress accumulation in the capsid, as the particle has enough time to relax between successive pixels (taken each 10 ms). This was to be expected, as the mechanical relaxation time of virus capsids measured from vibrational modes[99] is about 100 ps.

Force (pN)	100	125	150	200	250
One penton lost	0.91±0.06	0.92±0.14	1.04±0.34	0.94±0.17	1.64±0.58
Two pentons lost	0.96±0.08	0.88±0.15	1.12±0.22	0.46±0.24	0.69±0.22
Three pentons lost	0.84±0.08	0.62±0.16	1.00±0.24	1.05±0.23	0.55±0.41

Table 4.1. Weibull shape parameters, β, for the different forces and separated by pentons order.

We then estimate the average escape rates for the first, second and third penton, which correspond to well-defined, "relaxed" states of the capsid. Interestingly, we find that after the first penton is released, the average lifetime of the following pentons is reduced. For instance, at F=100 pN the average lifetime of the first penton is ~37.5 min (12.5 images), while, for the second and third pentons, we found ~27 min (9 and 8 images, respectively) (**Table 4.2**). This fact explains the increase in failure rate over image time observed in the Weibull analysis. The result indicates that pentamer disassembly events constitute a cooperative stepwise process, where the first step facilitates the following ones. Cooperativity has a sense of "purpose", which could be attributed to the need of the capsid to gradually dismantle to achieve successful infection.

	Force (pN)	Average lifetime	Standard deviation	N
Penton 1	100	12.5	11.6	18
	125	5.4	4.6	13
	150	3.8	3.2	12
	200	3.6	3.0	16
	250	4.0	2.2	11
Penton 2	100	9.0	10.2	18
	125	4.0	3.6	13
	150	3.0	2.3	12
	200	3.1	3.3	16
	250	3.2	2.8	11
Penton 3	100	8.0	9.3	18
	125	5.7	7.0	13
	150	3.7	2.9	12
	200	4.5	3.5	16
	250	1.6	1.5	11

Table 4.2. Average lifetime (λ) and standard deviation (in units of image) for the escape of the three pentons in experiments performed with increasing of indentation force F. The similar values of the average and deviations indicate an exponential distribution with a well-defined escape.

4.2.3 Estimation of the spontaneous penton scape rate

We now focus on an analytical determination of the probability of releasing the i^{th}-penton after taking n images $P_i(n)$ (i=1,2,3), which is amenable for comparison with experiments. We consider the pentons as if they were confined in potential energy wells (**Figure 4.6**) which are altered by mechanical intermittent strokes. From a theoretical point of view, the transition kinetics of penton release can be simplified as a two-state process (bound and unbound).

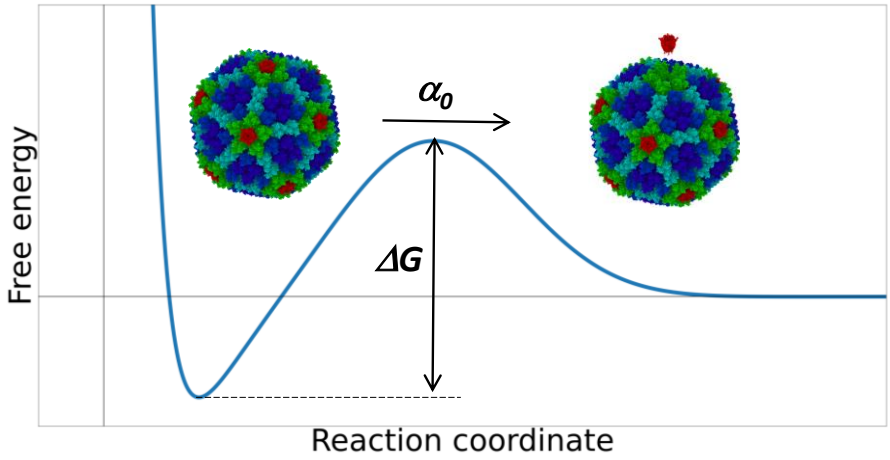

Figure 4.6. Energetic profile of penton release process when two states are considered.

In the absence of external mechanical perturbations (just the thermal bath) the transition rate α_0 for a penton to change from bound to unbound is related to the free energy well ΔG by a simple Arrhenius-type law

$$\alpha_0 = \omega_0 exp\left(\frac{-\Delta G}{k_B T}\right) \quad (4.2)$$

α_0 is usually called spontaneous or natural escape rate and ω_0 is the natural frequency of fluctuations of the penton in the energy well. To extract α_0 and then estimate ΔG we use a well-known strategy in transition theory[100], which consists in applying mechanical energy W into the system to lower the free energy well (ΔG-W) and accelerate the penton escaping-events to gather statistics in reasonable experimental times. In the jumping mode imaging of the AFM, the tip induces mechanical work to the capsid through an intermittent force $f_{AFM}(t)$ whose time dependence is similar to a tuneable top-hat function (**Figure 4.7**).

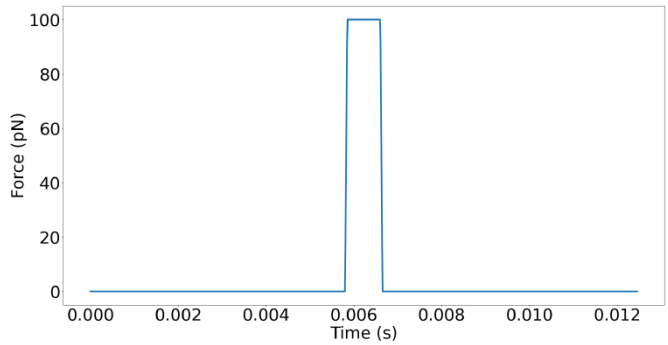

Figure 4.7 Indentation profile at 100 pN of applied force. Three parts of the curve can be distinguished. Two areas where the profile is null correspond to the approach and withdrawal processes. The central part corresponds to the indentation interval where the force is applied.

From the virus perspective, each stroke of this long series of indentations is extremely slow and during each single jump, the applied work W(t)>0 increases the transition rate to the unbonded state according to[100].

$$\alpha(t) = \alpha_0 \cdot e^{W(t)/k_B T} \quad (4.3)$$

Where k_B is the Boltzmann constant and T is the temperature. To further advance, we first propose a linear relation between the work applied by the AFM tip and the set point force (maximum F), $W = -Fx_{ef}$, where x_{ef} is a constant effective "indentation length". A second route consists of using the harmonic-well approximation, $F = -kx$ with an effective spring constant of the capsid, k. The indentation is then $x = \frac{-F}{k}$, and the applied work becomes quadratic in the applied force, $W = \left(\frac{1}{2}\right)\frac{F^2}{k}$, allowing us to compare theoretically estimated values of spring constants k with the experiments. The free parameters of the two-state model are α_0 and either x_{ef} or the effective spring constant k, which will be calculated by fitting the theoretical $P_i(n)$ with the experimental results.

The derivation of the single-penton escape probability$P_i(n)$ is detailed in Appendix 1 (A1). Starting from the expression for $\alpha(t)$ in Eq. (4.3), we first

calculate the probability $P_p(t)$ of penton failure after a given time, during a pixel. We are dealing with a Markov unidirectional process (from bound to unbound state) representing a first-order kinetic reaction. In an ensemble average, the increase in the number of unbound pentons, d$P_p(t)$, would be simply proportional to the population of bonded pentons, and the master equation reads,

$$dP_p(t) = \alpha(t) \cdot \left[1 - P_p(t)\right] \cdot dt \quad (4.4)$$

The applied force $f_{AFM}(t)$ used in Eq. (4.3) is experimentally known[61] (**Figure 4.7**) which permits us to perform a change of variable, mapping the image number "n" with real time in seconds. This is essential as Eq. (4.2) requires having the natural α_0 escape rate in proper inverse-of-time units, to estimate the energy barrier ΔG. Briefly, by integrating Eq. (4.4), we first determine the escape probability after a single pixel, then integrate over one complete image and finally over an arbitrary number n_i of images. The resulting expression for the probability of releasing the ith penton is,

$$P_i(n_i) = 1 - (1 - C_i)^{n_i} \quad (4.5)$$

where C_i, given in A1, depends on the applied force F and the free parameters we seek to find out (x_{ef}, k_i and the natural escape rate of the ith penton, $\alpha_{0,i}$). By fitting the theoretical probability $P_i(n)$ (Eq. (4.5) and A1) with the experimental results, we estimate x_{ef} and $\alpha_{0,i}$. The value of x_{ef} was found to be independent on the penton index, and the best fit (x_{ef}=0.18 ± 0.03 nm) was used for all the penton sequences. As shown in **Figure 4.8**, the theoretical model is in excellent agreement with experimental data. Additionally, we estimate an increase in the spontaneous escape rate as the penton-release order "i" increases: $\alpha_{0,1}$= (2.7±0.1)×10^{-4} s^{-1}, $\alpha_{0,2}$=(4.7±0.2)×10^{-4} s^{-1} and $\alpha_{0,3}$=(6.4±0.3) ×10^{-4} s^{-1} (first, second and third penton, respectively). Interestingly, the spontaneous escape rate of the third penton results to be about twice faster than the first

one. As a curiosity, these values of the spontaneous rates are of the same order of those reported in mechanical unfolding of proteins[101–103].

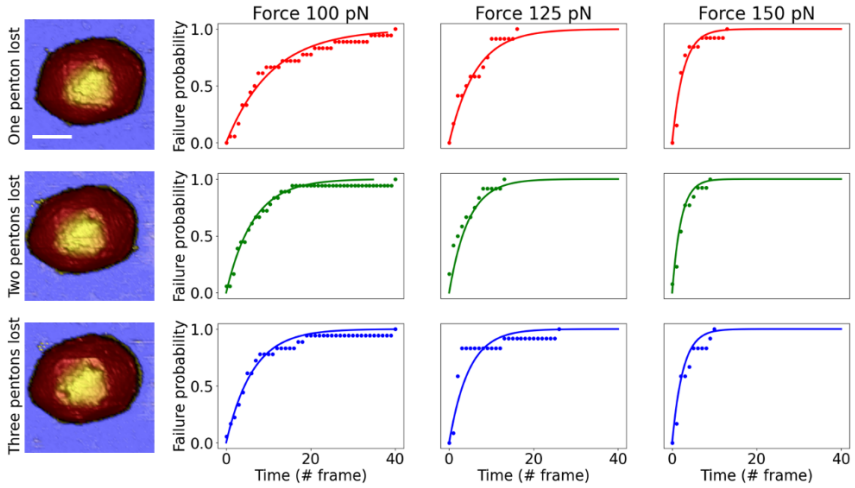

Figure 4.8. **Penton release distribution under Markov process model based on the ansatz $W=-F\times x_{ef}$.** AFM images were taken after the first, second and third penton escape events (left panel, scale bar corresponds to 44 nm). Cumulative probability of penton failure for successive penton escape when the capsid is exposed to strokes of forces of 100 pN, 125 pN and 150 pN (right panel). Dots represent the experimental data and solid lines represent the model results.

4.2.4 Weakening of the capsid stiffness

It has been reported that penton vacancies may be accompanied by a change in the global capsid stiffness[36,104]. Although this might seem logical, this is not a common feature in nanomaterials[105]. The increase in the failure rate we observed after the release of the first penton indicates a *global* effect, which could be ascribed to the capsid structure weakening. We can estimate the decrease in stiffness by using the ansatz $W = \left(\frac{1}{2}\right)\frac{F^2}{k}$, based on the energy of a harmonic-well with effective local stiffness k. The form of the theoretical failure probabilities were found to be in good agreement with the experimental trends (**Figure 4.9**) and allowed us to fit the theoretical $P_i(n)$ with the experimental

outcome to obtain estimations for the capsid stiffness. For intact capsids we got k_0=0.50±0.02 N/m, while for capsids without one or two pentons we obtained k_1=0.42±0.01 N/m and k_2=0.41±0.01 N/m, respectively. These values were compared with independent experimental data for intact capsids (k_0) and a group of 18 pentonless capsids (k_i). In these benchmark experiments, Ad5 pentonless particles were obtained by applying a temperature stress (T=40 ºC during 5 minutes in solution) which causes viral particles to lose at least one penton[94]. The benchmark experiments yield k_0=0.58±0.01 N/m N=53 [95] for intact particles and $k_{1,2,3}$=0.42±0.06 N/m N=18 [106] for heated capsids. These values are consistent with those obtained from escape probability distributions, where the penton number and release order were controlled. The similarity between the estimated values of k_i is remarkable if one considers that both experiments are radically different. The benchmark experiments measured k from the linear regime of the force-indentation curves, using single indentations with a force of a few nN, which ultimately cause large capsid deformations of tens of nm, cracks and capsid breaking. Here we are typically applying about 10^5 gentle AFM strokes of ~100 pN, at low frequency (10 ms). Notably, the present approach gets quite close to the mechanical cues in the cell environment.

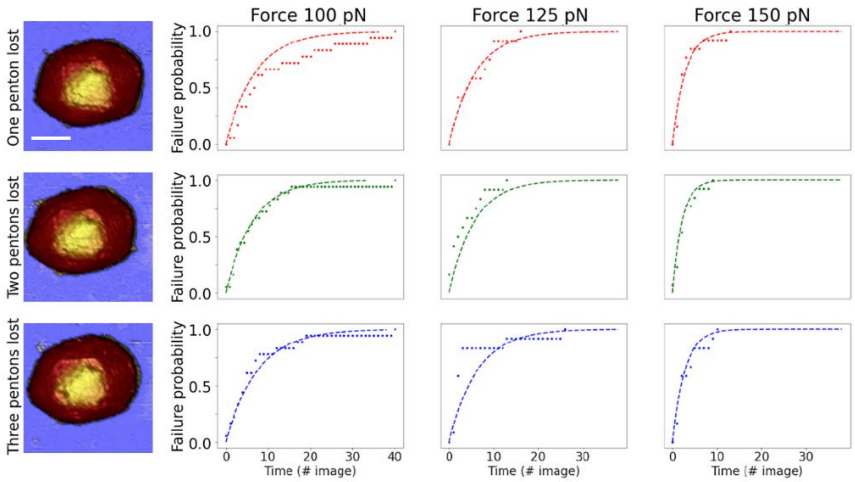

Figure 4.9. **Penton release distribution under Markov process model based on the ansatz W= (1/2) F^2/k.** The left panel illustrates AFM images taken after the first, second and third penton escape events (scale bar corresponds to 44 nm). Right panel shows the cumulative probability of penton failure for successive penton escape when the capsid is exposed to strokes of forces of 100 pN, 125 pN and 150 pN. Dots represent the experimental data and dashed lines represent the model results.

4.2.5 Estimation of the free energy barrier for penton release

A relevant question is how mechanical fatigue is altering the physical parameters of the capsid. We have seen that losing pentons affects the Ad5 particle in two ways: *i)* a gradual increase in the penton escape rate and *ii)* a decrease in the capsid stiffness. From the ratio $\alpha_{0,3}/\alpha_{0,1}$, Eq. (4.2) allows us to assess that the difference between the energy barriers of the third and first penton which is about ΔG_3-ΔG_1= -1 k_BT. This might indicate a small but noticeable modification in the molecular configuration of the residues sustaining the penton (after two partners are lost) which leads to the particle softening.

Our analysis also allows to estimate the average energy barrier for the penton release *ΔG*. For that, we need to estimate ω_0, the rate of exploration of the local well. A reasonable estimate is based on the balance of cohesion forces and environmental friction, and yields $\omega_0 = \frac{k}{\xi} \approx 10^{10} Hz$ (the penton's friction coefficient ξ is taken as the Stokes value in water, where the dynamic viscosity $\eta \sim 10^{-3}$Pa × s). Alternative estimations of ω_0 require the cut-off radius of the well λ (a sub-nanometric length of the order of the junction between the penton and the neighbouring hexamers). We infer that λ must be similar to the displacement produced by the limit force at which the loss of the penton can be seen as extremely fast (i.e. approximately within a single image), i.e. $\lambda = \frac{F_{limit}}{k} \simeq 0.5\, nm$. Thermal fluctuations lead to an average kinetic energy $Mv^2 = k_B T$and using $\omega_0 = \frac{v}{\lambda}$, this leads to $\omega_0 = 6.4 \times 10^9 Hz$. Vibrations around the quadratic potential lead $\omega_0 = (k/M)^{1/2}/(2\,\pi) = 10^{10}\, Hz$. These three estimations are quite close, and we conclude that $\omega_0 \approx 7.0 \times 10^9 Hz$. Taking logarithms in Eq. (5), and averaging over $\{\alpha_{0,i}\}$, we predict an energy barrier of $\Delta G \approx (30 \pm 1) k_B T$. This value is consistent with those reported in the literature on capsid assembly, either from coarse grained simulations[88] or calorimetry studies[107]. The pairwise interaction between capsid units is known to be between 5 and 6 k_BT. For the five contacts of the pentamer, this leads to a total binding free energy of ~ 30 k_BT, which agrees with our result.

4.3 Discussion

Theoretical simulations of virus assembly consider capsomer interactions to first neighbourhoods[88,107]. In principle, this type of building method might suggest that penton disruption is a local event depending solely on the neighbouring capsomers, i.e., hexons. However, we measured a significant increase in the

penton escape rate after the first penton is lost. In the Ad5 capsid, neighbouring pentons are ~45 nm away, so the loss of one penton is not expected to induce a strong local modification of the protein environment surrounding the other pentons. Since every penton is surrounded by similar hexons, the penton loss rate would then not depend on the chronological order as far as their local structural environment remains unchanged. However, our analysis clearly shows that, far from being a local event, penton disassembly depends on the global state of the capsid. Additionally, our analysis confirms a measurable softening of Ad5 capsids after one penton is lost. Both results suggest that the cooperativity in the penton-release process (aging) is related to a gradual modification in the global mechanical structure of the capsid. Notably, 45 nm would be the largest correlation distance identified between structural elements in a virus capsid[108] and other protein assemblies[109–112]. Further support of this conclusion is given in theoretical studies which reveal that the tangential stress distribution along the capsid presents long-range correlations connecting pentons, being particularly strong in T=25 capsids[90]. Aside from a global change in the particle stiffness, some enhancement in fluctuations and particle breathing, perhaps also influenced by loss of internal components such as protein VI or core protein V[94], might also facilitate the next penton escape.

4.3.1 Biological implications

We now explore the implications of our findings in the timeline of adenovirus uncoating[69]. In the initial stage, integrins bind to the penton base and induce the release of the associated penton. Penton loss facilitates externalization of protein VI, whose lytic activity disrupts the endosome membrane to allow virus escape at 15 min post infection (p.i.). Afterwards, the semi-disrupted particle is pulled along the microtubules, against the drag of the viscous cytoplasm, by

both dynein (minus-end) and kinesin (plus-end) motor proteins which bind to the capsid hexons[113,114]. During this randomized travel (active diffusion) along the microtubule network, the Ad5 capsid keeps losing capsomers [113,115]. Each stroke of the molecular motor introduces mechanical work (~10 k_BT [116]) into the capsid at a rate of about 10 Hz and corresponds to a step of about 5 nm. During the travel to the nucleus that covers between 5-10 μm [114], the partially disassembled capsids are subjected to thousands of these strokes. This energy is partly dissipated to the motor-protein linker and to the surrounding, but part of this mechanical energy (*W*) will reach the capsid, thus increasing the penton escape rate by the Boltzmann factor $e^{\frac{W}{k_BT}}$. We find that the penton lifetimes exponentially decay with the applied force, at least for 100 pN ≤F <200pN. As an educated guess, if $W \sim 2.5\ k_BT$ (a quarter of the protein-motor power stroke), the lifetime of a penton would be reduced by a factor 10. Once at the nuclear membrane (45-60 min p.i.), the virus particle is broken by the coupled action of the attached kinesin motor pushing in opposite directions [114]. At this stage, most virus particles appear to be weak enough to release the viral genome into the nuclear pore. The work introduced by each tap over the long series (~10^5) of gentle AFM strokes mimics the mechanical queues that the virion receives during its travel to the nucleus.

Our *in vitro* experiments reveal that genome ejection takes place after at least three pentons have been removed (**Figure 4.10a**). **Figure 4.10b** shows that the dsDNA escapes from the virus cage through big cracks that require the additional disassembly of hexons[61]. In vivo, semi-disrupted particles must be strong enough to preserve genome integrity when traveling from the endosome to the nucleus. Most likely, the uncoating process is adapted to achieve these two apparently contradictory goals: *i)* to keep the capsid stable enough during the transport to the nucleus and *ii)* to become weak enough once it arrives to the nuclear pore. Retaining a large number of pentons would guarantee a safe

trip to the nucleus, but it might delay or even preclude the final uncoating at the nuclear pore (**Figure 4.10c**). The survival analysis presented here estimates the average natural lifetime of the first penton in about $1/\alpha_{0,1}$ ~ 1 h. Lifetime is gradually reduced to $1/\alpha_{0,2}$ ~30 min (second penton) and $1/\alpha_{0,3}$ ~20 min (third penton). The whole process is over 50% faster than a non-cooperative penton escaping sequence.

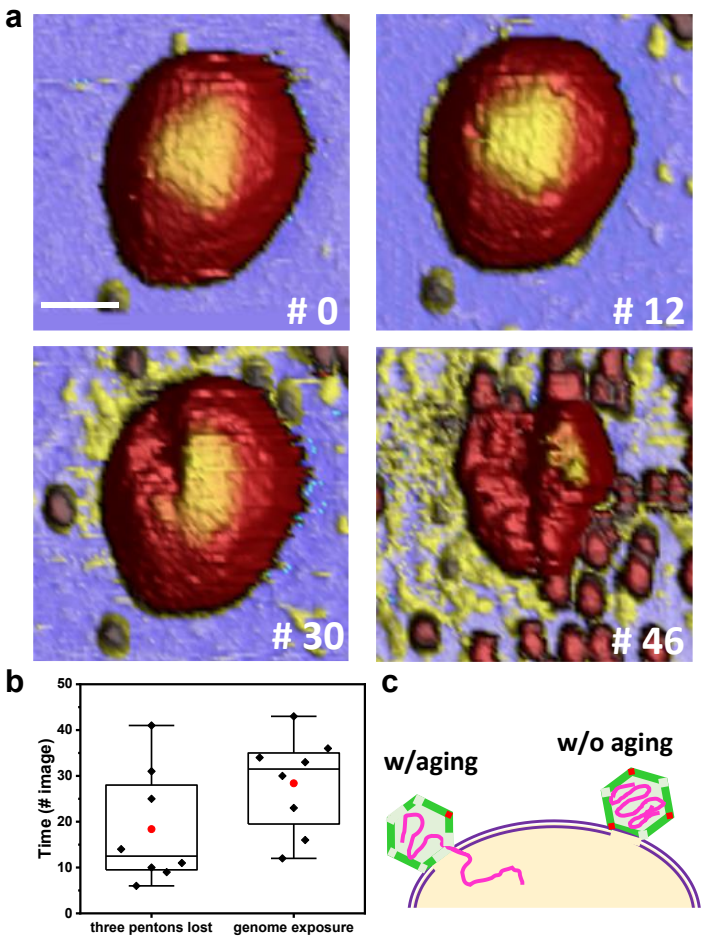

Figure 4.10. **Genome exposure and cooperative penton release. a)** Top left, virus particle showing three penton vacancies at frame #12. Top right, the same particle at frame #30 showing some DNA released. b) Chart presenting the # of frames required for releasing the pentons and inducing DNA exposure. c) Model of viral impaired uncoating at the nuclear pore assuming aging (left) and non-aging (right) penton release.

We conclude that the cooperative penton disassembly helps in achieving the required capsid aging on time for the genome to be successfully delivered at the nuclear pore (i.e. between 60 and 90 min p.i.). In view of the relatively adjusted times in the infectious cycle, a 50% delay might already prevent the virus from releasing its dsDNA on time (e.g. by allowing detection by cell defense mechanisms or finishing stuck on the nuclear pore) (**Figure 4.10c**). We, therefore, suggested that the increased disruption rate of the pentons is helping to fine tune the uncoating process of human adenovirus.

4.4 Conclusions

While aging is natural phenomenon mostly ascribed to materials, it has never been described in biomolecular structures. Icosahedral virus capsids are closed shells built up with a hexagonal lattice of proteins, which incorporate pentons at the fivefold symmetry axes. Human adenovirus capsids lose pentons during the initial steps of uncoating and throughout their travel to the nucleus, where DNA escapes from a partially disrupted virion across the nuclear pore. Adenovirus releases its pentons in a sequential way, but the mechanism governing this dynamic process that guarantees a successful genome delivery remains unknown.

Here survival analysis is used to analyze the penton disruption induced with atomic force microscopy on individual particles. We find a cooperative effect in the penton disassembly, such that the escape of one penton increases the release rate of the remaining ones. Consequently, pentons dismantling accelerates along the uncoating process because the probability of a penton to be removed increases as less pentons remain on the capsid structure. Therefore, this aging effect accelerates ~50% penton dismantling throughout the uncoating

process. Taking this into account, we develop a theoretical model that fits the experiments remarkably well and provides the energy barrier for penton release (~30 k_BT) and its spontaneous scape rate (~10^{-4} s^{-1}).

Our work uncovers a new paradigm about aging in biomolecular structures. In particular, we propose that aging fine tunes the uncoating process in order to produce weakened particles at the nuclear pore just ready for genome release. Strikingly, this aging is independent of the local molecular environment of pentons (first neighborhoods), revealing global factors never considered before in assembly/disassembly virus modeling. Besides, our study reports the largest cooperative phenomenon between proteins within a biological macromolecule to date: 45 nm inter-penton distance. Finally, although we have used human adenovirus as a model system, in view of the common geometric and mechanical features of penton vertices in virus design, this work may have general consequences on other icosahedral viruses that disassemble to release their genome inside the host.

CHAPTER 5

Acidification induces condensation of the adenovirus core

CHAPTER 5: Acidification induces condensation of the adenovirus core

5.1 Introduction

Virus particles must find the balance between the stability needed to survive harsh environments during transmission (extreme temperatures, osmotic pressure, ionic strength or pH)[117] and the ability to release their genome in the appropriate time and place. To achieve this goal, virus particles adopt metastable conformations, primed to disassemble under the appropriate cues provided by a host cell[118,119]. These cues induce the conformational changes required for genome uncoating, and depend on the virus and cell nature [120]. In animal viruses, such Adenovirus, after attachment to the cell receptor, virus particles use the host endocytic mechanisms to travel through the cytoplasm[121]. Disassembly triggering signals include virus-receptor interactions or exposure to low pH in the endocytic compartment, among others. For example, influenza virus uses the low pH in late endosomes as a cue for penetration by membrane fusion[122], and poxviruses undergo structural changes in the capsid under acidification[123]. Flaviviruses, such as dengue and Zika virus, undergo low pH-driven endosomal membrane fusion to release their genome into the cytoplasm during entry. Later, the immature virions undergo maturation during transport through the secretory pathway triggered by exposure to the more acidic pH environment of the trans-Golgi network[124].

As explained in Chapter 1, following internalization, the internal minor coat protein VI must be exposed to mediate membrane disruption of the early endosome (pH 6), facilitating AdV escape to the cytosol (pH 7.8) to continue its travel to the nuclear pore[41]. It seems logical, therefore, to expect that the

acidic nature of the early endosome could play a role in the initial stages of AdV uncoating, as shown for other viruses[122,125].

There have been two major approaches for investigating the role of acidification in AdV uncoating: looking at capsid disruption in purified virus particles and analyzing virus entry in the cell. It has long been known that dialysis against Tris-maleate buffers in the pH range 6.0-6.6 induces release of vertex proteins from the virions[126]. Additionally, extrinsic fluorescence spectroscopy assays, in which AdV particles are subjected to acidic conditions overnight, have shown that low pH destabilizes AdV particles[41,94]. On the contrary, other thermostability studies have demonstrated that overnight exposure to acidic conditions enhances Ad5 thermostability[127–129]. Conversely, when a buffer with high salt concentration was used in the same study, it was observed that virions were less thermostable upon acidification[128]. Finally, using a quantitative single-cell assay, it has been shown that membrane penetration during endosome escape does not require acidic endosomal pH, but other yet-unknown cellular mechanism[42]. Therefore, there is uncertainty regarding the role of acidification on AdV stability and function.

AFM studies have shown changes in the mechanical response of influenza virus across a pH range from early to late endosome[122]. In the dicistrovirus Triatoma virus, basic pH triggers uncoating by relaxing the stabilizing capsid-genome interactions, which results in a softening effect in the capsid[130]. Similarly, cowpea chlorotic mottle virus particles undergo swelling and softening transitions when the pH is raised from 5 to 7[131].

In this Chapter, we analyze how Ad5 mechanical properties and thermostability change upon acidification, simulating the conditions the particle may find as it traffics in the cell. We investigate the effect of short (~1 hour) exposure to low pH on Ad5 particles combining Atomic Force Microscopy (to explore changes in mechanical properties) with extrinsic

fluorescence spectroscopy and electron microscopy (to interrogate virion thermostability and genome exposure). We use mild acidic conditions mimicking the early endosome (pH 6), from where Ad5 has been demonstrated to escape[132]. We also use pH 5.5 that resembles the late endosome, motivated by the fact that the native trafficking pathway for HAdV-B7 involves residence in late endosomes and lysosomes[133]. Finally, our more extreme condition (pH 4), could resemble the harsh conditions of the gastro-intestinal tract, as not only the enteric HAdV-F41/40 but also Ad5 and other serotypes have been found in feces[134] and sewage waters[135].

5.2 Results

5.2.1 Acidification softens Ad5 viral particles

To examine the Ad5 mechanical properties in acidic conditions we performed nanoindentation experiments at four different pH values. The elastic constant for Ad5-wt at pH 7.8 was $k_{Ad5\text{-}wt}$ = 0.58 ± 0.02 N/m (mean ± SEM; N=53). In acidic conditions, the values obtained were: $k_{Ad5\text{-}wt}$ (pH 6) = 0.49 ± 0.02 N/m (mean ± SEM; N=56), $k_{Ad5\text{-}wt}$ (pH 5.5) = 0.50 ± 0.01 N/m (mean ± SEM; N=60), and $k_{Ad5\text{-}wt}$ (pH 4) = 0.44 ± 0.02 N/m (mean ± SEM; N=47) (**Figure 5.1 left, red symbols**). These data show that acidification makes Ad5-wt virions softer. To discern whether this softening is related to the capsid or to its contents (genome and core proteins), we analyzed empty capsids (Ad5-E). The stiffness value for empty particles at pH 7.8 was $k_{Ad5\text{-}E}$ = 0.44 ± 0.03 N/m (mean ± SEM; N=54) as previously described[36,95], and remained unchanged for all pH conditions tested (**Figure 5.1 right, red symbols**). These results demonstrate that virion softening induced by acidification is caused by changes in the core, or in the interactions between core and capsid. Breaking force values were

largely unaffected by acidification, with a value of 4.7 ± 0.2 nN for virions except for pH 4 where it decreased to 4.1 ± 0.1 nN (**Figure 5.1 left, blue symbols**). The breaking force value for empty particles was constant at ~2.6 ± 0.2 nN (**Figure 5.1 right, blue symbols**). The fact that the absence of core results in a ~50% decrease in the breaking force seems to indicate that the presence of the core significantly strengthens the capsid, as found previously for other viruses[136]. However, adenovirus immature particles contain all core components and present a breaking force similar to that of empty capsids, while the stiffness is intermediate between those of empty and mature capsids[36]. In immature particles, the genome is highly condensed due to the absence of proteolytic processing of core proteins VII and μ [36,58,59,104]. These observations suggest that it is not the presence of core components, but changes derived from maturation, which actually reinforce the Ad5 capsid.

Interestingly, our results show that at pH 4 the spring constant is similar in full and empty capsids, meaning that strong acidification causes an effect similar to the absence of mature core in capsid stiffness, but more pronounced This effect can be related to the moderate decrease in breaking force observed for virions at pH 4.

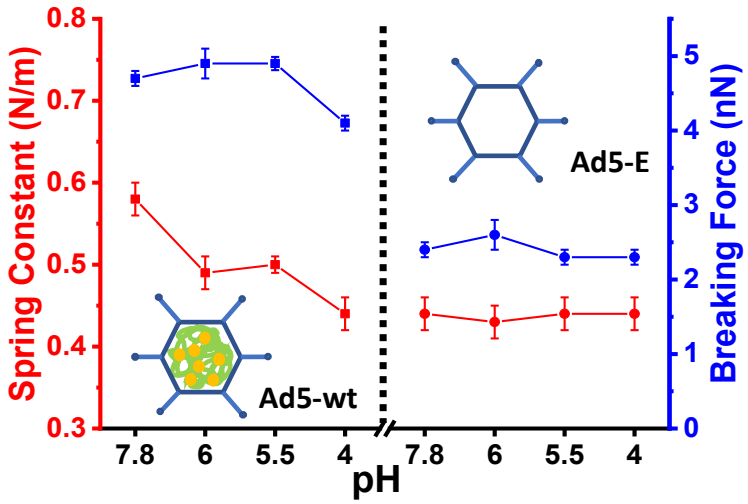

Figure 5.1. Mechanical properties of Ad5 wildtype (left, Ad5-wt) and empty particles (right, Ad5-E). Red symbols represent the spring constant, and blue symbols represent the breaking force, corresponding to the left and right axes, respectively.

5.2.2 Acidification increases core condensation in Ad5 viral particles

Since acidification softens Ad5-wt virions but not empty capsids, we wondered if low pH has a role in the physical state of the core, similarly to observations previously described for immature particles, where high core condensation results in lower internal pressure and a softer particle than in the mature virion[36,94]. We assessed core condensation by analyzing height (h) changes at the cracks created by single nanoindentations. We measured the height of the virion apex before performing a nanoindentation (**Figure 5.2a, before**), and of the lowest point in the crater afterwards (**Figure 5.2a, after**). The plot in **Figure 5.2a, right** shows an example of height profiles before (purple) and after (black) an indentation experiment obtained at the respective arrow lines of **Figure 5.2a, left**. The height of intact particles was similar for all the pH conditions (~85 nm) and close to the nominal Ad5 height[19] (**Figure 5.2b, "before"**). After nanoindentation, the lowest height in the crater (**Figure 5.2b, "after"**) at the different pH conditions was: $h_{pH\,7.8}$ = 63.7 ± 1.8 nm (mean ± SEM;

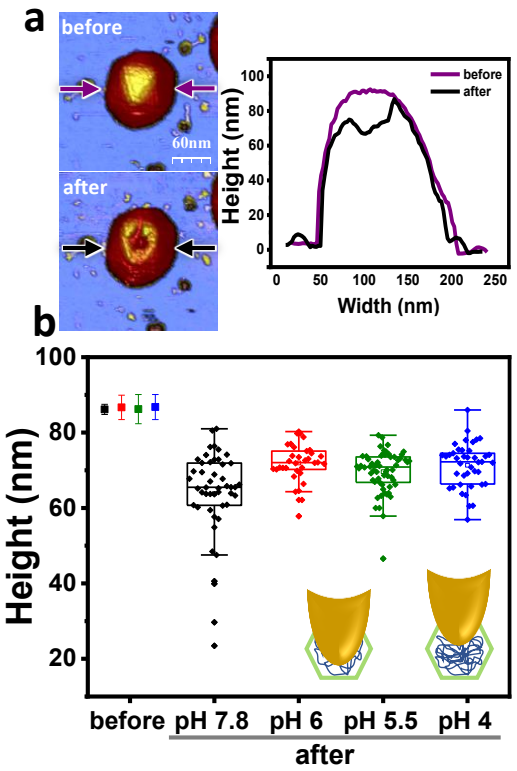

Figure 5.2. Height distribution before and after breakage of Ad5 particles. (a) Topography images of a single Ad5 particle before (top left) and after (bottom left) an indentation assay at pH 7.8. Arrows indicate the line at which the height profile before (purple) and after (black) an indentation curve was measured. (b) Heights measured before (average ±SEM) and after (boxplots) an indentation for the different pH conditions tested. The cartoons at the bottom show the AFM tip reaching two different depths after the capsid shell is broken by indentation.

N=48), $h_{pH\ 6}$ = 72.0 ± 0.9 nm (mean ± SEM; N=34), $h_{pH\ 5.5}$ = 69.7 ± 0.7 nm (mean ± SEM; N=50), and $h_{pH\ 4}$ = 71.3 ± 0.8 nm (mean ± SEM; N=41). ANOVA test indicates that all the populations are significantly different at a 0.05 level. That is, the AFM tip penetrates deeper (~20 nm) in the particles at neutral pH than at any other pH condition tested (≤15 nm). These results suggest that at pH 7.8 part of the core leaves the capsid after breakage, allowing the tip to penetrate deeper than at the rest of the conditions. Or, alternatively, in acidic conditions, the core is more condensed and hinders tip penetration inside the particle once the capsid shell breaks open (**Figure 5.2b, cartoon**).

5.2.3 Acidification decrease Ad5 genome accessibility

To obtain additional information on the effect of acidification on Ad5-wt virions, we carried out thermostability assays under different pH conditions, using extrinsic fluorescence and electron microscopy as indicators of genome accessibility and capsid integrity. These measurements were performed by Marta Pérez Illana and Mercedes Hernando Pérez. Technical information is in Section 3.7.

Incubation at the desired pH values was kept short (~1 hour) to mimic the situation in the AFM assays. At the initial temperatures (~30 ^{o}C), we did not find significant differences in fluorescence emission from particles treated at different pH values (**Figure 5.3a**), indicating that the amount of dsDNA accessible to the dye was not increased at the tested acidification conditions. In the same line, negative staining electron microscopy showed that particle morphology remained intact after 1 h treatment with acidic pH (**Figure 5.4,** 4^{o}C and 36^{o}C). These results agreed with the AFM observations showing mostly intact particles for all pH values before nanoindentation (**Figure 5.2a**, "before"). Analysis of the average fluorescence curves shown in **Figure 5.3b** yielded the following transition temperatures: $T_{0.5}$ pH 7.8 = 46.9 ± 0.8 ^{o}C; $T_{0.5}$ pH 6 = 54.2 ± 0.5 ^{o}C; $T_{0.5}$ pH 5.5 = 56.0 ± 0.3 ^{o}C; $T_{0.5}$ pH 4= 56.5 ± 0.1 ^{o}C, suggesting that acidification increases the thermostability of Ad5-wt virions. Additionally, lower increases in fluorescence emission were observed for decreasing pH values (**Figure 5.3a**). Considering that the adenovirus genome is heavily bound to core proteins, such decrease in fluorescence emission could be due to a lack of capsid dismantling events, or to a tighter interaction of core proteins with the adenovirus genome hampering the intercalation of the fluorophore.

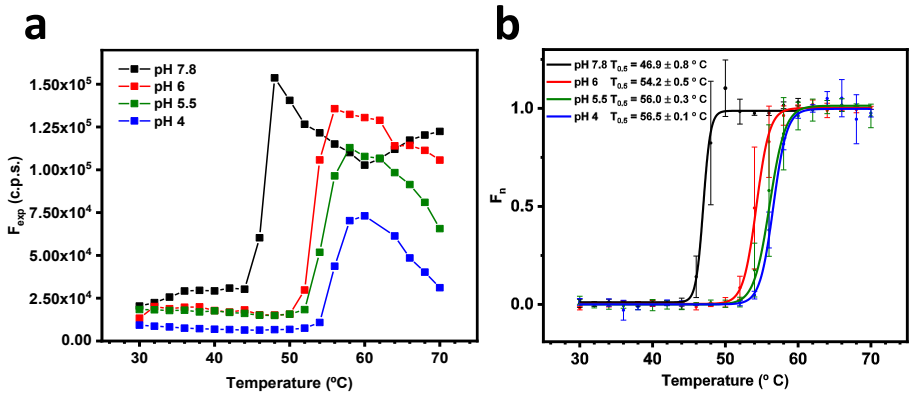

Figure 5.3. Effect of acidification and heating on Ad5-wt virions analyzed by extrinsic fluorescence. (a) Raw fluorescence signal of YOYO-1 (F_{exp}) as a function of temperature for Ad5-wt virions after incubation for 1 hour at the pH values indicated. The plot shows examples of single experimental curves recorded on the same day (experimental set). (b) Extrinsic fluorescence measurements normalized as described in Section 3.7.1. N=3 ± STD for pH6, 5.5 and 4; N=2 for pH7.8 and pH4 at 62ºC. Lines correspond to the Boltzmann sigmoid fitting to estimate the $T_{0.5}$ for each condition tested. For pH 7.8, fluorescence normalization was performed only until 60ºC since the post-transition base line is not considered linear anymore above 60ºC.

TEM images showed that at pH 7.8, Ad5 particles appear significantly disrupted starting from 48 ºC (above the $T_{0.5}$), in agreement with the rapid increase in YOYO-1 fluorescence (**Figure 5.4**). In the case of acidic pH (6, 5.5, 4), we started finding disrupted particles also at 48ºC. Although the disruption patterns observed varied, and not all particles appeared damaged, this observation indicates that in acidic conditions at 48 ºC there are openings in the capsid shell through which YOYO-1 could penetrate.

However, fluorescence does not appreciably increase (**Figure 5.3**). This observation supports the hypothesis that changes induced by acidification are largely due to a different, more condensed state of the Ad5 nucleoprotein core. At pH 4, both the maximum change in the raw fluorescence signal and the raw fluorescence at endpoint temperature (70 ºC, well beyond $T_{0.5}$) are notably lower than at the other pH conditions (**Figure 5.3a**). Additionally, capsid damage seems lower at pH 4 seems lower than for all other conditions

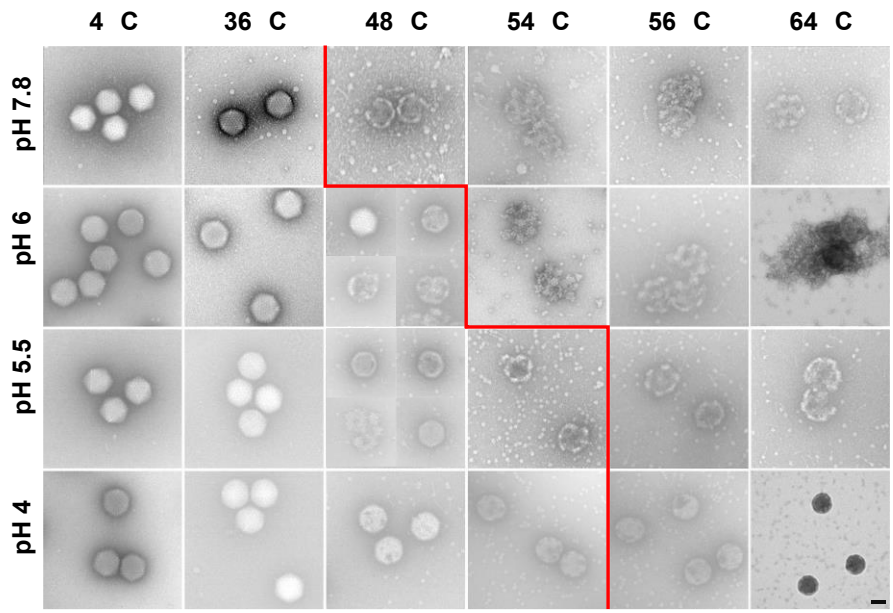

Figure 5.4. Structural effects of acidification and heating on Ad5-wt analyzed by negative staining electron microscopy. Red lines indicate approximately the experimental temperature point nearest to the calculated $T_{0.5}$ for each pH condition. Scale bar = 50 nm. For 48 ºC pH 6 and pH 5.5, four different fields of view were selected to represent the various particle populations observed.

tested throughout all the temperature range studied (**Figure 5.4**). That is, both capsid stability and shielding of dsDNA by core proteins seem to be maximally enhanced at this extreme pH.

5.3 Discussion

The results presented here indicate that short term acidic treatment of Ad5 particles by itself does not compromise capsid integrity, but has an impact on the core conformation, which reflects in capsid stiffness and genome accessibility to intercalating agents upon heating. We find a correlation between the elasticity of the Ad5-wt and genome exposure under acidic pH (**Figure 5.5**): the rigid particles at pH 7.8 present higher genome accessibility upon capsid disruption, while in the soft particles at pH 4 the genome is less

accessible to YOYO-1 intercalation even in the presence of capsid openings. These soft particles can support the thermal vibrations better than the stiffer virus structures, since they can reach higher deformations, and are more thermostable.

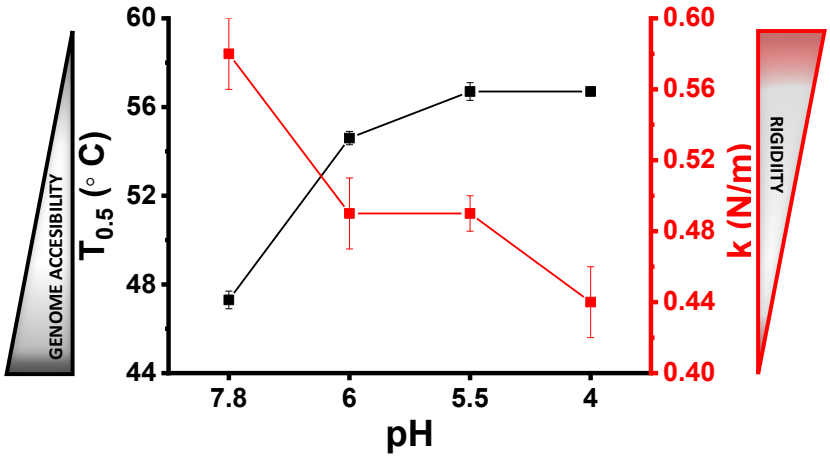

Figure 5.5. Summary of the effects of acidic pH on Ad5-wt observed by nanoindentation and extrinsic fluorescence experiments. Comparison of $T_{0.5}$ (extrinsic fluorescence, black symbols) and spring constant k (nanoindentation, red symbols) values obtained for all conditions tested

Our observation that acidification softens the Ad5 particle while increasing core condensation is reminiscent of the behaviour found for immature AdV particles, which are softer than the mature ones and also more thermostable[61,94]. Furthermore, when the capsid of immature particles is peeled away under mechanical fatigue, height measurements are compatible with an intact core (~70 nm), while for mature particles the remaining debris was only ~30 nm high, showing that most of the core components had diffused away[61]. These differences have been attributed to the higher condensation of the genome by the immature core proteins, which decreases internal capsid pressure[36]. The changes we observe in the mechanical properties of Ad5-wt virions subject to acidic pH also resemble those occurring in mature virions in

the presence of spermidine, a 3^+ charged polyamine known as a dsDNA condensing agent[36].

Why would acidification have a tightening effect on the Ad5 core similar to that of condensing counterions or proteins? One hypothesis is that the increment of proton concentration itself can promote DNA condensation. It is also conceivable that further proton uptake by histidine residues in acidic milieu, would increase the positive net charge of core proteins, strengthening their condensation action by screening the DNA negative charges[36,140]. Additionally, acidic residues (GLU, ASP) will reduce their negatively charged forms upon acidic conditions[140,141], which would further increase the positive charge of core proteins, and decrease their repulsion with the negatively charged DNA To this purpose we estimate theoretically the net charge at different pHs of core proteins using "Protein Calculator v3.4", employing the sequence of the core proteins and the copies number reported in[28]. Theoretical charge of the DNA of Ad5/attP, at different pHs was calculated according to the formula and pka values of 5'-nucleotides reported in[142]. The estimated percentage of non-screened negative DNA charges was calculated as follows:

$$\%\ of\ non-screened\ negative\ DNA\ charge = \frac{Core\ protein\ charge + DNA\ charge}{DNA\ charge}$$

With this information, we performed **Figure 5.6**.

However, it is also important to bear in mind that these changes in protein charges might also have counteracting effects. For example, neutralization of negatively charged forms by acidification could lead to a loss of salt bridges or favorable electrostatic interactions, thus having a negative impact on capsid and core protein stability.

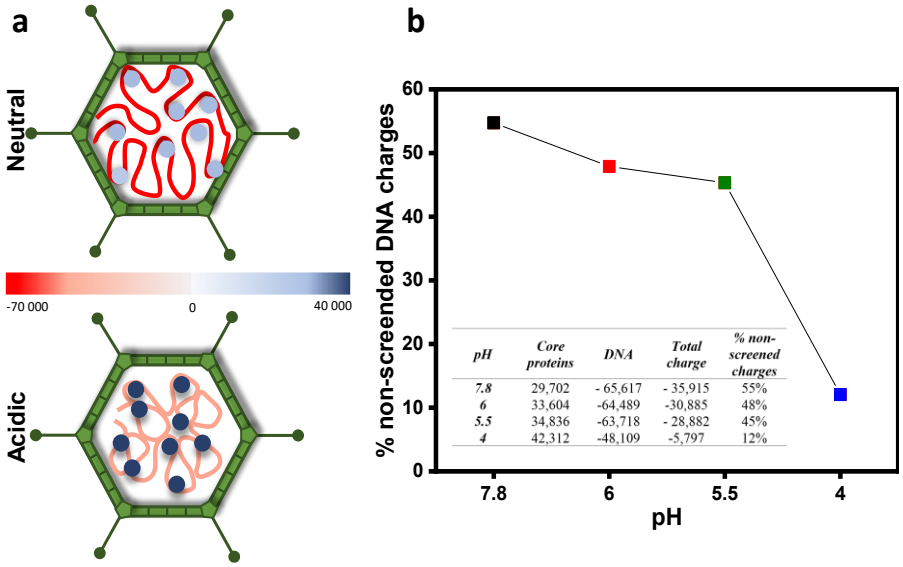

Figure 5.6. Effect on net charge of core proteins and DNA upon acidification. (a) Cartoon representing the condensation of the adenovirus core upon acidification. See main text for details. Core proteins are represented as blue spheres, indicating their positive charge, while DNA is represented as a red scribble, indicating its negative net charge. (b) Estimated percentage of non-screened negative DNA charge is lower for acidic pH4.

Two new cryo-electron microscopy studies of the structure of the enteric HAdV-F41 capsid, which is expected to resist the acidic conditions through the digestive tract[143,144], revealed that when comparing the structures of HAdV-F41 at neutral (7.4) and acidic (4) pH, no significant conformational changes were observed in the icosahedral capsid[143]. However, at neutral pH, HAdV-F41 is more thermostable than Ad5[144]. Since cryo-electron microscopy with icosahedral single particle averaging does not allow to observe the core structure, we propose that both, the higher thermostability of HAdV-F41 and the acidic milieu effect would have a role in the mechanical properties of the enteric adenovirus, yet to be explored.

Previous studies showed that both morphology and genome accessibility were affected by overnight acidification of Ad5-wt virions at 4 ^{o}C[41,94]. Here we do

not detect capsid disruption and genome accessibility by either TEM or extrinsic fluorescence after short term acidification (1 hour), although AFM analysis indicates that changes in the core have already started, causing particle softening and a moderate reduction of capsid strength (**Figure 5.1**). Only after the additional input of stress by heating do Ad5 capsids start to open (**Figure 5.4**), facilitating access of the intercalating dye to the genome (**Figure 5.3**). Stability modulation in viral particles is a complex problem where many factors play a role: ionic strength, divalent ions, pH, time, buffering capacity of the solution, age, and previous history of the specimen. In this regard, more studies with different conditions and techniques are needed to solve the discrepancies on the role of acidic pH on adenovirus capsid stability. Nevertheless, from the present work, we can conclude that acidification for time periods similar to those encountered while trafficking in the cell is not the sole responsible for Ad5 disassembly: other biological or chemical cues seem to be required to trigger uncoating. Our results also suggest that, in the endosome, acidification would contribute to keep the genome condensed, so that while the capsid starts to open and release internal components such as protein VI, the genome would stay protected inside the remaining shell to avoid misdelivery.

5.4 Conclusions

We have shown here that Ad5-wt virions subjected to acidic conditions for short time periods (~1 hour) become softer. This softening is related to changes in the core or in the interactions between core and capsid, but not to the capsid structure, as the mechanical properties of empty shells remain invariable upon acidification. Virion thermostability analyses by extrinsic fluorescence and electron microscopy indicate that genome accessibility

decreases at low pH, even when capsid openings are present, consistent with an increase in the condensation state of the core. Our work indicates that low pH *per se* is not enough to trigger adenovirus capsid disassembly, and conversely, suggests that acidification may play a role in keeping the Ad5 genome protected inside a defective shell to ensure its successful delivery at the nuclear pore. Finally, nanoindentation assays provide a new way to analyze subtle changes in viral particles in response to varying environmental conditions, which will contribute to our future understanding of the determinants of virus stability, assembly and disassembly.

CHAPTER 6

Adenovirus major core protein condenses DNA in clusters and bundles, modulating genome release and capsid internal pressure

CHAPTER 6: Adenovirus major core protein condenses DNA in clusters and bundles modulating genome realse and capsid internal pressure

6.1 Introduction

Regulation of dsDNA condensation is crucial for the management of genetic information. Major players in this regulation are specialized proteins which bend, wrap DNA, or form bridges between dsDNA strands [145]. In eukaryotes, wrapping by H2A, H2B, H3 and H4 histone octamers provides the first organization level of chromatin, with ~10 nm diameter nucleosomes forming a beads-on-string structure. Another histone, H1, is a bridger that clasps linker DNA at the nucleosome exit, stabilizing the structure[146]. In bacteria, nucleoid-associated proteins have mainly bending and bridging roles[147]. The highest known condensation of nucleic acids is the packing of viral genomes[148]. In tailed bacteriophages and herpesviruses, naked dsDNA is stored inside the capsid at very high volume fractions approximately in the form of a spool, with polyamines and cations helping to relieve the electrostatic repulsion between dsDNA strands[148,149]. In polyomaviruses, dsDNA is packed in complex with cell histones, forming a chromatin-like structure[150]. Adenoviruses and some of their structural relatives (asfarviruses, chloroviruses, mimiviruses, marseilliviruses) encode and package positively charged proteins with similarities to cell histones[151–154]. It has traditionally been thought that the main role of these proteins is to screen DNA-DNA electrostatic repulsion so that the viral genomes can be condensed to fit the limited space available inside the capsid. However, since these viruses have lower packing fractions than tailed phages (~0.3 *vs.* ~0.5), the actual need for genome condensation

agents is not that clear[155]. Furthermore, knowledge about the organization and properties of nucleoprotein complexes inside virus particles is scarce.

The best characterized system packing virus encoded proteins is Ad5. Previous studies have shown that cores released from Ad5 particles disrupted with pyridine contain polypeptides V, VII, and μ, and have a thick (15–30 nm) fibrous appearance when observed at the electron microscope after negative staining or metal shadowing[29]. After high ionic strength treatment of these cores, essentially only protein VII remains attached to the DNA, forming tangled structures with ~200 beads of 9.5 nm diameter located at highly variable distances (~10-130 nm)[29]. These observations suggested a chromatin-like organization for the adenovirus genome, with protein VII acting as a wrapper, while protein μ could have a bridging function to form the thicker fibers[32,36]. Currently, the only model for the core architecture *in situ* (in the crowded conditions within the intact virion) is based on cryo-electron tomography combined with molecular dynamics simulations, and proposes an organization of the DNA-protein complex as a fluid of soft repulsive particles[32].

As explained in Chapter 1 the Ad5 particle becomes fully infectious only after maturation, which involves cleavage of several capsid and core proteins by the viral protease[25]. Cleavage of proteins VII and μ results in decreased core condensation and increased internal pressure, priming the virion for sequential uncoating and facilitating genome release [61,62,94,137]. However, it has recently been shown that the hypothesized condensing role of protein VII, the most abundant core protein in Ad5 (60%~70% of the core protein mass), is not required for genome encapsidation. An Ad5 construct where the VII gene was excised from the genome using the Cre-lox recombination system has an assembly efficiency similar to the wild type virus (Ad5-wt), although the particles produced (Ad5-VII-) are not infectious due to a defect in entry[66]. The

actual cause for this entry defect is not clear. It has been hypothesized that, since the absence of VII represents a large loss of mass inside the virion, the entry defect may result from lack of internal pressurization, thereby hindering the start of the uncoating cascade. An alternative hypothesis is that the absence of VII would allow the genome to interact with positively charged proteins on the inner capsid surface, obstructing genome release[66]. Therefore, more work is required to ascertain the actual role of core protein VII in adenovirus assembly and disassembly. Theoretical models simulating the interactions of dsDNA and proteins within the capsid confinement predict that the presence of condensing proteins decreases internal capsid pressure, despite the decrease in free volume caused by their presence. These models also envisage that the natural tendency for the capsid contents to organize in layers near the confining capsid wall will increase when the strength of protein-DNA interactions is decreased[155]. Experimentally, AFM of single virus particles in liquid has proved the existence of internal pressure in tailed phages[136,156], where cryo-electron microscopy (cryo-EM) shows the naked genome ordered in concentric shells[149]. Tailed phages release this pressure to translocate their genome into the host[157]. No concentric shells are observed in Ad5 cryo-EM maps, and a change in internal pressure related to particle maturation has also been detected by AFM[36].

In this Chapter, we use AFM and cryo-EM to compare the mechanics and core organization of Ad5-wt and Ad5-VII- particles (**Figure 6.1a**), with the goal of understanding how protein VII influences the architecture and physical properties of adenovirus particles.

6.2 Results

6.2.1 Absence of protein VII stiffens the Ad5 intact particle

To investigate the role of protein VII in the physical properties of Ad5, we first analyzed the mechanics of Ad5-wt and Ad5-VII- intact particles by single nanoindentation assays (Chapter 1). AFM topography images that resolve individual protein capsomers revealed no substantial differences between Ad5-wt and Ad5-VII- particles (**Figure 6.1b, inset**). Height measurements of all particles included in this study (Ad5-wt, Ad5-VII- and empty shells) provided values around 86 nm (**Figure 6.1b**) consistent with the expected capsid diameter[61,75,76].

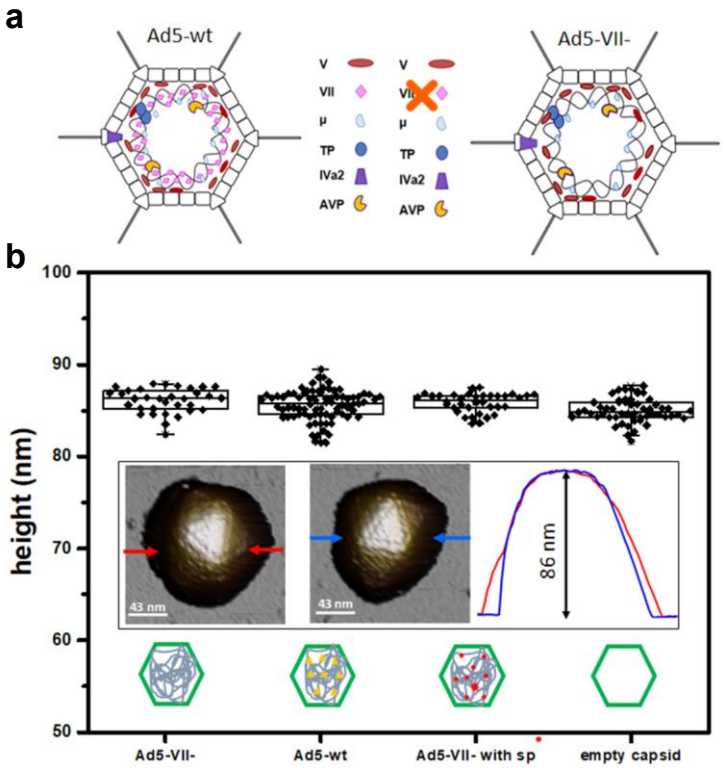

Figure 6.1. Ad5-wt and Ad5-VII– viral particles. (a) Schematic representation showing the core composition of the two specimens studied. Modified from Figure 1.20. (b) Height distribution of all the viral particles imaged with AFM. The inset shows AFM topography images of Ad5-wt (left), Ad5-VII– (center) particles, and the topographical profiles (right) corresponding to the line between the red (Ad5-wt) and blue (Ad5-VII-) arrows.

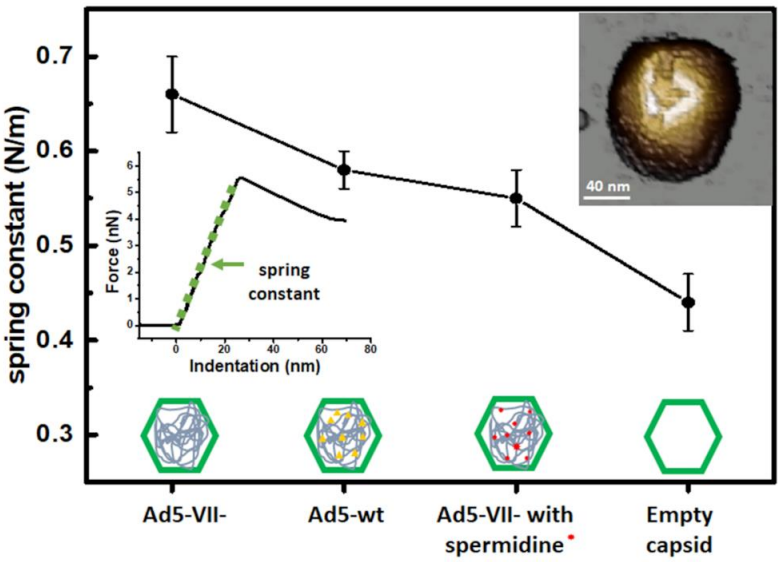

Figure 6.2. Mechanical properties of intact capsids. Stiffness (spring constants) measured for each specimen used in this work. Top right inset: Topography image of an adenovirus particle after performing a single indentation. Spring constant values are obtained from the force-indentation curve (FIC) (center left inset).

6.2.2 Absence of protein VII softens the Ad5 core

After the first deformation has fractured the capsid shell **(Figure 6.2, top right inset**), successive indentations probe directly the viral core[36]. **Figure 6.3a** presents the typical evolution of Ad5-wt and Ad5-VII- particles in a multiple indentation experiment, where the first indentation (FIC#0) on the intact shell (**Figure 6.3a#0**) opens a crack at the facet with a size similar to the apex of the AFM tip (~20 nm) (**Figure 6.3a#1**). As previously observed for Ad5 mature and immature particles[36], subsequent FICs present a non-linear Hertzian behaviour in contrast with the linear deformation found in intact particles (**Figure 6.3b and c**). Notice that tip reaches the substrate much earlier in Ad5-VII- (FIC#3 in **Figure 6.3c**) than in Ad5-wt (FIC#5, in **Figure 6.3b**). During the first indentation probing the core through the crack (**Figure 6.3a#1**), Ad5-wt cores are not indented beyond 40 nm at 3 nN, while Ad5-VII- cores undergo larger deformations, up to ~60 nm, at forces as low as 2 Nn (**Figure 6.3d**). This

difference indicates that it is easier for the AFM tip to penetrate/deform Ad5-VII- than Ad5-wt cores. That is, in the absence of protein VII the Ad5 core is softer and less condensed.

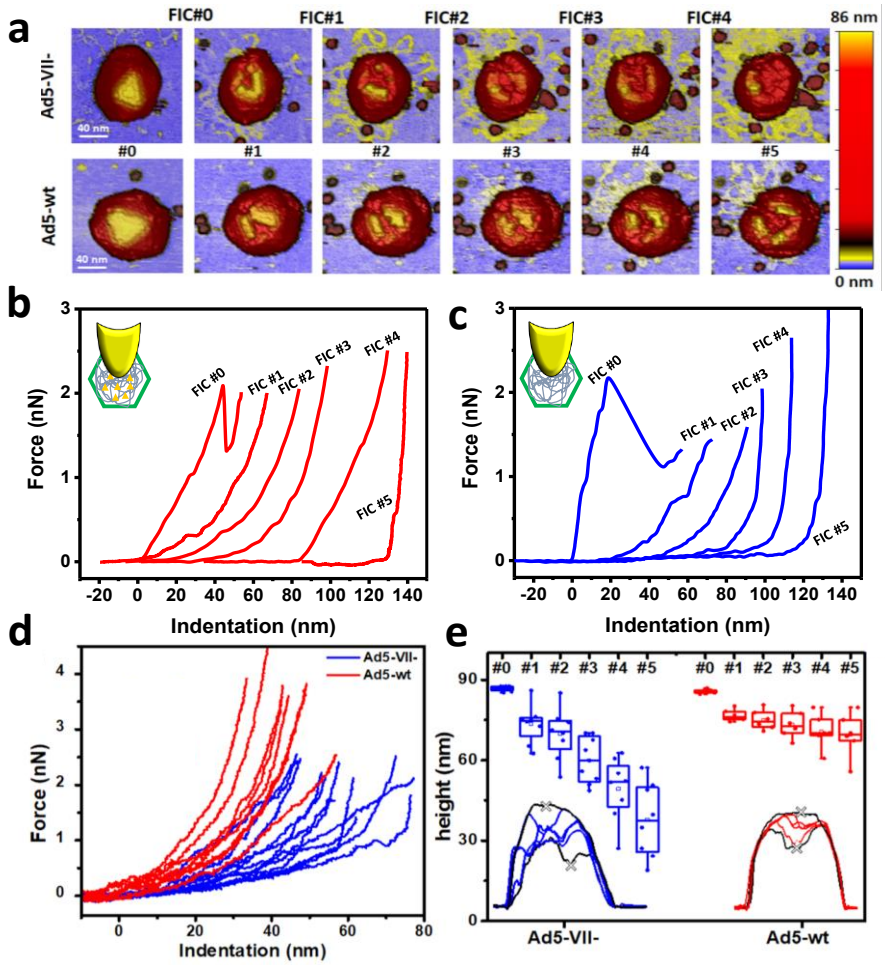

Figure 6.3. Mechanical properties of the core. (a) Images showing the evolution Ad5-wt and Ad5-VII– particles during multiple indentation assays. Images are colored by height, as indicated by the color bar at the right-hand side. (b) Indentation curves corresponding to the topographical evolution of the Ad5-wt and Ad5-VII- (c) Data have been horizontally shifted for the sake of clarity. (d) FIC curves corresponding to the first indentation performed on the core of 8 Ad5-wt (red) and 12 Ad5-VII– (blue) particles. (e) Evolution of the core (as indicated by the minimum height in the crater, grey crosses) for height Ad5-VII– and six Ad5-wt particles. Insets: Examples of topographical profiles obtained through the crater opened by the indentation.

6.2.3 Absence of protein VII increases de Ad5 internal pressure

It is generally accepted that viral genomes modulate the mechanics of virus particles by increasing their stiffness[73,82,158,159]. If the genome is assumed to be a solid material filling the cavity of the capsid, the deformation of the capsid-genome ensemble can be simplified by considering genome and capsid as individual springs associated in parallel. In this approximation, the spring constants of the Ad5 core in the presence or absence of protein VII would be $k_{wt}^{core} = k_{wt} - k_E = 0.14\ N/m$, and $k_{VII-}^{core} = k_{VII} - k_E = 0.22\ N/m$, predicting that the core in Ad5-wt would be softer than in Ad5-VII- when confined within the icosahedral shell. In contrast, one could expect that in the absence of VII, the core would be softer because it has less molecular mass. In fact, we found this tendency when directly probing the mechanics of the opened cores (**Figure 6.3d**). This behavior is reminiscent of our previous observation on the mechanics of Ad5 mature and immature particles, where we found that upon maturation the core becomes softer, but the capsid becomes stiffer due to an increase in internal pressure[36].

To investigate whether particle stiffening in Ad5-VII- was also related to changes in genome condensation and internal pressurization, we modified the factors governing the energetics of confined DNA (DNA bending and DNA-DNA electrostatic repulsion) by incubation with the condensing agent spermidine[36,136,160]. Spermidine is a trivalent polyamine that screens the phosphate negative charges, induces dsDNA condensation in solution and acts inside virus capsids[161,162]. We have previously shown that spermidine decreases the Ad5-wt elastic constant to $k_{wt}^{sp} = 0.49 \pm 0.02\ N/m$ (mean±SEM, N=36)[36]. We now find that upon incubation with spermidine, the Ad5-VII- particle spring constant decreased to $k_{VII-}^{sp} = 0.55 \pm 0.03 \frac{N}{m}$ (mean±SEM, N=36) which is similar to that of Ad5-wt (**Figure 6.2**). This result

indicates that genome condensation induced by spermidine softens the Ad5-VII- particle, and therefore informs about the role of protein VII in screening DNA negative charges.

Together, our data on core and particle stiffness show that the absence of protein VII loosens the core compaction, decreasing the rigidity of the virus core (**Figure 6.3d**) and increasing the pressure within intact particles (**Figure 6.2**). We can estimate the magnitude of the change in internal pressure using the continuous elasticity prediction for the spring constant of a pressurized thin spherical shell indented by a point force[163]:

$$k_1 = \frac{\pi}{2} k_0 \frac{(\tau^2-1)^{\frac{1}{2}}}{arctanh\left[(1-\tau^{-2})^{\frac{1}{2}}\right]} \quad (6.1)$$

Here $\tau = pR_1/k_0$ is a dimensionless parameter comparing the relative strength of pressure p against the elastic constant of the unpressurized shell k_0, and R_1 is the middle radius of the adenovirus capsid shell ($R_1 = 38$ nm). Taking $k_0 = k_{wt} = 0.58\ N/m$, and $k_1 = k_{VII-} = 0.66\ N/m$, and solving Eq. (6.1) for p, we obtain an estimate of 3.4 ± 0.7 MPa for the increase of pressure due to the lack of protein VII. This variation of pressure is like the generated during maturation (3 ± 1 MPa)[36], consistent with both effects resulting from changes in genome compaction by the core proteins. An increase in internal pressure is also consistent with the behavior predicted by theoretical models for weaker protein-DNA interaction regimes[32].

6.2.4 Absence of protein VII facilitates genome diffusion out of the Ad5 capsid

In multiple indentation experiments, elongated structures with a height compatible with dsDNA strands[164] (**Figure6.3a, yellow**) appeared on the

substrate surrounding Ad5-VII- particles after the first fracture of the shell (**Figure 6.3a#1, top**), but not in Ad5-wt (**Figure 6.3a, bottom**). Material consistent with unpacked DNA seemed to be more abundant in Ad5-VII- particles that in Ad5-wt for the equivalent indentation (**Figure 6.3a**). This qualitative observation suggests that it is easier to exit the disrupted shell for the VII-free genome than for the VII-bound one. An alternative possibility would be that the VII-free genome has a larger tendency to adsorb to the mica substrate than the VII-bound DNA. Measurements of the topographical profile across the crater produced by the successive indentations support the first possibility. Because topographical profiles include both the crater and its rims, we used the lowest height inside the crack as an indicator of the remaining core contents (**Figure 6.3e, insets**). Plotting the evolution of this parameter along 6 consecutive indentations for 8 Ad5-VII- and 6 Ad5-wt particles (**Figure 6.3e**) showed that, indeed, the core components are leaving faster the Ad5-VII- than the Ad5-wt cracked particles.

To further explore this aspect, we also compared how soon unpacked DNA was observed when particle disruption was induced by mechanical fatigue assays. Mechanical fatigue caused by repeated AFM imaging of the same particle at very low forces (~70 pN) promotes gradual disruption of the capsid, while allowing real time monitoring of the disassembly pathway from the initially intact to the final collapsed state (**Figure 6.4a**)[61]. Complete particle disruption by mechanical fatigue requires a different number of images for each individual particle. Thus, we quantify the time required to first observe dsDNA expelled from the capsid during a fatigue experiment as a percentage of the total particle life time. That is, 0% experiment time refers to the initial image when the particle is intact, and 100% to the final image when the particle is collapsed. These experiments indicated that dsDNA exits Ad5-VII-

particles earlier (30% experiment time) than Ad5-wt (70% experiment time) (**Figure 6.4b**).

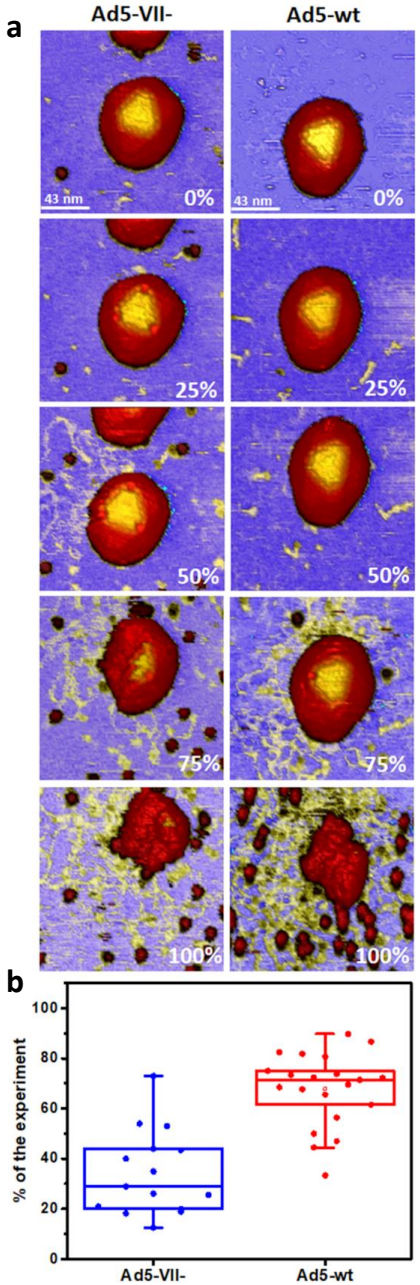

Figure 6.4. Genome exposure in mechanical fatigue experiments. (a) Topographical images of one Ad5-VII– (left) and one Ad5-wt (right) particle at different times in the experiment (indicated as percentage of the total experiment time). (b) Boxplot showing the percentage of experiment time when the genome was observed on the mica surface.

Because of the experimental design, at the end of mechanical fatigue or multiple indentation assays most of the analyzed particles have released their genome. However, in single indentation assays, only one image is taken after breakage of the capsid, and released DNA is not always observed, indicating that the genome can remain inside the cracked capsid shell. Unpacked DNA was observed in only 3% of Ad5-wt particles after a single indentation, in contrast to 42% of the Ad5-VII- particles (**Table 6.1**). All these results are compatible with a less condensed genome in Ad5-VII- that leaves the capsid faster than in Ad5-wt.

Type of Adenovirus	Single indentation assay	Multiple indentation assay	Mechanical fatigue assay
Ad5-VII-	42%(N=33)	88%(N=7)	100%(N=21)
Ad5-wt	3% (N=112)	71%(N=8)	100%(N=21)

Table 6.1. Exposure of core contents. Percentage of cases where structures compatible with released genome were observed for each kind of AFM.

6.2.5 Absence of protein VII reduces the thermal and mechanical stability of Ad5 viral particles

Using extrinsic fluorescence of the DNA intercalating agent YOYO-1 to characterize capsid disruption as a function of temperature in Ad5-wt and A5-VII- particles performed by Mercedes Hernando Perez and Marta Pérez Illana in[84]. The procedure was the same as made in Chapter 3. In both cases, the fluorescence emission of YOYO-1 increased with the temperature, as the genome became exposed to the solvent (**Figure 6.5**). The half-transition temperature ($T_{0.5}$) estimated for Ad5-wt was 47.35 ± 0.06 °C, in agreement with previous studies[41,94,127,137]. In contrast, for Ad5-VII- the maximum rate of

DNA exposure happened at 44.45 ± 0.10 °C. This result indicates that Ad5-VII- particles are thermally less stable than Ad5-wt.

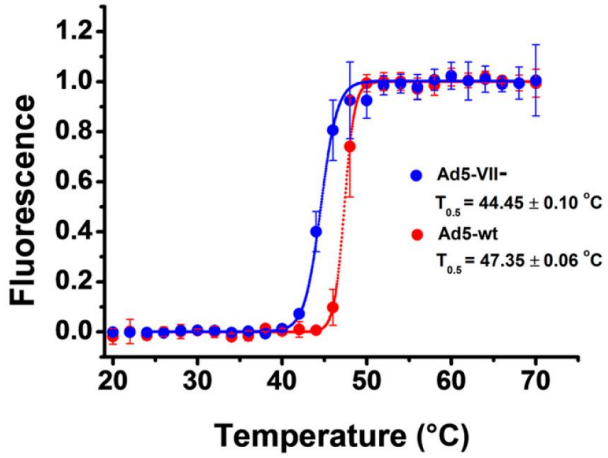

Figure 6.5. Thermal stability of adenovirus particles with or without protein VII. Extrinsic fluorescence measurements showing DNA exposure to solvent upon temperature increase for Ad5-VII- (blue) and Ad5-wt (red). Average values and error bars corresponding to the SD of four (Ad5-VII-) and six (Ad5-wt) experiments are plotted. Dotted lines correspond to the fit according to a Boltzmann sigmoid function.

To analyze the mechanical stability of the Ad5-VII- particles, we used mechanical fatigue induced by atomic force microscopy (AFM). This method involves repeated imaging of the same virus particle using very low forces (~100 pN), far below the breaking force of the capsid. In this way, we simultaneously induce and monitor the gradual disassembly of single virus particles[61]. Topography images taken at the beginning of the experiment showed no differences between Ad5-wt and Ad5-VII- particles (**Figure 6.6a#1**). As the experiment proceeded, mechanical fatigue caused the sequential removal of pentons, followed by complete particle collapse. In the example shown in **Figure 6.6a**, we show that for Ad5-VII- the first penton fell off the capsid at image #3, and the third penton at image #9. The capsid collapsed after #18 images. In contrast, in the Ad5-wt the first penton falls off at image #43, and the capsid collapsed at image #59 (**Figure 6.6a**). We quantified the

rate of penton loss for nine Ad5-VII- and seven Ad5-wt viral particles. In **Figure 6.6b**, pentons are considered independent identities, and the normalized penton population for all studied particles is plotted along the number of images taken. At the beginning of the experiment, all observable pentons are present for the 16 studied particles (penton population = 1). As the experiment proceeds, pentons fall off and the penton population decreases until there are no more observable pentons. The penton release distribution follows an exponential decay for both types of particles. The mean lifetime of a penton is 12 images for Ad5-VII-, and 26 images for Ad5-wt, indicating that penton loss occurs faster in Ad5-VII- particles (**Table 6.2**).

Type of Adenovirus	Penton release constant: λ (images^{-1})	Mean penton lifetime: 1/λ (images)	N
Ad5-VII-	0.08	12	9
Ad5-wt	0.04	26	7

Table 6.2. Exponential decay distribution for penton release. The penton distribution data follow an exponential decay function $N(t) = N_0 e^{-\lambda t}$, where t is the number of images taken, and parameters such as the penton release rate constant (λ) and mean life-time of a penton (1/λ) can be determined. The mean penton lifetime is given as number of images; the penton release rate constant represents the probability to release one penton in one image.

This higher propensity to release pentons agrees with our observation showing that lack of core protein VII increases the particle internal pressure. To further analyze the disassembly dynamics, we quantified the variation in particle volume during the mechanical fatigue assays (**Figure 6.6c**). At the beginning of the experiment, the particle volume remained constant for all particles analyzed. After losing the three pentons on the upper facet, the volume drops at a similar rate for both kinds of particles (13% volume loss per image for Ad5-VII-, 14% volume loss per image for Ad5-wt).

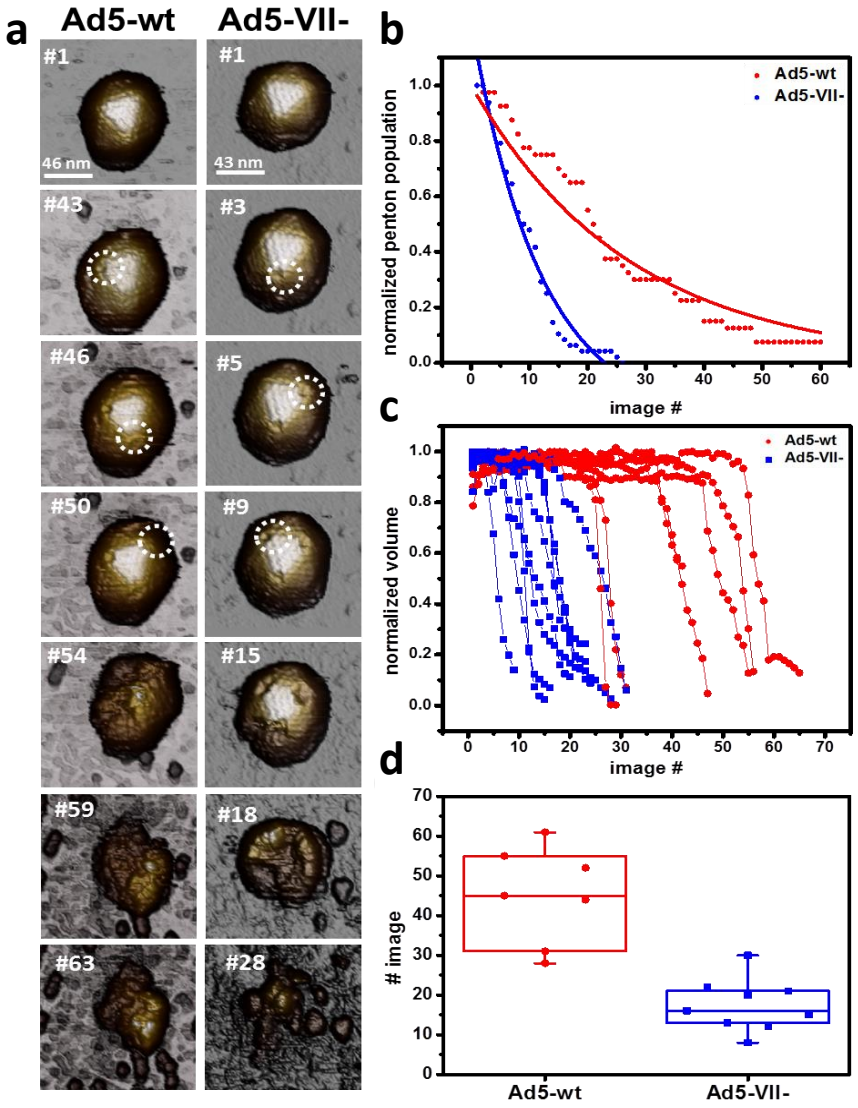

Figure 6.6. Mechanical stability of adenovirus particles with or without protein VII. (a) Representative AFM images along fatigue experiments for Ad5-VIIand Ad5-wt particles adsorbed on mica. Release of the first, second, and third pentons from the top facet are indicated with white circles. (b) Analysis of penton release for 9 Ad5-VII- and 7 Ad5-wt viral particles. At the beginning of the experiment, all visible pentons in the images are occupied (penton population = 1). The penton population decreases along the experiment. (c) Comparison of the evolution of Ad5-VII- and Ad5-wt particle volume during the fatigue experiment. (d) The image number at which each particle has undergone a 50% volume decrease is plotted for all particles analyzed

A clear difference, however, was the time elapsed until the particle volume starts to decrease: Ad5-wt particles lost 50% of their volume after being imaged ~50 times, while for Ad5-VII- the same decrease in volume occurred after only 15 images (**Figure 6.6d**). That is, Ad5-VII- particles start losing volume earlier than Ad5-wt particles, consistent with the penton release tendency. Therefore, penton resilience determines the stability of the virus particle under mechanical fatigue. In conclusion, our results so far indicate that Ad5-VII- particles are less stable than Ad5-wt under both thermal and mechanical stress.

6.2.6 Protein VII changes de organization of the Ad5 genome in virio and exvirio

6.2.6.1 In virio

To investigate how the absence of protein VII reflects on the Ad5 core organization inside the intact particle, we compared cryo-EM icosahedrally averaged maps for the Ad5-wt and Ad5-VII- particles (**Figure 6.7**). Cryo-EM experiments were performed by Dr. Mercedes Hernando-Pérez.

Although the Ad5 core is not icosahedrally ordered, interesting differences could be observed. In the Ad5-VII- particle, the core density was weaker and more heterogeneous than in Ad5-wt, as can be appreciated from visual inspection of the map cross-sections (**Figure 6.7a**) and comparison of gray level statistics. When gray levels in the region corresponding to the hexon shell were normalized to the same value range in both maps, in the Ad5-VII- core the average gray level was lower (**Figure 6.7c**). This observation indicates that, when protein VII (which accounts for 26~30% of the core mass) is not present, the particle contents are more loosely distributed within the capsid cavity. This looser conformation is consistent with the changes in core condensation detected with AFM experiments.

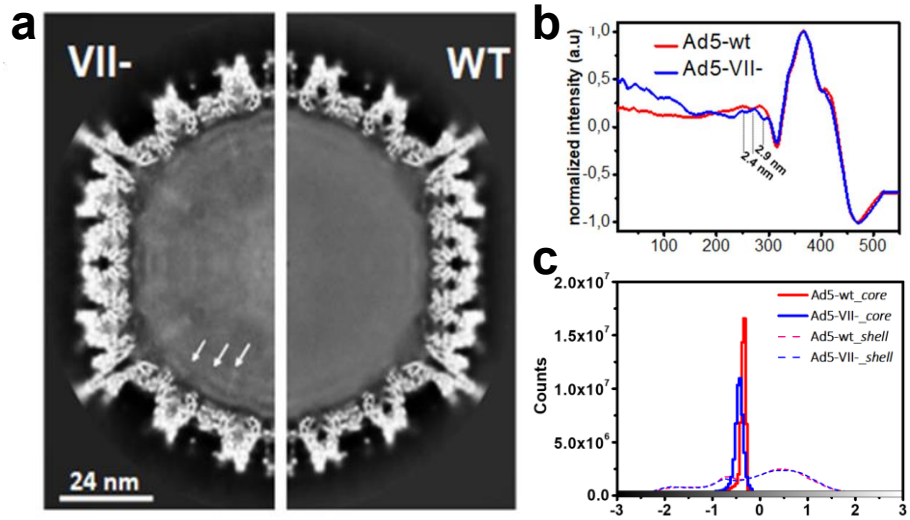

Figure 6.7. Organization of the core inside the virus particles. (a) Central section of 3D cryo-EM maps of Ad5-VII– and Ad5-wt. Higher density is shown in white. White arrows highlight the three concentric shells in Ad5-VII. (b) Radial average profiles of the Ad5-VII– and Ad5-wt maps. (c) Gray level histograms for the Ad5-wt and Ad5-VII- capsid shell and core regions in the cryo-EM maps.

In the Ad5-VII- map, three weak concentric shells appear near the inner wall of the capsid that are not present in Ad5-wt (**Figure 6.7a**). The distance between shells (2.4 and 2.9 nm, **Figure 6.7b**) is similar to the distances observed between the concentric layers of naked dsDNA in tailed bacteriophages[165,166]. The presence of these weak layers points to an organization of the Ad5-VII- genome somewhat similar to that found in viruses not packaging proteins. This organization agrees with theoretical model predicting that weakening the interactions between condensing proteins and DNA would result in an increased tendency to form layers beneath the confining capsid surface[155].

6.2.6.2 Ex virio

More information on the conformation of the Ad5 core nucleoprotein complex can be derived from the observation of unpacked contents at the end

of in situ AFM mechanical fatigue assays (**Figure 6.8**). Fibered shapes (yellow) and homogeneously dispersed formations (blobs, red) surround the major debris located at the center of the images (**Figure 6.8**).

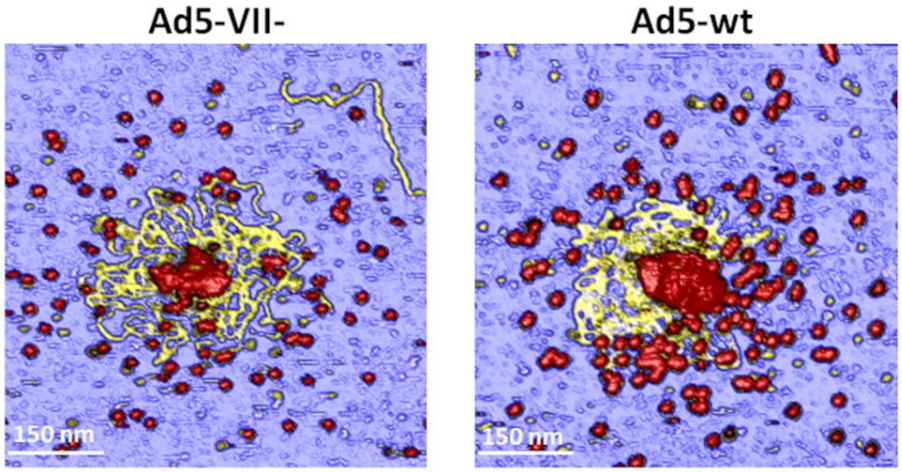

Figure 6.8. Final mechanical fatigue images. Example images showing the final stages of Ad5-VII– (left) and Ad5-wt (right) particles after mechanical fatigue disruption.

The characterization of structures with a size similar to the radius of the AFM tip apex is strongly influenced by dilation artefacts in the lateral dimension[56]. However, vertical measurements are not affected by these dilation effects. Therefore, we used the height as a size indicator of these objects to find that the vertical thickness of the fibered shapes is compatible with the dsDNA diameter as measured by AFM[164]. A close-up view of these areas reveals that some structures can be resolved as individual filaments (**Figure 6.9a**). However, topographical profiles show that in Ad5-wt the filament diameter is larger than in Ad5-VII- (**Figure 6.9c**, inset). Therefore, to analyse the height of the genome in the zoom in images we observed that DNA is a long molecule that extends over a large area and measuring heights with single profiles only provides local information. Therefore, we devised a procedure to estimate the diameter of DNA in a more objective way. First, we zoom into a region of the image where only substrate and genome are present. Then, we plot the

histogram of height values in the selected region. In this histogram, two peaks are observed, one corresponding to smaller heights (substrate), and the other to larger heights (objects lying on the substrate). The difference between the smaller and the larger heights indicated by Gaussian peaks fitted to the data gives the average value of the fiber height for each region (**Figure 6.9b**). A statistical analysis (**Figure 6.9c**) confirmed this aspect, with average filament heights of ~2 nm for Ad5-wt and 1.5 nm for Ad5-VII- (**Figure 6.9c**). Also, filament heights presented a broader dispersion (~1 nm to ~3nm) in Ad5-wt. We interpret the larger thickness in Ad5-wt filaments as being caused by the association of different regions in the dsDNA genome. The thickness dispersion indicates that this association would include at most three dsDNA chains. These results suggest that the presence of protein VII promotes condensation of dsDNA by formation of bundles, perhaps *via* bridging.

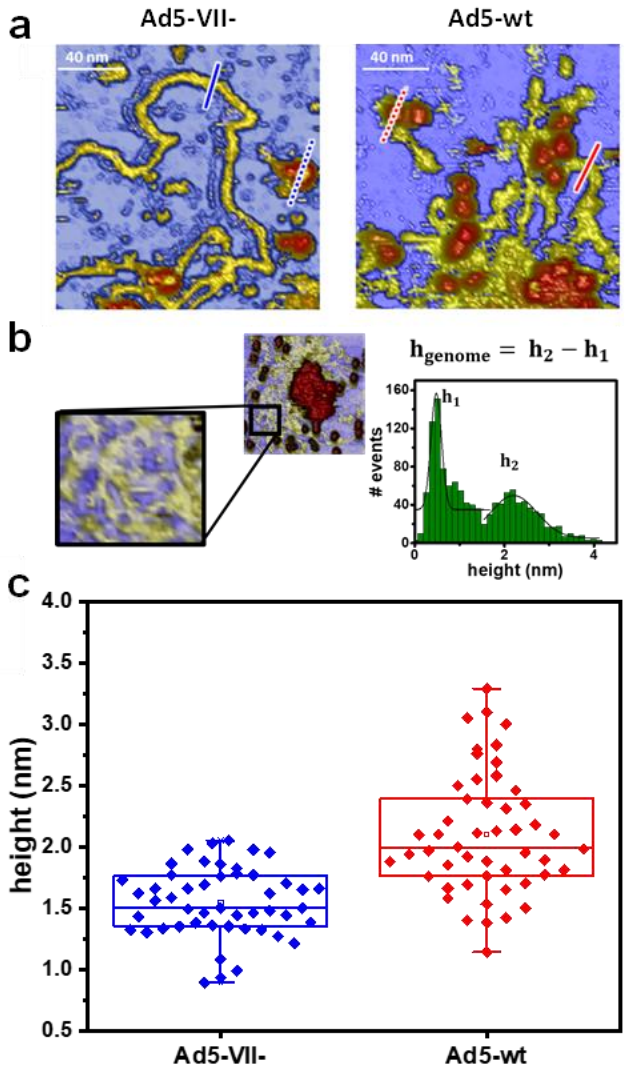

Figure 6.9. Analysis of unpacked core contents (yellow fibers). (a) Close-up details of the released contents from Figure 6.8. (b) Height analysis for fiber-like expelled objects (genome). (c) Statistics of fibered material heights calculated as explained in b. The inset shows two example topographical profiles across the fibered material (blue and red solid lines in a).

Topographical profiles (**Figure 6.10c, inset**) also pointed out to different heights for the blobs in the Ad5-wt and Ad5-VII- images (**Figure 6.9a**). These particles likely correspond to coat and core proteins coming from the collapsed virus particles after fatigue. We carried out a statistical analysis of

the blob heights for 11 Ad5-wt and 10 Ad5-VII- disrupted particles analysed in ~10 different experimental sessions. The last mechanical fatigue global image is flooded at ~6 nm (http://www.wsxm.es/) to isolate the particles for the count as much as possible. (**Figure 6.10a**) This flooding parameter was selected in order to avoid the genome contribution (2 to 4 nm). A histogram of normalized blob heights was calculated for each virus particle (**Figure 6.10b**). Then, histograms for all Ad5-wt or all Ad5-VII- particles were averaged (**Figure 6.10c**). These charts reveal a major population of objects between 12 and 13 nm for both Ad5-wt and Ad5-VII-, compatible with the size of adenovirus capsomers [19,73]. An additional population at ~10 nm was observed in Ad5-wt but not in Ad5-VII-. This size is close to the 9 nm beads previously observed in metal shadowed cores after high ionic strength treatments that removed most core proteins except VII[29]. We classified both the small and large blobs in Ad5-wt particles in two categories, depending on whether they were in contact with the DNA or isolated on the mica surface (**Figure 6.8** and **6.10a**). Objects found isolated on the substrate corresponded mainly to the larger blobs (**Figure 6.10d, empty red**), while most of the smaller blobs appeared associated with filaments (**Figure 6.10d, solid red**), pointing to their interaction with dsDNA. That is, Ad5-wt collapsed particles release objects smaller than capsomers and located preferentially in association with DNA strands, that do not appear when Ad5-VII- particles are disrupted. Therefore, these objects must correspond to the presence of core protein VII. A similar histogram was performed in Ad5-VII- particles to corroborate that the height of the objects is equal independently of the position (**Figure 6.10e**).

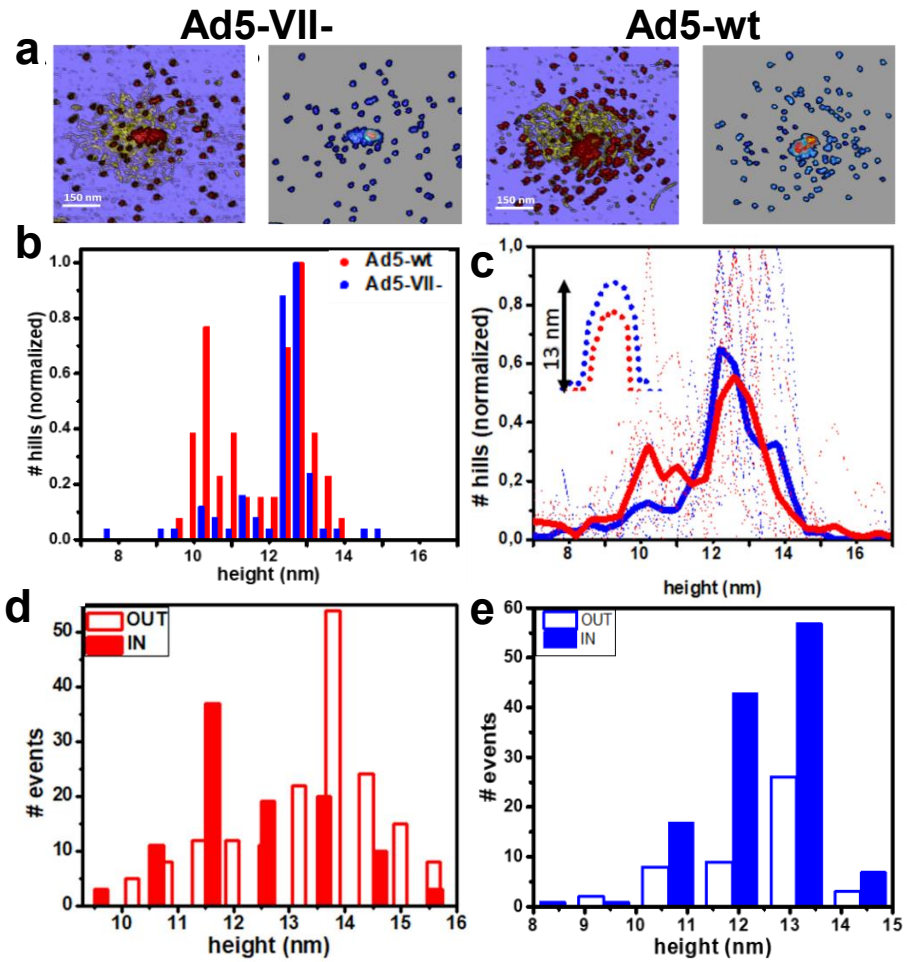

Figure 6.10. Analysis of unpacked core contents (red blobs). (a) Example of the last global image in a mechanical fatigue assay. and flooded image of Ad5-VII- and Ad5-wt viral particle. (b) Blob heights extracted from the flooded image. Data of each particle for histogram representation are normalized to the maximum number of blobs happening at a certain interval of heights. (c) Histograms of the blob height distribution were obtained for 11 Ad5-wt (red) and 9 Ad5-VII– (blue) disrupted particles. Solid lines present the average of the dotted lines coming from individual particles. Inset: example topographical profiles across the blobs (dashed lines in B). (d) Histograms showing the height of the Ad5-wt blobs in contact (red) and not in contact (white) with DNA. (e) Histogram showing the size of the blobs expelled from Ad5-VII- particles in contact (blue) and not in contact (white) with DNA.

We can estimate the number of protein VII monomers in a small blob by comparison with the known mass of the hexon trimer forming the larger blobs. The molecular mass of a hexon trimer is 324 kDa, while the molecular mass of

mature protein VII is 19 kDa[25]. If we consider the large and small blobs as spheres with radii r_L ~6.3 and r_S~ 5 nm, respectively, the number of protein VII monomers per small blob would be $\frac{324}{19} \times \left[\frac{r_S}{r_L}\right]^3$ ~9. However, several considerations from the previous literature would be reluctant with the formation of these VII nonamers. First, since in one Ad5 virion there are 252 capsomers (240 hexon trimers + 12 pentons) and between 500 and 800 copies of protein VII,[27,28] a fully disrupted particle should present at most (800/9)/(252+(800/9)) ~26% of small objects. In our Ad5-wt images we observe ~38% of small objects, above the highest expected value if the protein formed nonamers. This excess could be understood if a considerable number of capsomers remained bound forming capsid debris located at the center of the AFM images (**Figure 6.8** and **Figure 6.10a**). Second, assuming that the small blobs contain 9 protein VII monomers, the estimated number of VII oligomers per viral particle (55-88) would be 2-4 times smaller than the number of beads previously observed for pyridine cores[31]. Third, a high order multimer of VII would also be incompatible with previous cross-linking results on disrupted virions and extracted cores, where only dimers were detected[167].

It is also possible that we are overestimating the amount of VII monomers per blob, if part of the mass considered corresponds not only to protein VII, but also to associated DNA. In fact, an interesting model can be proposed if we consider each blob as a unit formed by one or several molecules of protein VII, wrapped or otherwise asymmetrically associated with a certain region of DNA. Protein VII appears to interact with DNA to a large extent electrostatically, as indicated by the experiments with spermidine (**Figure 6.2**). In each of these VII-DNA units, the repulsive monopole electrostatic interactions would be effectively screened. Remaining higher order (multipole) interactions in the protein-DNA complex combined with short range (steric) repulsion may act as

effective sticky “patches” and induce the formation of particularly stable clusters with conformations determined by the structural and interaction anisotropy of the individual complexes, such as cubes (8 effective particles), octahedra (6 effective particles) or tetrahedra (4 effective particles)[168]. Depending on the interaction details, clusters may be more or less polydisperse, but it is worth noting that we observe a reasonably sharp peak in the AFM small blob size distribution (**Figure 6.10c**) which suggests a largely monodisperse cluster population. The fact that clusters do not form in Ad5-VII- cores suggests that protein VII is essential for their formation. The clustering model should be taken with some care, as it does not take explicitly into account the role of other core proteins and the fact that the Ad5 DNA is a single topological entity. If this model is correct, it would mean that the interaction between the protein-DNA complexes is more complicated than previously proposed in the full confinement (isotropic, weakly repulsive potential) [32].

6.3 Discussion

In this work we have access to a mutant lacking protein VII that offers an inestimable opportunity to investigate the role of this protein in the physical properties and core organization of the adenovirus particle by using atomic force and cryo-electron microscopies. We find that in the absence of VII, the particle stiffness increases. Two possible reasons for stiffening in Ad5 have been described. First, upon maturation cleavage of proteins VII and μ, the screening of DNA-DNA electrostatic repulsion by the core proteins is decreased, resulting in an increase of internal pressure and a stiffer particle[36]. Second, a point mutation in capsid protein VI that partially hinders its maturation cleavage also produced an increase in particle stiffness[169]. Since it

has been observed that the Ad5-VII- particles also present deficient proteolytic cleavage of protein VI[66]. To unveil the cause of this stiffening we access to the core mechanics finding that the absence of protein VII results in a softer and less condensed core. As previous described[36,136], this behaviour is a signature of higher internal pressure due to the DNA-DNA repulsive interactions which are screened by this protein in the control virus (Ad5-wt). Moreover, lack of protein VII induces a reorganization of the adenovirus genome in a ring-like structure and accelerates genome diffusion out of semi-disrupted particles because of the higher internal pressure.

This last fact in the absence of protein VII show that the defect in virus entry previously observed is not due to a deficient internal pressure or a high mechanical or thermal stability, rather the opposite.

Taking a look of the AFM images of the Ad5 core as it is progressively extracted from the capsid in a physiological environment do not show beads-on-a-string structures as previously shown in released cores dried on a surface for EM analysis where most proteins but VII had been chemically removed[29]. Rather, we find beads that can be attributed to clusters of protein VII-DNA complexes, adjacent to bundles consisting of a few dsDNA chains that suggest condensing by a bridging interaction (**Figure 6.8** and **Figure 6.10a**, right). Since the bridging seems to happen away from the actual position of the VII-DNA cluster, we propose that protein VII promotes bundling of DNA by facilitating the bridging action of the small core protein μ[36]. The 9 kDa precursor form of protein μ is cleaved in three 20-30 residue long fragments by the Ad5 protease[25], which would correspond to objects of radii ~1.3 nm as estimated in a similar way as for the red blobs above. We suggest that protein VII could assist the action of μ by bending the DNA molecule so that two branches of it become closer, within the bridging range of μ (**Figure 6.11**).

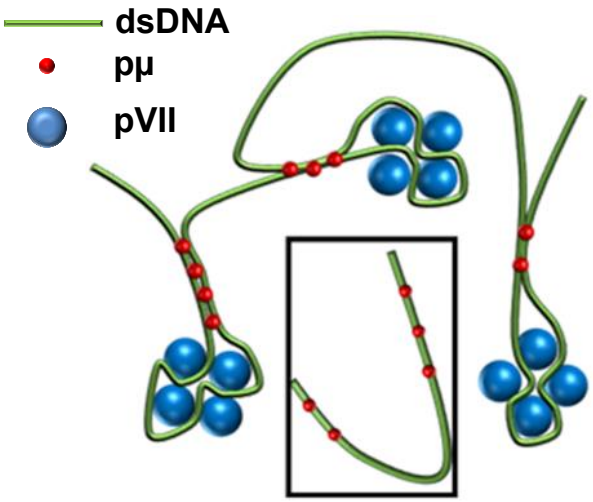

Figure 6.11. Model proposed of the condensing role of protein VII. Cartoon showing a hypothetical model for the condensing role of protein VII. Green, DNA; blue, protein VII; red, protein μ. The inset illustrates the situation where the bridging action of μ is hindered by the absence of clusters formed by the VII-DNA complexes.

In any case, our data show objects compatible with multimers of protein VII bound to DNA, and bundles of dsDNA, are present in Ad5-wt unpacked cores, but not in Ad5-VII-.

6.4 Conclusions

We have used AFM and cryo-EM to explore how the absence of core protein VII influences the physical properties and core organization of human adenovirus particles. In the absence of protein VII, the Ad5 particle becomes stiffer and the core becomes softer. Incubation with spermidine softens the Ad5-VII- particle. Thus, our results support the role of protein VII in screening the DNA negative charges, thereby modulating capsid pressure. A decrease in the core condensation when VII is not present accelerates genome diffusion through fractures of the capsid shell. Therefore, the defect in virus entry observed in Ad5-VII- particles[66] is not due to either lack of internal pressure or

trapping of the genome inside the particle. Our AFM imaging of the adenovirus core mechanically unpacked in real time from individual capsids indicates that protein VII induces dsDNA condensation by promoting a mixture of clustering and bridging mechanisms (**Figure 6.11).**

Although the condensing action of protein VII is not needed for DNA packaging during adenovirus assembly, it might play a role in other steps of the infectious cycle. Adenovirus uncoating in the cell occurs in a stepwise manner, starting at the plasma membrane and continuing at the early endosome, where vertex capsomers (pentons) and peripheral core components are released[69,170]. Afterwards the partially disrupted particle escapes the endosome and travels to the nuclear pore by traveling along the microtubular network[113]. We hypothesize that the condensation induced by protein VII may be required to keep the genome protected inside the semi-disrupted capsid while traveling to the nuclear pore.

CHAPTER 7

An unexpected role of core protein V in Human Adenovirus revealed by AFM

CHAPTER 7: An unexpected role of core protein V in human adenovirus revealed by AFM

7.1 Introduction

In the previous Chapter we have studied the role of protein VII in Ad5. We suggested that protein VII exists in VII-DNA complexes, adjacent to bundles of dsDNA chains condensed by a bridging action caused by protein μ[95]. Moreover, cryo-EM studies showed the same binding pocket inside the cavity of hexons for protein VII and VI[84] suggesting that apart from the condensing function of pVII, it plays an important role in maturation of Ad5 and in keeping the genome protected inside the capsid during uncoating[95,171].

The remaining core proteins should play an important role in Ad5 uncoating and stability. In this Chapter we will study core protein V.

Core protein V is specific for Mastadenoviruses[172]. Previous cross-linking studies identify the interaction among the core proteins, indicating the formation of dimers of pV and pVII. Moreover, this study suggests that pV exists in a complex with pVII and pμ but never found interaction VII-μ without pV, indicating that pVII and pμ are in close contact with pV[167]. Other studies show that recombinant protein V exists in dimer-monomer equilibrium and a direct association between protein V and protein VI suggesting that protein V bridges the DNA core with the capsid by interacting with protein VI[34]. This function of pV to bridge the core and the capsid through the interaction with protein VI has been already reported in previous works[167,173,174].

In a recent study, a mutant deleted of the protein V coding region (Ad5-ΔV) was produced to determine how protein V affects the viral uncoating in the host cell[175]. Therefore, protein V is dispensable for virion assembly. In this

study, they found that these virions were less thermostable [35] and less infectious due to a defect in genome delivery into the nucleus. In this vein, it is thought that the defect in the infectivity, due to an unscheduled release of Ad5-ΔV genome, comes from an intrinsic particle instability in the cytosol. In this sense, it is interesting to study the mechanical stability of these viral particles to deeply understand the protein V role from a multiple points of view.

Here, we use AFM and to compare the mechanics and core condensation state of Ad5-wt and Ad5- ΔV particles to understand how protein V influences the mechanical stability and physical properties of adenovirus particles.

7.2 Results

7.2.1 Absence of protein V reduces the viral capsid stiffness

We first investigated the mechanical properties of Ad5 in the absence of protein V to compare with Ad5-wt. Topographical images before the experiment revealed defectless intact virus particles (**Figure 7.1a, left and Figure 7.3a**) with a height ~85 nm compatible with the nominal diameter of these virus[18]. The force versus indentation curves (FICs) obtained in this study provided us information about the rigidity and the brittleness of the viral particles[176]. The spring constant was measured from the slope of the curve obtaining a value for Ad5-wt: $k_{Ad5-wt} = 0.58 \pm 0.01\ N/m$ (mean±SEM; N=53), value reported in previous Chapters. For Ad5-ΔV, the elastic constant was lower $k_{Ad5-\Delta V} = 0.45 \pm 0.02\ N/m$ (mean±SEM; N=30) (**Figure 7.1, left axes, black dots**) similar to the spring constant of the Ad5 empty capsid previously reported in Chapter 6. This result means that the absence of protein

V softens the Ad5 capsid, and could be ascribed with its bridging function between the capsid and the genome[167].

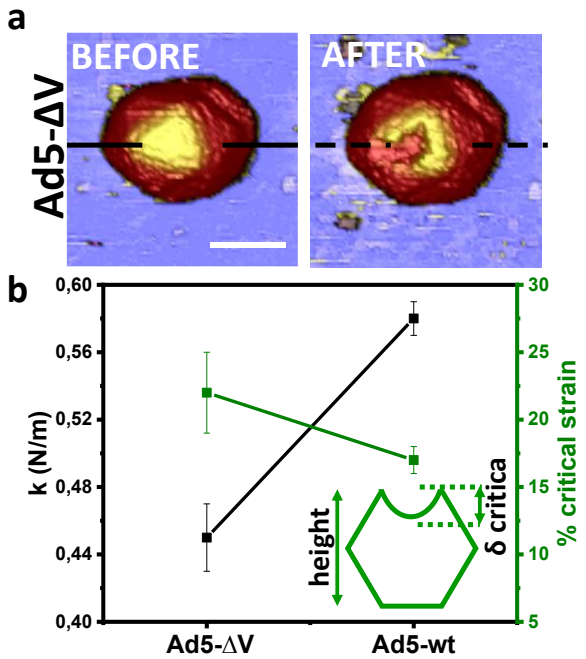

Figure 7.1. Mechanical properties of Ad5-ΔV and Ad5-wt viral particles. (a) Representative AFM images of Ad5-ΔV before and after an indentation experiment. (b) Stiffness (spring constants, black, left axes) and brittleness study (critical indentation, green, right axes) of the two specimens. This last value was obtained from the analysis showed in the inset.

Then, we estimated the ratio between the critical deformation ($\delta_{critical}$) and the viral particle height (**Figure 7.1, inset**), obtaining the critical strain that provides differences in brittleness[177]. The % critical strain obtained for Ad5-wt and Ad5-ΔV was 17±1% and 22±2% respectively (**Figure 7.1b, right axes, green dots**). The data show that the lack of protein V makes the viral particle more deformable confirming the fact that protein V acts as a mechanical reinforcement protein to the capsid.

7.2.2 Absence of protein V reduces the mechanical stability of Ad5

By performing mechanical fatigue assays, we can analyse the mechanical stability of the Ad5-ΔV viral particles against low force strokes. **Figure 7.2a** shows two examples of the of Ad5-ΔV (top) and Ad5-wt (bottom) particles disassembly . At the beginning of the experiment both particles showed similar topography and similar disassembly patterns. First, the three visible pentons located at the corners of the triangular facet are lost, then the gradual rupture of the capsid occurs until the particle crumples and collapses.

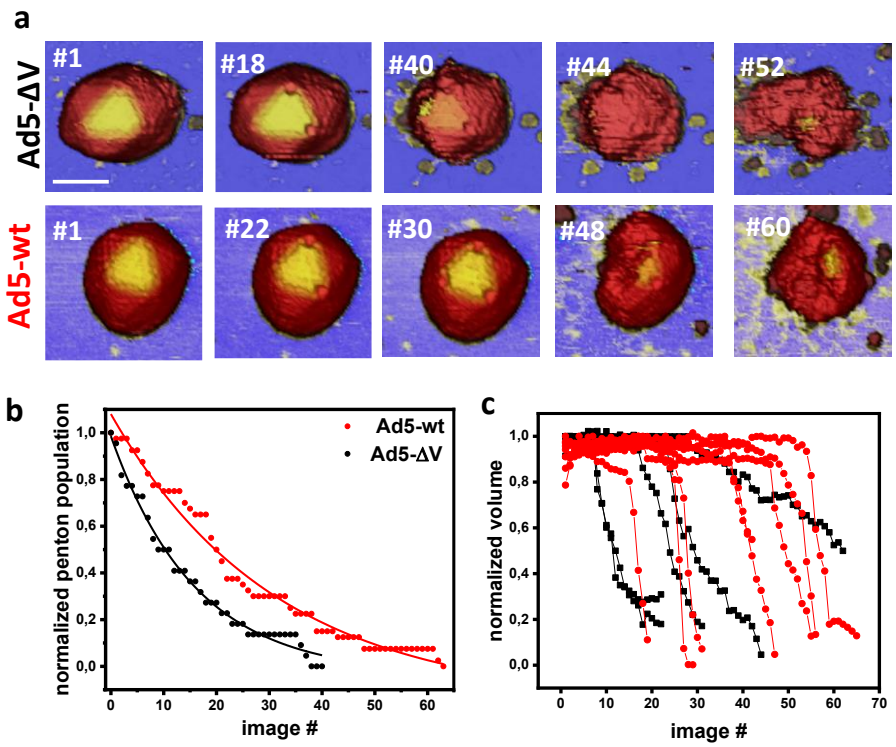

Figure 7.2. Mechanical stability by fatigue assays of Ad5-ΔV and Ad5-wt. (a) Examples of AFM images along Ad5-ΔV and Ad5-wt fatigue experiment. (b) Analysis of penton release distribution for all the viral particles studied. The penton release distribution follows an exponential decay. (c) Normalized volume evolution along a fatigue experiment for the two varieties studied.

Figure 7.2a shows that two pentons have been lost after #18 images for Ad5-ΔV until the final disassembly happens after #52 images. In the Ad5-wt example (**Figure 7.2a, bottom**), two pentons came out after #22 images and

the complete disassembly took place at frame #60. We quantitatively analyzed the mechanical fatigue assays of 8 Ad5-ΔV and 7 Ad5-wt particles. **Figure 7.2b** shows the rate of penton loss for all the particles studied, by plotting the normalized penton population along time (# of frames). While at the beginning of the experiments all the pentons are present, but they are released along time showing a population decrease until the three pentons are gone. The penton loss distribution follows an exponential decay, being able then to estimate the mean lifetime of a penton which is 16±1 images/penton for Ad5-ΔV and 26±2 images/penton for Ad5-wt. With this analysis, we observed that there is a higher propensity to release pentons in the absence of protein V.

Furthermore, we also quantified the volume loss of the viral particle during the fatigue experiments (**Figure 7.2c**). . Both Ad5-ΔV (black) and Ad5-ΔV (red) particles keep their volume constant during the first part of the mechanically induced disassembly process when only pentons are gone. After the three pentons are released, the virus particle volume decreases sharply in a few frames. In this regime, our data show that in the case of Ad5-ΔV the volume decreases slower (4±2% volume loss/image) than in the case of Ad5-wt (8±6% volume loss/image) by fitting the slope decrease of the volume.

7.2.3 Absence of protein V increases the core condensation state of Ad5

AFM images taken before and after a FIC (**Figure 7.1a**) demonstrated the rupture of the shell, which caused a crack whose topography demonstrated a loos of height. By measuring the height at the lowest part of the crack, we can estimate the remaining core inside the disrupted capsid after the particle is broken. **Figure 7.3a** shows box plots of a statistical analysis of the viral height before and after viruses are broken. The results present that height reduction

is lightly larger in Ad5-wt (red, N=48) than in Ad5-ΔV (black, N=25) particles. Although one-way ANOVA test at the 0.05 level revealed that populations means are not significantly different it seems that it is more difficult for the AFM tip to penetrate in Ad5-ΔV than in Ad5-wt, in agreement with **Figure 7.2c**. Therefore, it appears that the absence of protein V tends to retain core inside the broken particles.

To go further in the analysis of the disassembly, we have examined the variation in virus height along the fatigue assays[61]. To do so, we have measured the height evolution of a point with an influence radius of 2 nm located at the centre of the three-fold symmetry for 7 Ad5-wt and 6 Ad5-Δ5. In **Figure 7.3b**, we have plotted the normalized height evolution along time for single Ad5-wt (red) and Ad5-V (black) particles (dashed lines). From the average curve (solid lines) we estimated the height evolution of Ad5-wt and Ad5-ΔV. The height of Ad5-wt starts at 86 nm from the beginning of the experiment (0.0) until 0.75, meaning that during this period the capsid remains mostly intact. However, afterwards the height decreases dramatically until 20 nm at the end of the experiment (1.0). This means that along the fatigue experiment, once the virus particles have lost the three pentons of the upper face the AFM tip peels the virus and it reaches deeply inside , because the virus cores are being released as soon as the protein capsid is broken. In Ad5-ΔV particles (red) the particle peeling starts at t = 0.3, well before than in Ad5-wt case. In contrast with Ad5-wt, the Ad5-V particles are disrupted progressively until reaching a height of 45 nm at the end of the experiment (t = 1.0). In the mutant case part of the core remains inside the disrupted capsid while the capsid components fall apart.

Altogether, the mechanical fatigue assays revealed that Ad5-ΔV dissasembles in less volume/image, and its core is more condensed than in Ad5-wt particles.

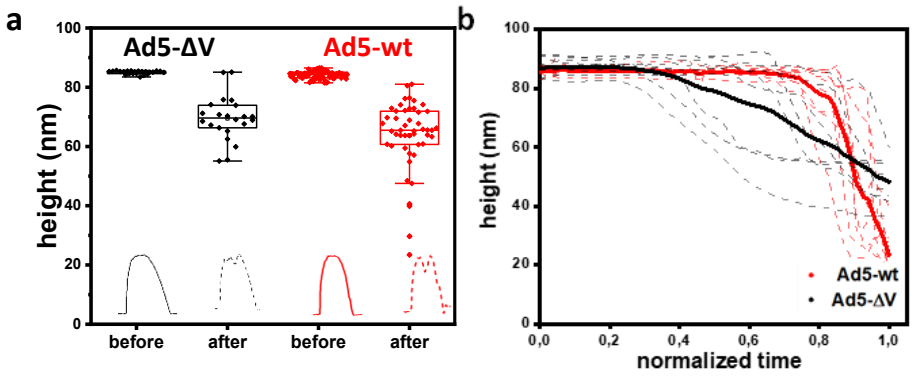

Figure 7.3. Height analysis provides information about the core condensation state. (a) Height distribution of all the viral particles imaged with AFM before and after an indentation. (b) Height evolution along the mechanical fatigue experiments (dash lines). Average of the experiments are represented in solid lines.

7.2.4 Absence of protein V reduces the genome diffusion out of the capsid

Other approach to study the core diffusion is to monitor the DNA appearing on the surface[178] after the virus has been crumpled by mechanical fatigue assays. In particular, in the previous Chapter we have resolved the genome organization and proteins dispersion of Ad5 in the topography of gradually collapsed virus particles. In the present case, in both mutant and wild type particles (**Figure 7.4a**) we can observe the debris of the capsid in the centre of the image and the genome (in yellow) spread on the surroundings. In the case of Ad5-ΔV, the genome was only seen in 25% of the fatigue experiments and the small amount of genome appears to be very close to the central debris of the capsid (**Figure 7.4a, top**). However, in Ad5-wt the genome was present in 100 % of the experiments and its diffusion was efficient enough to mostly occupy the full substrate under study (**Figure 7.4a, bottom**).

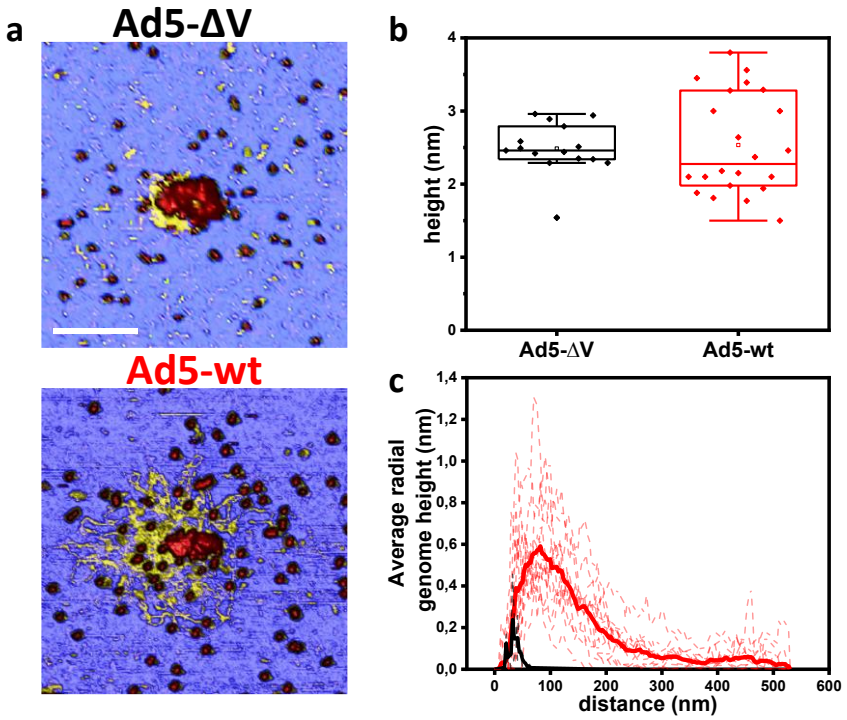

Figure 7.4. Genome analysis after mechanical fatigue assays. (a) AFM examples of Ad5-ΔV (top) and Ad5-wt (bottom) disruption after a mechanical fatigue assay. (b) Genome height distribution of the two adenoviral particles studied. (c) Radial average genome height distribution of Ad5-ΔV and Ad5-wt. Solid lines represent the average distribution for all the cases studied.

Beyond this qualitative perception, we performed a quantitative characterization of the genome strands thickness. This quantity can be determined by tracing height profiles on the topographical images in which DNA is spread. By taking the maximum height of a large number of profiles, it is possible to make a statistical study of the genome thickness for each viral particle. The results of this analysis, shown in **Figure 7.4b** suggest that the genome thickness presents a similar average value in both specimens close to 2 nm [164]. However, it is interesting to highlight that the thickness of the wt genome presents a higher dispersion (0.59) than the mutant one (0.36). This is probably related to the lack of pV in the mutant, which allows the DNA strands to be more disentangled than in the wt case.

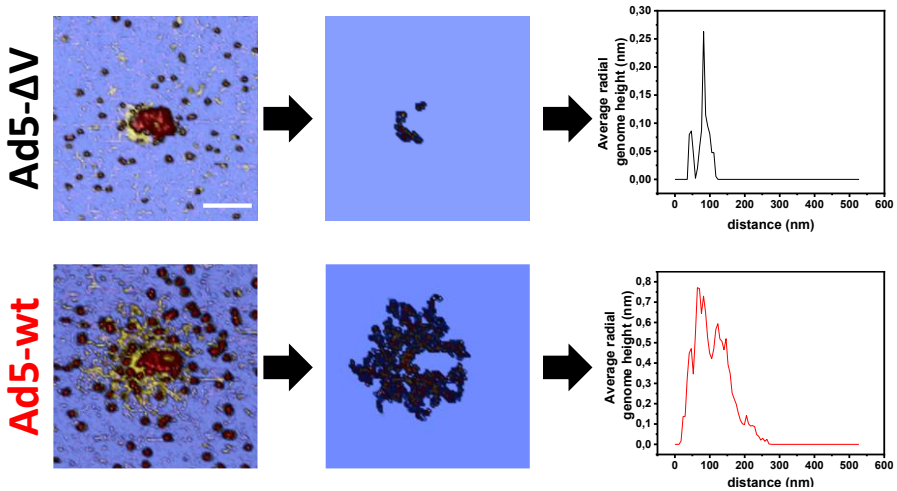

Figure 7.5. Average radial genome height analysis. (a) Final mechanical fatigue global image. Scale bar corresponds to 150 nm. (b) Flooded final mechanical fatigue image to isolate the genome height contribution (2 to 4 nm). (c) Radial average genome height distribution of the examples images of Ad5-ΔV (black) and Ad5-wt (red). The analysis is performed with WsXM software (http://www.wsxm.es/)

The presence of dsDNA on the surface allows us to quantify how far the virus genome is spread after escaping from the crumpled virus particles (**Figure 7.4a and 7.5**). These measurements provide information about the condensation level of the DNA in the virus core[62]. In our case we determine the genome diffusion level by performing a radial average of the topographical height at the end of the fatigue experiment (**Figure 7.5**). The radial average consists of estimating the average height of points that are located at the same distance to the centre of the virus. In **Figure 7.4c**, the radial average as a function of distance is shown for each viral particle studied (dashed lines), and the averaged data in solid lines. This chart shows that the genome of wt particles reaches distances up to 500 nm away from the center of the virus. However, the mutant data hardly spread beyond 60 nm. From these analyses, we can conclude that the genome of Ad5-ΔV particles does not leave the broken capsid as easily as in the Ad5-wt case.

7.3 Discussion

Core proteins play an important role in Ad5 uncoating and stability because it has been suggested that they help to condense the DNA inside the capsid cavity[29,32]. However, in recent studies, it has been reported that some core proteins are dispensable for the assembly of adenoviral particles but not for successful infection [35,66,175,179].

Previous AFM studies have thrown some light in the influence of the core proteins on the virus particle stability. For example, in Chapter 6 using a mutant in which core protein VII is absent[66] we reported stiffer and less thermostable viral particles due to the reduction of the core condensation and the consequent internal pressure increment[84,95]. In other case we found that immature AdV virions are softer and more thermostable compared to wildtype. In this case, the AFM experiments revealed a reduction in the internal pressure caused by an increase in the core condensation[36,94]. This was corroborated by mechanical fatigue assays in which the final size of immature particles was larger when comparing to wildtype[61].

In order to derive the pV role in the biophysical properties of virus particles, it is convenient to recall that pV displays connection with VI and the genome acting as a bridge between the capsid and the core [167]. In this vein, although the genus Mastadenovirus is the only one encoding protein V[172], a recent structural study of an atadenovirus showed the existence of a protein (p32k) that may play the same role as pV in Mastadenovirus[180]. Another cryo-EM study in enteric human AdV-41 revealed the position of pV confirming its interaction with DNA and pVI, thereby part of pV is bridging the core and the surrounding capsid[144].

Our studies show that the absence of core protein V softens the AdV capsid. This decrease in stiffness is similar to previous observations reported in empty capsid. In fact, it is known that the nucleic acids mechanically reinforce the capsids [82,181,182]. Our stiffness data suggest that in the absence of protein V the viral particle might be less pressurized, although the virus particle crumpling experiments indicate that Ad5-V particles present a more solid core than Ad5-wt.

The absence of pV bridging in Ad5-V particles could result in a softening and less brittle virus structure. In addition, our mechanical fatigue studies revealed that when pV is not present, pentons are lost faster than in wildtype (**Figure 7.2b**), probably due to the absence of protein V support below the pentons. This early loos of pentameric capsomers is compatible with in a less thermostable particle that would facilitate the access of fluorescence dye to the genome[175].

Beyond the structure stability, it is important to pay attention to the influence of pV in virus function (infectivity). Three adenoviral particles have been developed in the absence of protein V so far. The first was a deletion mutant with a dramatic decrease in thermostability and infectivity [35]. On the other hand, deletion of pV in bovine AdV-3 results in non-infectious particles and that pV is required for proper viral assembly[179]. In the third case it has been suggested that virions lacking protein V can assemble and presented no differences in the rest viral proteins but they were less infectious probably because they presented an unscheduled release of the genome in the cytoplasm[175].

Our experiments reveal that Ad5-V cracked particles show a solid core that remains more condensed than Ad5-wt (**Figure 7.2c and 7.3**). It seems that pV does not help in core condensation, because when it is absent in the Ad5-V particles DNA is not as easily released as in the wt case (**Figure 7.4**). Thus, the

role of protein V is different from this of histones[183]. However, the thickness of genome strands is similar in both viral particles suggesting that the rest core proteins (VII and μ) bind equally to DNA. Proteins VII and μ mediate DNA-DNA binding condensing the core, while protein V induces capsid-DNA interactions that pull DNA to the capsid lumen against core condensation (**Figure 7.6**). From these observations, we suggest that protein V competes with VII/μ.

It is important to consider that most of protein V of Ad5 is retained inside the shell until the translocation of the genome at the nuclear pore where the protein V is removed[170]. In this vein, protein V seems to play an important role during the cellular trafficking of Ad5. The same literature also reports that some protein V is lost before reaching the nuclear pore[170], which causes the genome to be detached from the capsid and to remain more condensed in order to help traffic through the pore more efficiently than when the genome is decondensated. In our AFM experiments we have found that the core remains condensed in the capsid, while in cellular trafficking experiments the genome detaches from the capsid[175] In AFM, during the disassembly of Ad5-wt partcles, protein V competes with pVII/μ and helps the genome to be released as the virus structure is gradually crumpled, while in Ad5-V particles this competition does not exist and the core is kept condensed. Therefore, when the protein capsid is peeled the core remains condensed. In bulk Ad5-wt experiments, the bridging action of protein V helps to keep the genome attached to the capsid while in Ad5-ΔV core and capsid are separated in the cytoplasm. However, in AFM experiments core and capsid are adsorbed together on the surface and they do not appear separated as in the trafficking experiments[175].

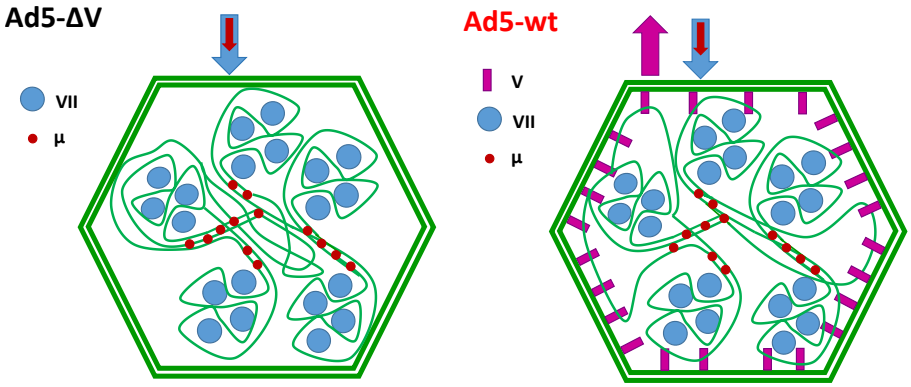

Figure 7.6. Model of viral particles for competition between core proteins V, VII and μ. In Ad5-ΔV (left) the condensing action of protein VII and μ is more efficient. In Ad5-wt (right) all the core proteins are present. In this situation proteins VII and μ condense the genome while protein V makes contacts with the core and the capsid. Two difference forces are acting in the genome represented with arrows.

7.4 Conclusion

In this work we have used AFM to study how the absence of core protein V influences in the mechanics and stability of human adenovirus. In the absence of pV adenoviral particles become softer and less brittle when comparing to Ad5-wt. This result reveals the role of pV as a mechanical reinforcement protein acting as a bridge between capsid and genome. Moreover, mechanical fatigue assays in the absence of pV showed that the core is more relaxed as it spreads more slowly and the genome does not diffuse as fast as in the wt particles. Overall, unveil the mechanical/stability consequences of the pV bridging action between core and capsid.

CHAPTER 8

Virucidal action mechanism of alcohol and divalent cations against human adenovirus

CHAPTER 8: Virucidal action mechanism of alcohol and divalent cations against human adenovirus

8.1 Introduction

Understanding the mode of action of a biocidal products has been shown to be relevant for establishing scientific principles, improvement of biocidal products as well as usage optimization, and combatting emerging resistance by target microorganism[184]. Biocides are multi-target antimicrobial agents with broad spectrum of action. Understanding their interactions with microbial targets, here viruses, informs our knowledge of mechanisms contributing to viral inactivation or viral resistance mechanisms, and contributes to improving efficacy through formulation design and better usage recommendation of the product in practicer[185]. Non-enveloped viruses offer less targets for virucidal action compared to enveloped ones. These targets comprise mainly the capsid, viral encoded receptor binding proteins and viral genomesj[186]. The mechanisms of virucidal action against non-enveloped viruses remain poorly studied.

The increased use of alcohols over other antimicrobials can be attributed to their rapid and broad-spectrum antimicrobial activity against bacteria, viruses and fungi[187,188]. Alcohols show substantial virucidal activity against enveloped viruses as compared to non-enveloped ones, which suggests that the viral lipid envelope is a potential target[189]. Alcohol in concentrations between 59-90% (w/v) show a fast acting and broad-spectrum of antimicrobial action[187,190,191], but persistence of efficacy is relatively low as alcohols evaporate quickly, and their residual activity after short periods of time is thus compromised[191,192]. Moreover, usage of 60-90% (w/v) alcohol in surface and hand disinfectants can be problematic mostly due to increased flammability, toxicity and generation of high amounts of volatile organic compounds (VOCs) affecting user safety[193].

VOCs generated by household products containing aforementioned alcohol concentrations may have short and long-term adverse health effects on animal and human in indoor environments including sensory irritation, allergies, asthma and leukemia[194]. The design of formulations that accommodate a decrease in alcohol concentration while retaining an appropriate virucidal activity is thus essential. Alcohols in synergistic combination with other antimicrobials (e.g. metals) are being studied not only to address those issues but to confer higher efficacy and persistence to a biocidal product as well[195]. The usage of zinc salts and oxides as antimicrobial agents is still limited. The main usage of zinc is as preservative in combination with other active ingredients in biocidal products used as pesticide in agriculture[196], as hand and skin antisepsis in household and healthcare products[188,197], and as antifouling agent in paints for metal surface treatment[198]. The combination of alcohol and zinc salts has not been widely reported, but the use of zinc pyrithione has shown some benefit on formulation antimicrobial activity and persistence[188]. Usage of other zinc salts such as zinc sulphate (as used in the present study) in combination with alcohol has not been reported commercially or academically yet.

In this context, the main goal of this study was to analyse the capacity of ethanol/zinc salt combination to present virucidal activity against non-enveloped viruses with identification of possible targets leading to a better understanding of the mechanism(s) of action. The influence of such combination against mammalian virus (adenovirus-Ad5-) capsid susceptibility to mechanical stress and virus integrity was verified through nano-indentation analysis by AFM. Furthermore, virucidal efficacy testing alongside viral purification and subsequent DNA extraction after exposure to formulations was performed in order to elucidate whether viral nucleic acid is a potential target for the formulation system under study.

Overall, this Chapter sought to confirm the potentiation of the virucidal activity of formulated ethanol with zinc sulphate, and to understand the mechanisms of

action for such activity against human adenovirus. This study was developed thanks to the collaboration with Jean-Yves Maillard group in Cardiff University. Leonam Gonzalvez performed the virucidal efficacy tests and the DNA damage analysis.

8.2 Results

The formulations tested where obtained from Reckitt Benckiser and their basic composition are described in Table 8.1. Excipients (non-active ingredients) are not disclosed due to proprietary issues. The virucidal efficacy of unformulated biocides are most commonly studied, and investigation of formulation is rarely reported in the literature. This study looked at the effect of the formulation and controls consisted of formulated ethanol (RB-ethanol) and zinc (RB-zinc).

Formulation	Composition
RB-Full	40% (w/v) ethanol + 0.1% (w/v) zinc sulphate + excipients; pH 10.5
RB-Ethanol	40% (w/v) ethanol + excipients; pH 10.5
RB-Zinc	0.1% (w/v) zinc sulphate + excipients; pH 10.5
RB-Control	Excipients; pH 10.5

Table 8.1. Formulations studied and their composition.

8.2.1 Virucidal activity of formulations

Following the use of the BS EN14476 protocol (the procedure is detailed in Appendix 2-A2-), the virucidal activity of the different formulations after 60 min exposure in hard water but with no organic load showed that the full formulation and the formulated ethanol (RB-Full and RB-Ethanol) (**Figure 8.1)** showed a significant reduction in PFU/ml compared to the formulated zinc or

the control containing excipients only ($p<0.05$). The formulation control (RB-Control) which contained excipients only did not show any reduction in HAdV2 infectivity and the lack of virus inactivation was comparable to RB-Zinc (**Figure 8.1**). Furthermore, there was no difference in activity between RB-Full and RB-Ethanol.

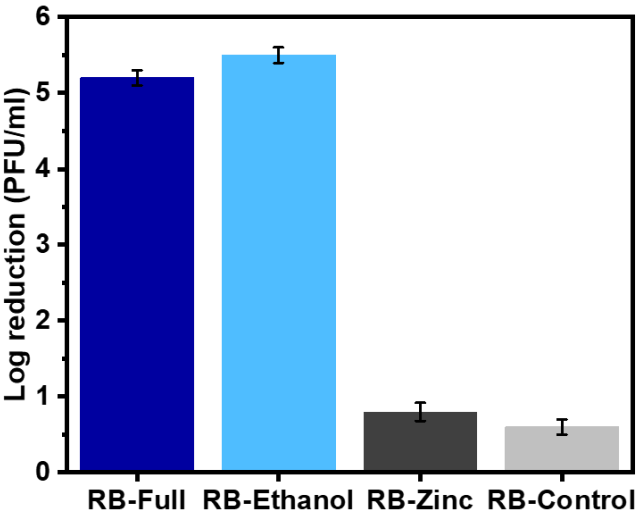

Figure 8.1. Virucidal activity test. Efficacy of the different formulations against HAdV2 using the EN14776 suspension test. Test conditions: 60 min contact time, hard water, no organic load.

8.2.2 DNA damage analysis

Potential damage to viral DNA was evaluated for HAdV2 (details in A2). There was no apparent DNA damage following virus exposure to any of the formulations. Severe damage associated with random multiple breaks in DNA[199,200] would take the form of a smear (**Figure 8.2a**). In addition, the use of restriction enzymes, which would indicate random DNA breaks, did not show any differences in DNA band pattern following virus exposure to different formulations (**Figure 8.2b**).

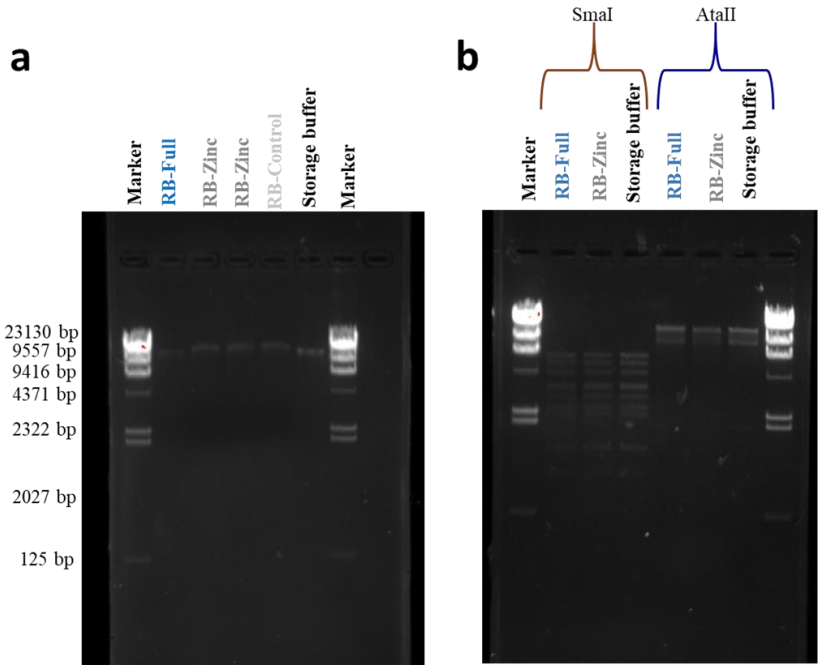

Figure 8.2. HAdV2 DNA damage analysis after exposure to formulations. (a) HAdV2 DNA bands extracted after exposure to different formulations. (b) HAdV2 DNA bands obtained after exposure to formulations and digested separately by SmaI and AatII restriction enzymes (see text).

8.2.3 Morphologial analysis

The effect of the different formulations in Ad5 particle morphology was analysed using AFM imaging in liquids and TEM. Ad5 particles were imaged after exposure to the different formulations at various incubation times. **Figure 8.3a** shows a typical AFM topography of a random population of Ad5 particles obtained in liquid condition before treatment. The topographical profile of one of the particles, marked by a green line in **Figure 8.3c** indicated that the particle size is ~ 86 nm. The impact of the different formulations on the particle morphology following different incubation times was then measured. In **Figure 8.3b** we showed an example of Ad5 incubation in RB-Full for 5 min, that resulted in drastic morphological alterations. The topographical profile (red line in **Figure 8.3c**) demonstrated that the height for the particle taken as an example

decreased to ~ 45 nm (a 50% reduction for this particular virion). Analysis of a particle height dataset showed decreases with increasing RB-Full exposure time up to 52% after 10 min (**Figure 8.3d**), indicative of capsid disruption or collapse.

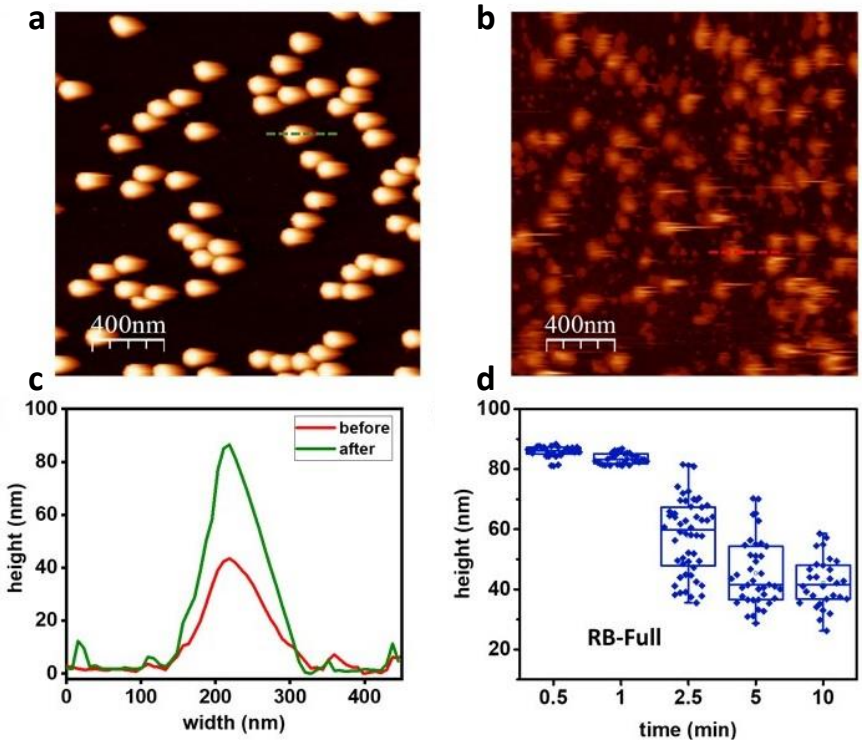

Figure 8.3. Morphology changes induced by formulation RB-Full. (a) Control: AFM image taken before treatment. (b) AFM image taken after 5 min contact with RB-Full. (c) Profiles of one viral particle and before (green line) and after (red line) treatment with RB-Full. (d) Box plot showing the evolution of particle height as a function of treatment time with RB-Full.

Moreover, RB-Ethanol significantly induced morphological changes in Ad5 (**Figure 8.4**). This is supported by a decrease in height with increasing incubation time. RB-Full decreased the height of the particle by 52% after 5 min of exposure time, whilst RB-ethanol decreased virus particle height by 62% after 2.5 min. RB-Zinc and RB-Control did not produce any height reduction in viral particles, regardless of the exposure time (**Figure 8.4**). RB-Full which contains both ethanol and zinc seemed to have a lesser effect on the integrity of the viral

particles causing less damage when compared to the formulation containing only ethanol (RB-Ethanol).

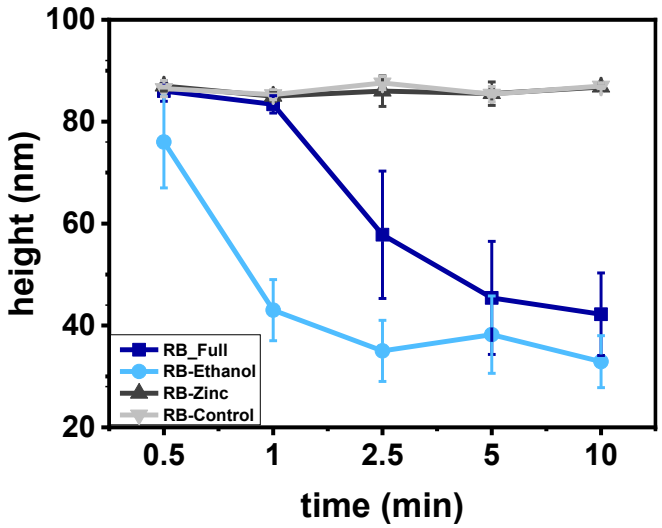

Figure 8.4. Particle height evolution after treatment with the different formulations as a function of time. Height average values and standard deviation are plotted. The N=50 for all the formulations and contact times.

On the other hand, TEM images only revealed damage when treated with RB-Ethanol after 5 minutes of incubation (**Figure 8.5**). The other formulations did not reveal any gross morphological changes in Ad5 particles independently of the contact time when only HBS was present (**Figure 8.5).** The apparent discrepancy between the AFM and TEM results with RB-Full formulation may originate from the differences in the experimental setup between the two imaging techniques. In particular, AFM imaging of Ad5 particles adsorbed to mica requires the presence of Ni^{+2} ions in the buffer[61]. We hypothesized the possibility of a synergistic effect between RB-Full and nickel salt used for the AFM assays. To verify this hypothesis, we repeated the TEM experiments adding Ni_2Cl to the HBS buffer at the same concentration used in the AFM protocol. This addition showed some damaged viral particles after 5 min of incubation by TEM

(**Figure 8.5**), which still do not suffice to provide the average height showed in AFM (**Figure 8.4, dark blue**). The excess of disrupted particles found in AFM can be ascribed to the fact that virus specimens are typically subjected to forces of ~100 pN during imaging. It is known that such low force can disrupt previously weakened virus structures[61]. In the present case, it is likely that virus particles are deteriorated by the combination of RB-Full and $NiCl_2$ and demolished during AFM imaging. Therefore, a combination of RB-Full with 5 mM $NiCl_2$ is responsible for the structural damage observed using both AFM and TEM.

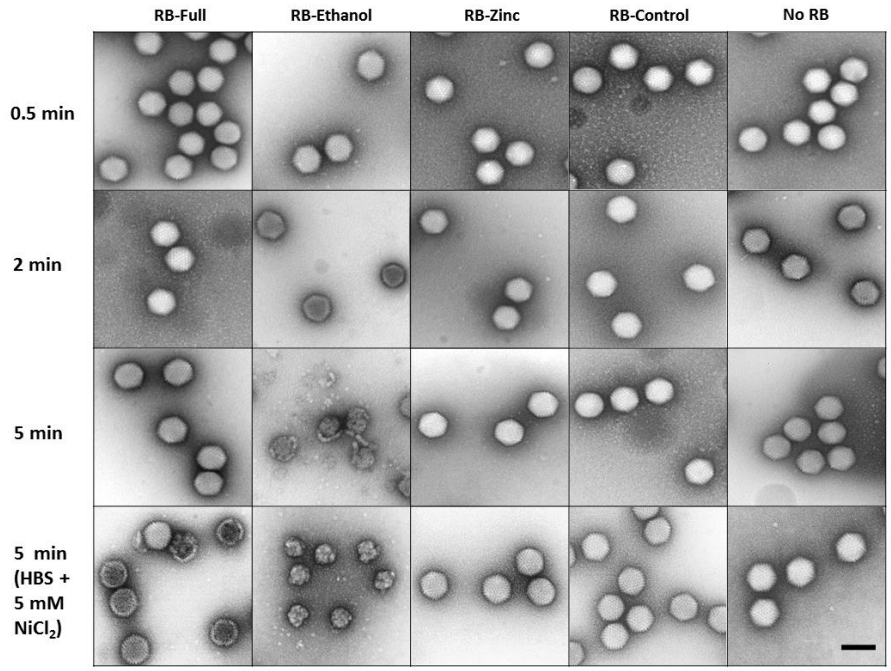

Figure 8.5. Morphology changes observed by TEM. Negative staining TEM imaging of Ad5 particles treated with the indicated formulations for different time lengths and buffer conditions. Scale bar 100 nm.

8.2.4 Mechanical properties

Changes in the mechanical properties of the Ad5 virions were measured. An incubation time of 0.5 min with the formulations diluted 1:1 in Milli-Q H_2O was chosen to have structurally intact viral particles that can be analysed mechanically. Using this contact time, we ensured there was no reduction in height of Ad5 caused by the formulation. The particle spring constant was significantly (ANOVA, $p<0.05$) lower in samples exposed to the formulations when compared to untreated control, showing that particles became softer when incubated with the formulations (**Figure 8.6**). However, no significant variation was found between the effect of the four formulations, as indicated by a Kolmoworov-Smirnov test of the measurements. This observation indicates that the excipients and highly basic pH present in all formulations tested alter Ad5 particle stiffness. In contrast, exposure of Ad5 to RB-Ethanol significantly decreased the breaking force indicating a weakening of the viral capsid when comparing with the other formulations. The maximum required force to break the particle is decreased in this case showing that the viral particles are more brittle (i.e. for the same deformation the force to break the particle is lower).

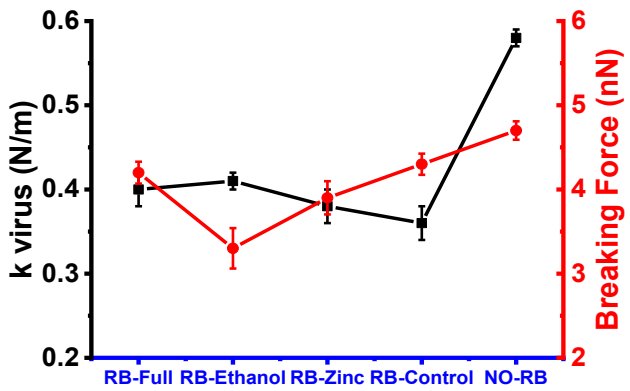

Figure 8.6. Changes in mechanical properties of Ad5 capsids following exposure to formulations. Black symbols represent the spring constant and red symbols represent the breaking force for the three formulations tested and the untreated control.

8.3 Discussion

Biocidal products play an important role for the control or elimination of microbial contamination in a wide range of settings. Some microorganisms, and notably non-enveloped viruses are more challenging to inactivate than enveloped ones due to the lack of a lipid bilayer envelope as a potential target[201]. The development of synergistic formulations based on combining active ingredients or/and selecting appropriate formulation excipients is important as this can lead to significant increase in disinfection efficacy while reducing toxicity and improving surface compatibility. Overall, there is little understanding of the mechanisms underlying virucidal activity of alcohol and metal ions in a given formulation. In this study, we aimed to produce a better insight of the use of zinc salt to potentiate the virucidal activity of a ethanol formulation against a non-enveloped virus. In our experimental set up we decided to use ethanol and the different control in a formulation as this would represent better the use of a final disinfectant product. Besides the impact of a formulation on biocidal activity is rarely investigated, hindering the application of findings to the efficacy of a final product in practice.

The RB-Full (40% w/v ethanol + 0.1% w/v zinc salt; pH 10.5) and the RB-Ethanol (40% (w/v) ethanol + excipients; pH 10.5) formulations were virucidal against HAdV2 (> 5 $\log_{10}$ reduction) within 60 min at room temperature and without organic load. RB-Zinc (0.1% (w/v) zinc sulphate + excipients; pH 10.5) on the control (excipients only) were not. Unformulated ethanol is considered to have a rapid virucidal activity (within 2 min) against adenovirus type 2 at concentrations between 55 and 85%. For adenovirus type 5, the reported effective concentration of unformulated ethanol ranges between 45 and 95%[202]. No gross structural damage of the virions was observed by TEM using RB-Full which contrasted with the damaging effect of RB-Ethanol. Although TEM observations cannot be directly correlated to the level virucidal activity, the

mechanisms of virions inactivation between the 2 formulations could be different, since both RB-Full and RB-Ethanol showed the same virucidal efficacy. These findings also questioned the role of zinc in the full formulation. We originally hypothesise that sufficient damage to the viral capsid imparted, for example, by ethanol would allow zinc penetration and its interaction with viral DNA. Zinc has been shown to interact directly with dsDNA[156]. Free zinc ions (Zn^{2+}) have been shown to be able to bind to DNA and change its secondary structure mainly through interactions with DNA phosphate sugar backbone as well as guanine and cytosine[203]. A high ratio of Zn^{2+} to DNA has also been shown to destabilise the DNA double helix decreasing its melting temperatures[204,205]. In addition, the viral genome can impact on capsid mechanics[206,207]. However, we did not observe that zinc caused any damage to viral dsDNA.

Although no major structural damage of the virions was observed by TEM using RB-Full, the addition of Ni^{2+} produced gross alterations of the viral particles. Such gross damage was confirmed with AFM suggesting capsid weakening with increased incubation time. We hypothesise that $NiCl_2$ was necessary to observe gross viral particle alteration when combined to the RB-Full formulation. The use of $NiCl_2$ in the AFM protocol was necessary because divalent ions are required for virus adsorption on mica. The potential mechanistic synergistic effect combining the RB-Full formulation with $NiCl_2$ was not expected and opens an interesting avenue for further formulation optimisation. The mechanical properties of the viral capsid such as stiffness and capacity to withstand pressure such as DNA packing and cell entry process, and extracellular conditions including osmotic pressure, desiccation and pH, plays a significant role for their viability[208,209]. Research on the mechanical properties of adenovirus resulted in a reduction of the capsid rigidity. The observed lower breaking force in this study indicates that the virus would be more susceptible to environment chemical and mechanical stress[210]. RB-Ethanol affected the ability of the virus to withstand pressure rather than its stiffness, ultimately

decreasing the viral capsid ability to withstand mechanical stress[210]. The mechanical properties of the virions were measured on intact particles in order to avoid the influence of structural defects (cracks, vacancies, etc). In this way, we to subtle changes on the capsomer bonds induced by the formulations. From our data (**Figure 8.6**) differences in the mechanical alterations of viruses between formulations were not extensive. However, we observed that all the formulations tested produced changes in the virus mechanics which contrasts with untreated viruses (**Figure 8.6**).

Although it is tempting to explain virucidal activity with the observed damage to the viral particles, there is no direct correlation between gross viral particle alteration and infectivity assays.

8.4 Conclusion

The need for biocidal product manufacturers to decrease alcohol concentration for environmental, regulatory and commercial reasons, while maintaining virucidal activity is challenging. We hypothesised that the addition of zinc might potentiate a low (non virucidal) concentration of ethanol (here 40%). We combined different techniques to investigate the interplay between the infectivity, integrity and mechanical effects of ethanol and zinc salt as active ingredients against Ad5. We observed that Ad5 particles were inactivated (5 $\log_{10}$ reduction in PFU/ml) when exposed to the RB-full and RB-Ethanol for 60 minutes in clean conditions, although only the formulated ethanol produced gross morphological change to the viral particles after 5 min exposure. It was interesting to observe that the presence of 5 mM $NiCl_2$ contributed to the structural damage imparted by the full formulation. AFM confirmed that capsid topography reduced considerable when virus was exposed to the full formulation in te presence of $NiCl_2$. Although the addition of zinc did not seem to improve the efficacy of the formulation, the addition of $NiCl_2$ contributing to

a weakening of the viral capsid offers an interesting avenue to pursue.

The use of AFM was instrumental in making such observations and as such, AFM has shown to be an important tool for understanding the mechanistic impact of virucidal formulation.

GENERAL CONCLUSIONS

In this thesis we have characterized the specific roles of two adenovirus core proteins, the dynamics of penton release, and the virion response to acidic conditions and virucidal agents, by using as a principal technique atomic force microscopy.

In **Chapter 4**, we used mechanical fatigue to study penton release dynamics. We found a cooperative effect in the penton release by using survival analysis, such that the escape of one penton increases the release rate of the remaining ones. Consequently, penton dismantling accelerates along uncoating, because the probability of a penton to be removed increases as less pentons remain on the capsid structure. Taking this into account, we developed a theoretical model that fits the experiments remarkably well and provides the energy barrier for penton release (~30 *kBT)* and its spontaneous escape rate (~10^{-4} s^{-1}). We proposed that aging fine tunes the uncoating process to provide weakened particles at the nuclear pore just ready for genome release. Strikingly, penton aging is independent of the local molecular environment of pentons (first neighborhoods), revealing long distance factors (~45 nm inter-penton distance) never considered before in modeling virus assembly/disassembly.

In **Chapter 5**, we explored the changes in Ad5 particles subject to short term acidification, mimicking the conditions occurring during infection. We found that low pH *per se* is not enough to trigger adenovirus capsid disassembly, which starts only after an additional stress (heating) is applied. However, upon acidification we detected a softening of the virion and a reduction in genome accessibility to an intercalating dye, even when capsid openings are present. The mechanical properties of empty capsids remained invariable at all pH conditions

tested, and penetration of the AFM tip inside broken virions is hindered at acidic pH. All these observations are consistent with an increase of the condensation state of the Ad5 nucleoprotein core due to acidification. In this Chapter, we discussed that cellular cues other than low pH are required to trigger Ad5 uncoating, and suggests that acidification may play a role in keeping the Ad5 genome protected inside a defective shell to ensure its successful trafficking through the cell.

In **Chapter 6**, we study a mutant lacking the major core protein of Ad5 (protein VII). We find that in the absence of VII, the particle stiffness increases, as a signature of higher internal pressure due to the DNA-DNA repulsive interactions which are screened by this protein in the control virus. Lack of protein VII induces a slight ordering of the adenovirus genome inside the capsid, and accelerates genome diffusion out of semi-disrupted particles because of the higher internal pressure. Moreover, we have observed that the absence of protein VII reduces the mechanical stability and thermostability of Ad5. AFM imaging of the adenovirus core mechanically unpacked in real time from individual capsids indicates that protein VII induces dsDNA condensation by promoting a mixture of clustering and bridging mechanisms. This study provided novel information on the role of viral histone-like proteins in the architectural organization of the genome and its influence on the viral core functionalities. While DNA condensation by VII is not needed for adenovirus assembly, we propose that it helps retaining the genome inside fractured capsids, protecting it from cell defenses while the semi-disrupted particle travels through the cytoplasm to the nuclear pore.

In **Chapter 7**, as in the previous one we study a mutant is which core protein V is absent. We have discovered that the presence of protein V reinforces the capsid stiffness and the particle is more brittle when protein V is present. This

result supports the action of protein V as a mechanical reinforcement protein acting as a bridge between capsid and genome. Moreover, mechanical fatigue assays revealed that, in the absence of protein V, the system is more relaxed during disassembly, losing less volume per image and the genome does not release from the capsid. Overall, it seems that core protein V, contrary to its expected role, decondenses the genome and helps cellular trafficking of the virus to protect from cell immune response.

In **Chapter 8**, we combine different techniques to investigate the interplay between the infectivity, integrity and mechanical effects of ethanol and divalent cations against Ad5. We characterize the virucidal action of alcohol in combination with zinc. We report a strong virucidal activity of a formulation containing both compounds and provide evidence that structural alterations in the virus capsid are responsible for the inactivation.

Adenovirus is a complex virus in which numerous factors are involve for a successful infection. In this thesis I aim to show some factors involve in uncoating such as penton release dynamics and acidification. Furthermore, the core adenovirus study helps to determine the role of the proteins inside the shell and their function, which opens a path for the study of the unknown adenovirus core.

CONCLUSIONES GENERALES

En esta tesis hemos caracterizado los roles específicos de dos proteínas del núcleo del adenovirus, la dinámica de la liberación de los pentones y la resistencia del virión a condiciones ácidas y a agentes virucidas, utilizando como técnica principal la microscopía de fuerzas atómicas.

En el **Capítulo 4**, utilizamos la fatiga mecánica para estudiar la dinámica de liberación del pentón. Encontramos un efecto cooperativo en la liberación de los pentones usando análisis de supervivencia, de tal manera que el escape de un pentón aumenta la tasa de liberación de los pentones restantes. En consecuencia, la liberación de los pentones se acelera a lo largo del desensamblaje, porque la probabilidad de que un pentón sea liberado aumenta a medida que quedan menos pentones en la estructura de la cápside. Teniendo esto en cuenta, desarrollamos un modelo teórico que se ajusta notablemente bien a los experimentos y proporciona la barrera energética para la liberación de pentones (~30 kBT) y su tasa de escape en ausencia de fuerza (~10-4 s^{-1}). Propusimos que el envejecimiento del sistema ayuda el proceso de desensamblaje para alcanzar partículas suficientemente debilitadas en el poro nuclear, listas para la liberación del genoma. Sorprendentemente, el envejecimiento de los pentones es independiente del ambiente molecular local de los pentones (primeros vecinos), revelando factores que afectan a larga distancia (~45nm de distancia entre pentones) nunca antes considerados en el modelado del ensamblaje/desensamblaje del virus.

En el **Capítulo 5**, exploramos los cambios en las partículas Ad5 sujetas a acidificación a tiempos cortos, imitando las condiciones que ocurren durante la infección. Encontramos que el bajo pH por sí mismo no es suficiente para desencadenar el desensamblaje de la cápsida del adenovirus, que comienza sólo después de que se aplique un estrés adicional (calentamiento). Sin embargo, al acidificarse detectamos un ablandamiento del virión y una reducción de la accesibilidad del genoma a un fluoróforo intercalante de ácidos nucleicos, incluso cuando hay defectos en la cápside. Las propiedades mecánicas de las cápsides vacías permanecieron invariables en todas las condiciones de pH estudiadas, y la penetración de la punta de AFM dentro de los viriones rotos se ve obstaculizada a pH ácido. Todas estas observaciones son consistentes con un aumento del estado de condensación del núcleo de Ad5 debido a la acidificación. En este capítulo, hemos discutido que se requieren otras señales celulares aparte del bajo pH para desencadenar el desensamblaje de Ad5, y sugiere que la acidificación puede jugar un papel en el mantenimiento del genoma de Ad5 protegido dentro de una cápsida defectuosa para asegurar su viaje a través de la célula.

En el **Capítulo 6**, estudiamos un mutante que carece de la proteína principal del núcleo de Ad5 (proteína VII). Encontramos que en ausencia de VII, la rigidez de la partícula aumenta, como consecuencia de una mayor presión interna debido a las interacciones de repulsión ADN-ADN que son examinadas por esta proteína en el virus de referencia (Ad5). La falta de proteína VII induce un ligero ordenamiento del genoma del adenovirus dentro de la cápside y acelera la difusión del genoma fuera de las partículas semirrotas debido a la mayor presión interna. Además, hemos observado que la ausencia de la proteína VII reduce la estabilidad mecánica y la termoestabilidad del Ad5. Las imágenes de AFM del núcleo del adenovirus desemsanblado mecánicamente en tiempo real de cápsidas individuales indica que la proteína VII induce la condensación de dsADN al promover una mezcla de mecanismos de

agrupamiento y puenteo. Este estudio proporcionó información novedosa sobre el papel de las proteínas similares a las histonas virales en la organización arquitectónica del genoma y su influencia en las funcionalidades del núcleo viral. Si bien la condensación del ADN por VII no es necesaria para el ensamblaje de adenovirus, proponemos que ayuda a retener el genoma dentro de cápsides rotas, protegiéndolo de las defensas celulares mientras la partícula viaja a través del citoplasma hasta el poro nuclear.

En el **Capítulo 7**, al igual que en el anterior, estudiamos un mutante en el que la proteína V del núcleo está ausente. Hemos descubierto que la presencia de la proteína V refuerza la rigidez de la cápside y la partícula es más frágil cuando la proteína V está presente. Este resultado apoya la acción de la proteína V como una proteína de refuerzo mecánico que actúa como puente entre la cápside y el genoma. Además, los ensayos de fatiga mecánica revelaron que, en ausencia de la proteína V, el sistema se relaja más durante el desensamblaje, perdiendo menos volumen por imagen y el genoma no se libera de la cápside. En general, parece que la proteína V del núcleo, en contraposición con su función esperada, descondensa el genoma y ayuda al tráfico celular del virus a protegerse de la respuesta inmunológica de la célula.

En el **Capítulo 8**, combinamos diferentes técnicas para investigar la relación entre la infectividad, la integridad y los efectos mecánicos del etanol y los cationes divalentes en el Ad5. Caracterizamos la acción virucida del alcohol en combinación con el zinc.Además, descubrimos una fuerte actividad virucida de una formulación que contiene ambos compuestos y proporcionamos pruebas de que las alteraciones estructurales en la cápside del virus son responsables de la inactivación.

El adenovirus es un virus complejo en el que intervienen muchos factores para que la infección tenga éxito. En esta tesis pretendo mostrar algunos factores implicados en el desensamblaje del adenovirus como la dinámica de liberación de los pentones y la acidificación. Además, el estudio del núcleo del adenovirus ayuda a determinar el papel de las proteínas dentro de la cápside y su función, abriéndose un camino para el estudio del desconocido núcleo del adenovirus.

ABBREVIATIONS

AdV	Adenovirus
Ad5	Adenovirus type 5
AFM	Atomic force microscopy
ANOVA	Analysis of variance
AVP	Adenoviral protease
CAR	Coxsackie and adenovirus receptor
CPS	Counts per second
Cryo-EM	Cryo electron microscopy
DNA	Deoxyribonucleic acid
dsDNA	Double stranded DNA
EDL	Electrostatic double layer
EM	Electron microscopy
FIC	Force Indentation curve
FZC	Force versus Z-piezo curve
GFP	Green fluorescent protein
GON	Group of nine
GOS	Group of six
HDMS	Hexamethyldisilazane
HOPG	Highly oriented pyrolitic graphite
HPI	Hours post infection
ITR	Inverted terminal repeats
JM	Jumping mode
JM+	Jumping mode plus
MLP	Major late proteins
NPC	Nuclear pore complex
PFU	Plaque forming unit
RGD	Arginine-glycerine-asparagine
RNA	Ribonucleic acid
S2	Two-fold symmetry
S3	Three-fold symmetry
S5	Five-fold symmetry
SD	Standard deviation
SEM	Standard error of the mean
Si	SIlicon
SPM	Scanning probe microscopy
STM	Scanning tunneling microscopy
TEM	Transmision electron microscopy
TP	Terminal protein
VA RNA	Virus associated RNA

BIBLIOGRAPHY

1. Roos, W. H., Bruinsma, R. & Wuite, G. J. L. Physical virology. *Nat. Phys.* **6**, 733–743 (2010).
2. Wen, A. M., Rambhia, P. H., French, R. H. & Steinmetz, N. F. Design rules for nanomedical engineering: from physical virology to the applications of virus-based materials in medicine. *J. Biol. Phys.* **39**, 301–325 (2013).
3. Singh, P., Gonzalez, M. J. & Manchester, M. Viruses and their uses in nanotechnology. *Drug Dev. Res.* **67**, 23–41 (2006).
4. Selivanovitch, E. & Douglas, T. Virus capsid assembly across different length scales inspire the development of virus-based biomaterials. *Curr. Opin. Virol.* **36**, 38–46 (2019).
5. Lundstrom, K. Viral Vectors in Gene Therapy. *Dis. (Basel, Switzerland)* **6**, (2018).
6. Rowe, W. P., Huebner, R. J., Gilmore, L. K., Parrott, R. H. & Ward, T. G. Isolation of a cytopathogenic agent from human adenoids undergoing spontaneous degeneration in tissue culture. *Proc. Soc. Exp. Biol. Med.* **84**, 570–573 (1953).
7. Virus Taxonomy - 1st Edition. https://www.elsevier.com/books/virus-taxonomy/king/978-0-12-384684-6.
8. Robinson, C. M. *et al.* Molecular evolution of human adenoviruses. *Sci. Rep.* **3**, 1812–1812 (2013).
9. Leen, A. M. & Rooney, C. M. Adenovirus as an emerging pathogen in immunocompromised patients. *British Journal of Haematology* vol. 128 135–144 (2005).
10. Gonçalves, M. A. F. V. & De Vries, A. A. F. Adenovirus: From foe to friend. *Reviews in Medical Virology* vol. 16 167–186 (2006).
11. Cots, D., Bosch, A. & Chillón, M. Helper Dependent Adenovirus Vectors: Progress and Future Prospects. *Curr. Gene Ther.* **13**, 370–381 (2013).
12. Dobbelstein, M. Replicating adenoviruses in cancer therapy. *Current Topics in Microbiology and Immunology* vol. 273 291–334 (2004).
13. McConnell, M. J. & Imperiale, M. J. Biology of adenovirus and its use as a vector for gene therapy. *Hum. Gene Ther.* **15**, 1022–1033 (2004).
14. Fields, B. N., Knipe, D. M. & Howley, P. M. *Fields virology*. (Wolters Kluwer Health/Lippincott Williams & Wilkins, 2007).
15. Ma, Y. & Mathews, M. B. Structure, function, and evolution of adenovirus-associated RNA: a phylogenetic approach. *J. Virol.* **70**, 5083–5099 (1996).
16. Van der Vliet, P. C. Adenovirus DNA replication. *Curr. Top. Microbiol. Immunol.* **199 (Pt 2**, 1–30 (1995).
17. Gräble, M. & Hearing, P. Adenovirus type 5 packaging domain is composed of a repeated element that is functionally redundant. *J. Virol.* **64**, 2047–2056 (1990).
18. Dai, X., Wu, L., Sun, R. & Zhou, Z. H. Atomic Structures of Minor Proteins VI and VII in Human Adenovirus. *J. Virol.* **91**, (2017).
19. San-Martín, C. Latest insights on adenovirus structure and assembly. *Viruses* **4**, 847–877 (2012).
20. Burnett, R. M., Grütter, M. G. & White, J. L. The structure of the adenovirus capsid. I. An envelope model of hexon at 6 A resolution. *J. Mol. Biol.* **185**, 105–123 (1985).
21. Liu, H. *et al.* Atomic structure of human adenovirus by cryo-EM reveals interactions among protein networks. *Science* **329**, 1038–1043 (2010).
22. Zubieta, C., Schoehn, G., Chroboczek, J. & Cusack, S. The structure of the human adenovirus 2 penton. *Mol. Cell* **17**, 121–135 (2005).
23. van Raaij, M. J., Mitraki, A., Lavigne, G. & Cusack, S. A triple beta-spiral in the adenovirus fibre shaft reveals a new

structural motif for a fibrous protein. *Nature* **401**, 935–938 (1999).

24. Liu, H., Wu, L. & Zhou, Z. H. Model of the trimeric fiber and its interactions with the pentameric penton base of human adenovirus by cryo-electron microscopy. *J. Mol. Biol.* **406**, 764–774 (2011).
25. Mangel, W. F. & San Martín, C. Structure, function and dynamics in adenovirus maturation. *Viruses* **6**, 4536–4570 (2014).
26. Maier, O., Galan, D. L., Wodrich, H. & Wiethoff, C. M. An N-terminal domain of adenovirus protein VI fragments membranes by inducing positive membrane curvature. *Virology* **402**, 11–19 (2010).
27. van Oostrum, J. & Burnett, R. M. Molecular composition of the adenovirus type 2 virion. *J. Virol.* **56**, 439–448 (1985).
28. Benevento, M. *et al.* Adenovirus composition, proteolysis, and disassembly studied by in-depth qualitative and quantitative proteomics. *J. Biol. Chem.* **289**, 11421–11430 (2014).
29. Vayda, M. E., Rogers, A. E. & Flint, S. J. The structure of nucleoprotein cores released from adenovirions. *Nucleic Acids Res.* **11**, 441–460 (1983).
30. Lischwe, M. A. & Sung, M. T. A histone-like protein from adenovirus chromatin. *Nature* **267**, 552–554 (1977).
31. Mirza, M. A. & Weber, J. Structure of adenovirus chromatin. *Biochim. Biophys. Acta* **696**, 76–86 (1982).
32. Pérez-Berná, A. J. *et al.* Distribution of DNA-condensing protein complexes in the adenovirus core. *Nucleic Acids Res.* **43**, 4274–4283 (2015).
33. Giberson, A. N., Davidson, A. R. & Parks, R. J. Chromatin structure of adenovirus DNA throughout infection. *Nucleic Acids Res.* **40**, 2369–2376 (2012).
34. Perez-Vargas, J. *et al.* Isolation and Characterization of the DNA and Protein Binding Activities of Adenovirus Core Protein V. *J. Virol.* **88**, 9287–9296 (2014).
35. Ugai, H., Borovjagin, A. V., Le, L. P., Wang, M. & Curiel, D. T. Thermostability/Infectivity Defect Caused by Deletion of the Core Protein V Gene in Human Adenovirus Type 5 Is Rescued by Thermo-selectable Mutations in the Core Protein X Precursor. *J. Mol. Biol.* **366**, 1142–1160 (2007).
36. Ortega-Esteban, A. *et al.* Mechanics of Viral Chromatin Reveals the Pressurization of Human Adenovirus. *ACS Nano* **9**, 10826–10833 (2015).
37. Bergelson, J. M. *et al.* Isolation of a common receptor for Coxsackie B viruses and adenoviruses 2 and 5. *Science* **275**, 1320–1323 (1997).
38. Chiu, C. Y., Mathias, P., Nemerow, G. R. & Stewart, P. L. Structure of adenovirus complexed with its internalization receptor, alphavbeta5 integrin. *J. Virol.* **73**, 6759–6768 (1999).
39. Lindert, S., Silvestry, M., Mullen, T.-M., Nemerow, G. R. & Stewart, P. L. Cryo-electron microscopy structure of an adenovirus-integrin complex indicates conformational changes in both penton base and integrin. *J. Virol.* **83**, 11491–11501 (2009).
40. Medina-Kauwe, L. K. Endocytosis of adenovirus and adenovirus capsid proteins. *Adv. Drug Deliv. Rev.* **55**, 1485–1496 (2003).
41. Wiethoff, C. M., Wodrich, H., Gerace, L. & Nemerow, G. R. Adenovirus protein VI mediates membrane disruption following capsid disassembly. *J. Virol.* **79**, 1992–2000 (2005).
42. Suomalainen, M. *et al.* A direct and versatile assay measuring membrane penetration of adenovirus in single cells. *J Virol* **87**, 12367–12379 (2013).
43. Greber, U. F., Webster, P., Weber, J. & Helenius, A. The role of the adenovirus protease on virus entry into cells. *EMBO J.* **15**, 1766–1777 (1996).
44. Cotten, M. & Weber, J. M. The adenovirus protease is required for

virus entry into host cells. *Virology* **213**, 494–502 (1995).

45. Greber, U. F. & Flatt, J. W. Adenovirus Entry: From Infection to Immunity. *Annu. Rev. Virol.* **6**, 177–197 (2019).
46. Binnig, G., Quate, C. F. & Gerber, C. Atomic Force Microscope. *Phys. Rev. Lett.* **56**, 930–933 (1986).
47. Baró, A. M. *et al.* Determination of surface topography of biological specimens at high resolution by scanning tunnelling microscopy. *Nature* **315**, 253–254 (1985).
48. Ortega-Esteban, A. *et al.* Minimizing tip-sample forces in jumping mode atomic force microscopy in liquid. *Ultramicroscopy* **114**, 56–61 (2012).
49. Horcas, I. *et al.* WSXM: A software for scanning probe microscopy and a tool for nanotechnology. *Rev. Sci. Instrum.* **78**, (2007).
50. Weisenhorn, A. L., Maivald, P., Butt, H.-J. & Hansma, P. K. Measuring adhesion, attraction, and repulsion between surfaces in liquids with an atomic-force microscope. *Phys. Rev. B* **45**, 11226–11232 (1992).
51. García, R. & Pérez, R. Dynamic atomic force microscopy methods. *Surf. Sci. Rep.* **47**, 197–301 (2002).
52. Israelachvili, J. N. Intermolecular and Surface Forces. 706.
53. Ohnesorge, F. & Binnig, G. True Atomic Resolution by Atomic Force Microscopy Through Repulsive and Attractive Forces. *Science (80-.).* **260**, 1451 LP – 1456 (1993).
54. Hernando-Pérez, M. *et al.* Quantitative nanoscale electrostatics of viruses. *Nanoscale* **7**, 17289–17298 (2015).
55. Martínez, L. *et al.* Aspect-ratio and lateral-resolution enhancement in force microscopy by attaching nanoclusters generated by an ion cluster source at the end of a silicon tip. *Rev. Sci. Instrum.* **82**, 23710 (2011).
56. Villarrubia, J. S. Algorithms for Scanned Probe Microscope Image Simulation, Surface Reconstruction, and Tip Estimation. *J. Res. Natl. Inst. Stand. Technol.* **102**, 425–454 (1997).
57. Sader, J. E., Chon, J. W. M. & Mulvaney, P. Calibration of rectangular atomic force microscope cantilevers. *Rev. Sci. Instrum.* **70**, 3967–3969 (1999).
58. Kuznetsov, Y. G. & McPherson, A. Atomic force microscopy in imaging of viruses and virus-infected cells. *Microbiol. Mol. Biol. Rev.* **75**, 268–285 (2011).
59. Alba, R., Hearing, P., Bosch, A. & Chillon, M. Differential amplification of adenovirus vectors by flanking the packaging signal with attB/attP-PhiC31 sequences: implications for helper-dependent adenovirus production. *Virology* **367**, 51–58 (2007).
60. Weber, J. Genetic analysis of adenovirus type 2 III. Temperature sensitivity of processing viral proteins. *J. Virol.* **17**, 462–471 (1976).
61. Ortega-Esteban, A. *et al.* Monitoring dynamics of human adenovirus disassembly induced by mechanical fatigue. *Sci. Rep.* **3**, 1–7 (2013).
62. Ortega-Esteban, A. *et al.* Fluorescence Tracking of Genome Release during Mechanical Unpacking of Single Viruses. *ACS Nano* **9**, (2015).
63. Seki, T. *et al.* Artificial Extension of the Adenovirus Fiber Shaft Inhibits Infectivity in Coxsackievirus and Adenovirus Receptor-Positive Cell Lines. *J. Virol.* **76**, 1100–1108 (2002).
64. Alba, R., Hearing, P., Bosch, A. & Chillon, M. Differential amplification of adenovirus vectors by flanking the packaging signal with attB/attP-ΦC31 sequences: Implications for helper-dependent adenovirus production. *Virology* **367**, 51–58 (2007).
65. Condezo, G. N. *et al.* Structures of Adenovirus Incomplete Particles Clarify Capsid Architecture and Show Maturation Changes of Packaging Protein L1 52/55k. *J Virol* **89**, 9653–9664 (2015).
66. Ostapchuk, P. *et al.* The adenovirus major core protein VII is dispensable for virion assembly but is essential for

lytic infection. *PLoS Pathog.* **13**, 1–24 (2017).

67. Hearing, P. & Shenk, T. The adenovirus type 5 E1A transcriptional control region contains a duplicated enhancer element. *Cell* **33**, 695–703 (1983).
68. Warming, S., Costantino, N., Court, D. L., Jenkins, N. A. & Copeland, N. G. Simple and highly efficient BAC recombineering using galK selection. *Nucleic Acids Res.* **33**, 1–12 (2005).
69. Greber, U. F., Willetts, M., Webster, P. & Helenius, A. Stepwise dismantling of adenovirus 2 during entry into cells. *Cell* **75**, 477–486 (1993).
70. Larson, I. & Pugh, R. J. Qualitative Adsorption Measurements with an Atomic Force Microscope. *Langmuir* **14**, 5676–5679 (1998).
71. Mu, Y. Effects of surface hydrophobicity on the conformational changes of polypeptides of different length. *Phys. Rev. E* **84**, 31906 (2011).
72. Gun'ko, V. M., Vedamuthu, M. S., Henderson, G. L. & Blitz, J. P. Mechanism and Kinetics of Hexamethyldisilazane Reaction with a Fumed Silica Surface. *J. Colloid Interface Sci.* **228**, 157–170 (2000).
73. Snijder, J. *et al.* Integrin and defensin modulate the mechanical properties of adenovirus. *J. Virol.* **87**, 2756–2766 (2013).
74. Kienberger, F. *et al. Single molecule tools. Part B: Super-Resolution, Particle Tracking, Multiparameter, and Force Based Methods*. (Elsevier/Academic Press, 2010).
75. Llauró, A., Schwarz, B., Koliyatt, R., De Pablo, P. J. & Douglas, T. Tuning Viral Capsid Nanoparticle Stability with Symmetrical Morphogenesis. *ACS Nano* **10**, 8465–8473 (2016).
76. Zeng, C. *et al.* Contact Mechanics of a Small Icosahedral Virus. *Phys. Rev. Lett.* **119**, 38102 (2017).
77. Butt, H. J. Measuring local surface charge densities in electrolyte solutions with a scanning force microscope. *Biophys. J.* **63**, 578–582 (1992).
78. Butt, H.-J., Cappella, B. & Kappl, M. Force measurements with the atomic force microscope: Technique, interpretation and applications. *Surf. Sci. Rep.* **59**, 1–152 (2005).
79. D, L. L. & M, L. E. *Theory of Elasticity*. (Pergamon Press, 1989).
80. Ivanovska, I. L. *et al.* Bacteriophage capsids: Tough nanoshells with complex elastic properties. 6.
81. Schaap, I. A. T., Carrasco, C., de Pablo, P. J., MacKintosh, F. C. & Schmidt, C. F. Elastic response, buckling, and instability of microtubules under radial indentation. *Biophys. J.* **91**, 1521–1531 (2006).
82. Carrasco, C., Castellanos, M., De Pablo, P. J. & Mateu, M. G. Manipulation of the mechanical properties of a virus by protein engineering. *Proc. Natl. Acad. Sci. U. S. A.* **105**, 4150–4155 (2008).
83. Evans, E. Probing the relation between force--lifetime--and chemistry in single molecular bonds. *Annu. Rev. Biophys. Biomol. Struct.* **30**, 105–128 (2001).
84. Hernando-Pérez, M. *et al.* Dynamic competition for hexon binding between core protein VII and lytic protein VI promotes adenovirus maturation and entry. *Proc. Natl. Acad. Sci. U. S. A.* **117**, 13699–13707 (2020).
85. Flint, S. J., Racaniello, V. R., Rall, G. F., Skalka, A. M. & Enquist, L. W. *Principles of virology*. (2015).
86. Caspar, D. L. & Klug, A. Physical principles in the construction of regular viruses. *Cold Spring Harb. Symp. Quant. Biol.* **27**, 1–24 (1962).
87. Klug, W. S. *et al.* Failure of viral shells. *Phys. Rev. Lett.* **97**, 1–4 (2006).
88. Zandi, R., Reguera, D., Bruinsma, R. F., Gelbart, W. M. & Rudnick, J. Origin of icosahedral symmetry in viruses. *Proc. Natl. Acad. Sci. U. S. A.* **101**, 5 (2014).
89. Klug, W. S., Roos, W. H. & Wuite, G. J. L. Unlocking internal prestress from protein nanoshells. *Phys. Rev. Lett.* **109**, 1–5 (2012).
90. Zandi, R. & Reguera, D. Mechanical properties of viral capsids. *Phys. Rev.*

E **72**, 21917 (2005).

91. Patterson, D. *et al.* Virus-like particle nanoreactors: Programmed encapsulation of the thermostable CelB glycosidase inside the P22 capsid. *Soft Matter* **8**, 10158–10166 (2012).
92. Nakano, M. Y., Boucke, K., Suomalainen, M., Stidwill, R. P. & Greber, U. F. The First Step of Adenovirus Type 2 Disassembly Occurs at the Cell Surface, Independently of Endocytosis and Escape to the Cytosol. *J. Virol.* **74**, 7085–7095 (2000).
93. Burckhardt, C. J. Drifting Motions of the Adenovirus Receptor CAR and Immobile Integrins Initiate Virus Uncoating and Membrane Lytic Protein Exposure. 13.
94. Pérez-Berná, A. J. *et al.* The role of capsid maturation on adenovirus priming for sequential uncoating. *J. Biol. Chem.* **287**, 31582–31595 (2012).
95. Martín-González, N. *et al.* Adenovirus major core protein condenses DNA in clusters and bundles, modulating genome release and capsid internal pressure. *Nucleic Acids Res* **47**, 9231–9242 (2019).
96. Arkhipov, A., Roos, W. H., Wuite, G. J. L. & Schulten, K. Elucidating the Mechanism behind Irreversible Deformation of Viral Capsids. *Biophys. J.* **97**, 2061–2069 (2009).
97. Waloddi Weibull, B. A Statistical Distribution Function of Wide Applicability. *J. Appl. Mech.* **Vol. 18**, 293–297 (1951).
98. Nakagawa, T. & Osaki, S. The Discrete Weibull Distribution. *IEEE Trans. Reliab.* **R**-**24**, 300–301 (1975).
99. Stephanidis, B., Adichtchev, S., Gouet, P., McPherson, A. & Mermet, A. Elastic properties of viruses. *Biophys. J.* **93**, 1354–1359 (2007).
100. Bell, G. Models for the specific adhesion of cells to cells. *Science (80-.).* **200**, 618–627 (1978).
101. Carrion-Vazquez, M. *et al.* Mechanical and chemical unfolding of a single protein: A comparison. *Proc. Natl. Acad. Sci.* **96**, 3694 LP – 3699 (1999).
102. Valbuena, A. *et al.* On the remarkable mechanostability of scaffoldins and the mechanical clamp motif. *Proc. Natl. Acad. Sci.* **106**, 13791–13796 (2009).
103. Stigler, J. & Rief, M. Ligand-induced changes of the apparent transition-state position in mechanical protein unfolding. *Biophys. J.* **109**, 365–372 (2015).
104. Roos, W. H. *et al.* Scaffold expulsion and genome packaging trigger stabilization of herpes simplex virus capsids. *Proc. Natl. Acad. Sci. U. S. A.* **106**, 9673–9678 (2009).
105. López-Polín, G. *et al.* Increasing the elastic modulus of graphene by controlled defect creation. *Nat. Phys.* **11**, 26–31 (2015).
106. Ortega-Esteban, A. Biophysical Determinants for Adenovirus Uncoating & Infectivity. *Dr. Thesis* (2015).
107. Perlmutter, J. D., Qiao, C. & Hagan, M. F. Viral genome structures are optimal for capsid assembly. *Elife* **2**, e00632 (2013).
108. Roy, A. & Post, C. B. Long-distance correlations of rhinovirus capsid dynamics contribute to uncoating and antiviral activity. *Proc. Natl. Acad. Sci.* **109**, 5271 LP – 5276 (2012).
109. Callaway, D. J. E. & Bu, Z. Nanoscale protein domain motion and long-range allostery in signaling proteins—a view from neutron spin echo spectroscopy. *Biophys. Rev.* **7**, 165–174 (2015).
110. Li, J., Callaway, D. J. E. & Bu, Z. Ezrin induces long-range interdomain allostery in the scaffolding protein NHERF1. *J. Mol. Biol.* **392**, 166–180 (2009).
111. Domínguez-Gil, T. *et al.* Activation by Allostery in Cell-Wall Remodeling by a Modular Membrane-Bound Lytic Transglycosylase from Pseudomonas aeruginosa. *Structure* **24**, 1729–1741 (2016).
112. Williams, M. R., Lehman, S. J., Tardiff, J. C. & Schwartz, S. D. Atomic resolution probe for allostery in the

regulatory thin filament. *Proc. Natl. Acad. Sci. U. S. A.* **113**, 3257–3262 (2016).

113. Bremner, K. H. *et al.* Adenovirus transport via direct interaction of cytoplasmic dynein with the viral capsid hexon subunit. *Cell Host Microbe* **6**, 523–535 (2009).
114. Zhou, J., Scherer, J., Yi, J. & Vallee, R. B. Role of kinesins in directed adenovirus transport and cytoplasmic exploration. *PLOS Pathog.* **14**, e1007055 (2018).
115. Rentsendorj, A. *et al.* Typical and atypical trafficking pathways of Ad5 penton base recombinant protein: implications for gene transfer. *Gene Ther.* **13**, 821–836 (2006).
116. Howard, J. Mechanics of Motor Proteins and the Cytoskeleton Sunderland. in *Mechanics of Motor Proteins and the Cytoskeleton* vol. 55 (2001).
117. Moreno-Madrid, F. *et al.* Atomic force microscopy of virus shells. *Biochem. Soc. Trans.* **45**, 499–511 (2017).
118. Moyer, C. L. & Nemerow, G. R. Viral weapons of membrane destruction: variable modes of membrane penetration by non-enveloped viruses. *Curr. Opin. Virol.* **1**, 44–49 (2011).
119. Mateu, M. G. Assembly, stability and dynamics of virus capsids. *Arch. Biochem. Biophys.* **531**, 65–79 (2013).
120. Yamauchi, Y. & Greber, U. F. Principles of Virus Uncoating: Cues and the Snooker Ball. *Traffic* **17**, 569–592 (2016).
121. Lopez, S. & Arias, C. %J N. E. How viruses hijack endocytic machinery. **3**, 16 (2010).
122. Li, S. *et al.* pH-Controlled two-step uncoating of influenza virus. *Biophys J* **106**, 1447–1456 (2014).
123. Schmidt, F. I., Bleck, C. K. E. & Mercer, J. Poxvirus host cell entry. *Curr. Opin. Virol.* **2**, 20–27 (2012).
124. Tan, T. Y., Fibriansah, G. & Lok, S. M. Capsid protein is central to the birth of flavivirus particles. *PLoS Pathog* **16**, e1008542 (2020).
125. Mani, B. *et al.* Low pH-dependent endosomal processing of the incoming parvovirus minute virus of mice virion leads to externalization of the VP1 N-terminal sequence (N-VP1), N-VP2 cleavage, and uncoating of the full-length genome. *J. Virol.* **80**, 1015–1024 (2006).
126. Prage, L., Pettersson, U., Höglund, S., Lonberg-Holm, K. & Philipson, L. Structural proteins of adenoviruses. IV. Sequential degradation of the adenovirus type 2 virion. *Virology* **42**, 341–358 (1970).
127. Rexroad, J. *et al.* Structural stability of adenovirus type 5. *J Pharm Sci* **92**, 665–678 (2003).
128. Rexroad, J., Evans, R. K. & Middaugh, C. R. Effect of pH and ionic strength on the physical stability of adenovirus type 5. *J Pharm Sci* **95**, 237–247 (2006).
129. Rexroad, J., Martin, T. T., McNeilly, D., Godwin, S. & Middaugh, C. R. Thermal stability of adenovirus type 2 as a function of pH. *J Pharm Sci* **95**, 1469–1479 (2006).
130. Snijder, J. *et al.* Probing the biophysical interplay between a viral genome and its capsid. *Nat Chem* **5**, 502–509 (2013).
131. Wilts, B. D., Schaap, I. A. T. & Schmidt, C. F. Swelling and softening of the cowpea chlorotic mottle virus in response to pH shifts. *Biophys J* **108**, 2541–2549 (2015).
132. Gastaldelli, M. *et al.* Infectious adenovirus type 2 transport through early but not late endosomes. *Traffic* **9**, 2265–2278 (2008).
133. Miyazawa, N., Crystal, R. G. & Leopold, P. L. Adenovirus serotype 7 retention in a late endosomal compartment prior to cytosol escape is modulated by fiber protein. *J. Virol.* **75**, 1387–1400 (2001).
134. Lenaerts, L., De Clercq, E. & Naesens, L. Clinical features and treatment of adenovirus infections. *Rev Med Virol* **18**, 357–374 (2008).
135. Hartmann, N. M., Dartscht, M., Szewzyk, R. & Selinka, H.-C.

Monitoring of adenovirus serotypes in environmental samples by combined PCR and melting point analyses. *Virol. J.* **10**, 190 (2013).

136. Hernando-Pérez, M. *et al.* Direct Measurement of Phage phi29 Stiffness Provides Evidence of Internal Pressure. *Small* **8**, 2365.
137. Pérez-Berná, A. J. *et al.* Structure and Uncoating of Immature Adenovirus. *J. Mol. Biol.* **392**, 547–557 (2009).
138. Pérez-Berná, A. J. *et al.* The Role of Capsid Maturation on Adenovirus Priming for Sequential Uncoating. *J. Biol. Chem.* **287**, 31582–31595 (2012).
139. Ortega-Esteban, A. *et al.* Monitoring dynamics of human adenovirus disassembly induced by mechanical fatigue. *Sci. Rep.* 7.
140. Dumetz, A. C., Chockla, A. M., Kaler, E. W. & Lenhoff, A. M. Effects of pH on protein-protein interactions and implications for protein phase behavior. *Biochim Biophys Acta* **1784**, 600–610 (2008).
141. Voet, D., Voet, J. G. & Pratt, C. W. *Fundamentals of biochemistry*. (2000).
142. Cameselle, J. C., Ribeiro, J. M. & Sillero, A. Derivation and use of a formula to calculate the net charge of acid-base compounds. Its application to amino acids, proteins and nucleotides. *Biochem. Educ.* **14**, 131–136 (1986).
143. Pérez-Illana, M. *et al.* Cryo-EM structure of enteric adenovirus HAdV-F41 highlights structural divergence among human adenoviruses. 2020.07.01.177519 (2020) doi:10.1101/2020.07.01.177519 %J bioRxiv.
144. Rafie, K. *et al.* The structure of enteric human adenovirus 41 - a leading cause of diarrhoea in children. 2020.07.01.181735 (2020) doi:10.1101/2020.07.01.181735 %J bioRxiv.
145. Luijsterburg, M. S., White, M. F., van Driel, R. & Dame, R. T. The major architects of chromatin: architectural proteins in bacteria, archaea and eukaryotes. *Crit. Rev. Biochem. Mol. Biol.* **43**, 393–418 (2008).
146. Zhou, B.-R. *et al.* Structural insights into the histone H1-nucleosome complex. *Proc. Natl. Acad. Sci. U. S. A.* **110**, 19390–19395 (2013).
147. Gruber, S. Multilayer chromosome organization through DNA bending, bridging and extrusion. *Curr. Opin. Microbiol.* **22**, 102–110 (2014).
148. Teif, V. B. & Bohinc, K. Condensed DNA: Condensing the concepts. *Prog. Biophys. Mol. Biol.* **105**, 208–222 (2011).
149. Black, L. W. & Thomas, J. A. Condensed genome structure. *Adv. Exp. Med. Biol.* **726**, 469–487 (2012).
150. Germond, J. E., Hirt, B., Oudet, P., Gross-Bellark, M. & Chambon, P. Folding of the DNA double helix in chromatin-like structures from simian virus 40. *Proc. Natl. Acad. Sci.* **72**, 1843 LP – 1847 (1975).
151. Borca, M. V *et al.* A structural DNA binding protein of African swine fever virus with similarity to bacterial histone-like proteins. *Arch. Virol.* **141**, 301–313 (1996).
152. Okamoto, K. *et al.* Cryo-EM structure of a Marseilleviridae virus particle reveals a large internal microassembly. *Virology* **516**, 239–245 (2018).
153. Wulfmeyer, T. *et al.* Structural organization of DNA in chlorella viruses. *PLoS One* **7**, e30133 (2012).
154. Xiao, C. *et al.* Structural studies of the giant mimivirus. *PLoS Biol.* **7**, e92 (2009).
155. Marion, S., San Martín, C. & Šiber, A. Role of Condensing Particles in Polymer Confinement: A Model for Virus-Packed 'Minichromosomes'. *Biophys. J.* **113**, 1643–1653 (2017).
156. Evilevitch, A. *et al.* Effects of Salts on Internal DNA Pressure and Mechanical Properties of Phage Capsids. *J. Mol. Biol.* **405**, 18–23 (2011).
157. González-Huici, V., Salas, M. & Hermoso, J. M. The push-pull mechanism of bacteriophage Ø29

DNA injection. *Mol. Microbiol.* **52**, 529–540 (2004).

158. Carrasco, C. *et al.* DNA-mediated anisotropic mechanical reinforcement of a virus. *Proc. Natl. Acad. Sci.* **103**, 13706 LP – 13711 (2006).
159. Sae-Ueng, U. *et al.* Solid-to-fluid DNA transition inside HSV-1 capsid close to the temperature of infection. *Nat. Chem. Biol.* **10**, 861–867 (2014).
160. Grønbech-Jensen, N., Mashl, R. J., Bruinsma, R. F. & Gelbart, W. M. Counterion-Induced Attraction between Rigid Polyelectrolytes. *Phys. Rev. Lett.* **78**, 2477–2480 (1997).
161. Leforestier, A. & Livolant, F. Structure of toroidal DNA collapsed inside the phage capsid. *Proc. Natl. Acad. Sci.* **106**, 9157 LP – 9162 (2009).
162. Bloomfield, V. & Crothers, D. M. *Nucleic acids: structures, properties and functions*. (2000).
163. Vella, D., Ajdari, A., Vaziri, A. & Boudaoud, A. The indentation of pressurized elastic shells: from polymeric capsules to yeast cells. *J. R. Soc. Interface* **9**, 448–455 (2012).
164. Moreno-Herrero, F., Colchero, J. & Baró, A. M. DNA height in scanning force microscopy. *Ultramicroscopy* **96**, 167–174 (2003).
165. Lander, G. C. *et al.* DNA bending-induced phase transition of encapsidated genome in phage λ. *Nucleic Acids Res.* **41**, 4518–4524 (2013).
166. Comolli, L. R. *et al.* Three-dimensional architecture of the bacteriophage phi29 packaged genome and elucidation of its packaging process. *Virology* **371**, 267–277 (2008).
167. Chatterjee, P. K., Vayda, M. E. & Flint, S. J. Interactions among the three adenovirus core proteins. *J. Virol.* **55**, 379–386 (1985).
168. Zhang, Z. & Glotzer, S. C. Self-Assembly of Patchy Particles. *Nano Lett.* **4**, 1407–1413 (2004).
169. Denning, D. *et al.* Maturation of adenovirus primes the protein nano-shell for successful endosomal escape. *Nanoscale* **11**, 4015–4024 (2019).
170. Puntener, D. *et al.* Stepwise Loss of Fluorescent Core Protein V from Human Adenovirus during Entry into Cells . *J. VIROL.* **85**, 16 (2011).
171. Karen, K. A. & Hearing, P. Adenovirus Core Protein VII Protects the Viral Genome from a DNA Damage Response at Early Times after Infection. *J. Virol.* **85**, 4135–4142 (2011).
172. Davison, A. J., Benko, M. & Harrach, B. Genetic content and evolution of adenoviruses. *J. Gen. Virol.* **84**, 2895–2908 (2003).
173. Matthewst, D. A. & Russell, W. C. Adenovirus core protein V is delivered by the invading virus to the nucleus of the infected cell and later in infection is associated with nucleoli. *J. Gen. Virol.* **79**, 1671–1675 (1998).
174. Moyer, C. L. & Nemerow, G. R. Disulfide-bond formation by a single cysteine mutation in adenovirus protein VI impairs capsid release and membrane lysis. *Virology* **428**, 41–47 (2012).
175. Bauer, M., Gomez-Gonzalez, A., Suomalainen, M., Hemmi, S. & Greber, U. F. The E3 ubiquitin ligase Mind bomb 1 enhances nuclear import of viral DNA by inactivating a virion linchpin protein that suppresses exposure of virion pathogen-associated molecular patterns. *bioRxiv* 2020.08.29.242826 (2020) doi:10.1101/2020.08.29.242826.
176. Mateu, M. G. Mechanical properties of viruses analyzed by atomic force microscopy: A virological perspective. *Virus Res.* **168**, 1–22 (2012).
177. Llauró, A. *et al.* Cargo-shell and cargo-cargo couplings govern the mechanics of artificially loaded virus-derived cages. *Nanoscale* **8**, 9328–9336 (2016).
178. Kellermayer, M. S. Z., Vörös, Z., Csík, G. & Herényi, L. Forced phage uncorking: viral DNA ejection triggered by a mechanically sensitive switch. *Nanoscale* **10**, 1898–1904 (2018).

179. Zhao, X. & Tikoo, S. K. Deletion of pV affects integrity of capsid causing defect in the infectivity of bovine adenovirus-3. *J. Gen. Virol.* **97**, 2657–2667 (2016).

180. Marabini, R., Condezo, G. N., Gómez-Blanco, J. & Martín, C. S. Near Atomic Structure of an Atadenovirus Reveals a Conserved Capsid-Binding Motif and Intergenera Variations in Cementing Proteins. *bioRxiv* 2020.07.24.220046 (2020) doi:10.1101/2020.07.24.220046.

181. Ivanovska, I., Wuite, G., Jönsson, B. & Evilevitch, A. Internal DNA pressure modifies stability of WT phage. *Proc. Natl. Acad. Sci. U. S. A.* **104**, 9603–9608 (2007).

182. Michel, J. P. *et al.* Nanoindentation studies of full and empty viral capsids and the effects of capsid protein mutations on elasticity and strength. *Proc. Natl. Acad. Sci. U. S. A.* **103**, 6184–6189 (2006).

183. Teif, V. B. & Bohinc, K. Condensed DNA: Condensing the concepts. *Prog. Biophys. Mol. Biol.* **105**, 208–222 (2011).

184. Condell, O. *et al.* Efficacy of biocides used in the modern food industry to control salmonella enterica, and links between biocide tolerance and resistance to clinically relevant antimicrobial compounds. *Appl. Environ. Microbiol.* **78**, 3087–3097 (2012).

185. Russell, A. D. Biocide use and antibiotic resistance: The relevance of laboratory findings to clinical and environmental situations. *Lancet Infectious Diseases* vol. 3 794–803 (2003).

186. Maillard, J. Y. Virus susceptibility to biocides: An understanding. *Reviews in Medical Microbiology* vol. 12 63–74 (2001).

187. Mcdonnell, G., Russell, A. D., Operations, L. & Louis, S. *Antiseptics and Disinfectants: Activity, Action, and Resistance*. *CLINICAL MICROBIOLOGY REVIEWS* vol. 12 (1999).

188. Guthery, E., Seal, L. A. & Anderson, E. L. Zinc pyrithione in alcohol-based products for skin antisepsis: persistence of antimicrobial effects. *Am. J. Infect. Control* **33**, 15–22 (2005).

189. van Engelenburg, F. A. C., Terpstra, F. G., Schuitemaker, H. & Moorer, W. R. The virucidal spectrum of a high concentration alcohol mixture. *J. Hosp. Infect.* **51**, 121–125 (2002).

190. Macinga, D. R., Sattar, S. A., Jaykus, L. A. & Arbogast, J. W. Improved inactivation of nonenveloped enteric viruses and their surrogates by a novel alcohol-based hand sanitizer. *Appl. Environ. Microbiol.* **74**, 5047–5052 (2008).

191. Alhmidi, H. *et al.* Dissemination of a nonpathogenic viral DNA surrogate marker from high-touch surfaces in rooms of long-term care facility residents. *Am. J. Infect. Control* **45**, 1165–1167 (2017).

192. Rutala, W. A. & Weber, D. J. Selection of the Ideal Disinfectant. *Infect. Control Hosp. Epidemiol.* **35**, 855–865 (2014).

193. Kramer, A. *et al.* Virucidal activity of a new hand disinfectant with reduced ethanol content: comparison with other alcohol-based formulations. *J. Hosp. Infect.* **62**, 98–106 (2006).

194. Suchomel, M., Gnant, G., Weinlich, M. & Rotter, M. Surgical hand disinfection using alcohol: the effects of alcohol type, mode and duration of application. *J. Hosp. Infect.* **71**, 228–233 (2009).

195. Gaonkar, T. A., Geraldo, I., Shintre, M. & Modak, S. M. In vivo efficacy of an alcohol-based surgical hand disinfectant containing a synergistic combination of ethylhexylglycerin and preservatives. *J. Hosp. Infect.* **63**, 412–417 (2006).

196. Rajasekaran, P., Kannan, H., Das, S., Young, M. & Santra, S. Comparative analysis of copper and zinc based agrichemical biocide products: materials characteristics, phytotoxicity and in vitro antimicrobial efficacy. *AIMS Environ.*

Sci. **3**, 439–455 (2016).

197. Gonçalves, K. de J., Graziano, K. U. & Kawagoe, J. Y. Revisão sistemática sobre antissepsia cirúrgica das mãos com preparação alcoólica em comparação aos produtos tradicionais . *Revista da Escola de Enfermagem da USP* vol. 46 1484–1493 (2012).
198. Ytreberg, E., Karlsson, J. & Eklund, B. Comparison of toxicity and release rates of Cu and Zn from anti-fouling paints leached in natural and artificial brackish seawater. *Sci. Total Environ.* **408**, 2459–2466 (2010).
199. Maillard, J.-Y., Beggs, T. S., Day, M. J., Hudson, R. A. & Russell, A. D. Effects of biocides on the transduction of Pseudomonas aeruginosa PAO by F116 bacteriophage. *Lett. Appl. Microbiol.* **21**, 215–218 (1995).
200. Elnifro, E. M., Cooper, R. J., Klapper, P. E. & Bailey, A. S. PCR and restriction endonuclease analysis for rapid identification of human adenovirus subgenera. *J. Clin. Microbiol.* **38**, 2055–2061 (2000).
201. Ijaz, M. K. & Rubino, J. Should Test Methods for Disinfectants Use Vertebrate Viruses Dried on Carriers to Advance Virucidal Claims? *Infect. Control Hosp. Epidemiol.* **29**, 192–194 (2008).
202. Kampf, G. Efficacy of ethanol against viruses in hand disinfection. *J. Hosp. Infect.* **98**, 331–338 (2018).
203. Aich, P. *et al.* M-DNA: A complex between divalent metal ions and DNA which behaves as a molecular wire. *J. Mol. Biol.* **294**, 477–485 (1999).
204. De Souza, J. R., De Castro, C. S. P. & Bloch, C. Zinc Binding to Lambda Phage DNA Studied by Voltammetric Techniques. *J. Braz. Chem. Soc.* **11**, 398–404 (2000).
205. Labiuk, S. L., Delbaere, L. T. J. & Lee, J. S. Cobalt(II), nickel(II) and zinc(II) do not bind to intra-helical N(7) guanine positions in the B-form crystal structure of d(GGCGCC). *J. Biol. Inorg. Chem.* **8**, 715–720 (2003).
206. Labiuk, S. L., Delbaere, L. T. J. & Lee, J. S. Gamma and Ultraviolet Radiation Cause DNA Crosslinking in the Presence of Metal Ions at High pH¶. *Photochem. Photobiol.* **73**, 579 (2001).
207. Roos, W. H., Ivanovska, I. L., Evilevitch, A. & Wuite, G. J. L. Viral capsids: Mechanical characteristics, genome packaging and delivery mechanisms. *Cell. Mol. Life Sci.* **64**, 1484–1497 (2007).
208. Carrasco, C. *et al.* Built-in mechanical stress in viral shells. *Biophys. J.* **100**, 1100–1108 (2011).
209. Greber, U. F. Virus and Host Mechanics Support Membrane Penetration and Cell Entry. *J. Virol.* **90**, 3802–3805 (2016).
210. Hernando-Pérez, M., Lambert, S., Nakatani-Webster, E., Catalano, C. E. & de Pablo, P. J. Cementing proteins provide extra mechanical stabilization to viral cages. *Nat. Commun.* **5**, 4520 (2014).

APPENDICES

APPENDIX 1: Supplementary information of Chapter 4

A.1.1 Probabilistic Markovian model description

The objective of this section is to develop a model that allows us to reproduce the results obtained as well as to make estimates on certain physical properties related to the capsomers and the virus itself. First of all, it is important to identify which are the experimental data to which we have access. In this work we have the penton population as a function of the number, n, of images taken over the experiment. As mentioned in Chapter 4, the statistical treatment of the escape events (in terms of n) results reveals that the process of escape has memory as the escape events become more frequent once some penton is lost. This behaviour complicates the theoretical treatment. By contrast, when we discern between successive penton escape events and study the statistics of the lag-time between events, we find out survival probability distributions compatible with Poissonian memory-less processes from which we obtain the escape rates associated to each penton, in chronological order. This fact allows us to use the standard tools of Markovian process to develop a theoretical model. The possibility of using these tools, which are frequently used in a wide variety of problems, greatly simplifies the development of the model.

We separately consider the survival times for the first, second and third penton; taking the survival "time" (in image units) as the difference

between successive events (e.g. between the second and first escape event). The theoretical model introduces profile of the AFM indentation force overtime, F(t), to reproduce experimental data. Each data set is then classified according to the number of pentons previously lost and the maximal AFM force F. In order to reproduce the experimental data, the theoretical model should reconstruct each step of the image acquisition process, which is composed of three parts: first, each individual pixel (or indentation) is resolved; second, many individual pixels are combined to conform an image (which is the experimental unit) and third, many images are taken before an escape event is observed. We calculate the probability of losing a penton over each step of the whole process.

Aside from the temporal evolution of the process, we need to consider some spatial details of the indentation. We consider two possible cases: i) the indentation touches an area which "stimulates" a penton or ii) it touches a region which does disturb the penton. In the first case, we consider that certain work "W" is applied to the penton, while in the latter case the applied work is zero. The latter case, moreover, includes two subgroups: indentations outside the capsid (on the substrate) and indentations in a region of the capsid which has already lost its penton. By inspecting many experimental images, we calculate the average fraction of image covered by the capsid, which is noted as the parameter ν. Moreover, if the indentation is performed on the area of a penton that has been previously lost, we assume that such indentation will not stimulate the

remaining pentons, due to the local nature of the indentation process. Within the capsid domain, the fraction of the image which corresponds to the "region of influence" of an exposed penton, is noted as $\rho_i \nu$, where ρ_i is the fraction of remaining exposed pentons. Since there are three pentons exposed to the AFM tip (Figure 4.1), this parameter will take the values ρ_1 =1, when no penton has been lost, ρ_2=2/3 when one penton has left the virus and finally ρ_3=1/3 when only one penton remains. Let P^{out} be the probability of losing a penton even if the indentation does not "touch" the penton, and P^{in} the probability of losing a penton after "touching" it with the AFM tip, then, the total probability of losing the "i-th" penton after resolving one pixel is,

$$B_i \coloneqq (1-\nu)P^{out} + \left(\rho_i P^{in} + (1-\rho_i)P^{out}\right) \quad (1)$$

We now deduce the form of P^{out} and P^{in} and integrate over pixels and images to derive the probability of losing the "i-th" penton after a number n of images. This is precisely the quantity amenable for comparison with experiments.

A.1.1.1 Two state Markovian continuous model for the indentation process

The master equation for the probability for the pentons being in the "free" (unbonded) state at time t, $P_f(t)$, is equivalent to a first order kinetic reaction. The rate of increase of free pentons is proportional to the escape rate α(t) times the probability of being bounded, 1-$P_f(t)$,

$$dP_f(t) = \alpha(t)\left(1 - P_f(t)\right)dt \quad (2)$$

To solve Eq. (2), we need to evaluate the transition rate α(t). To this end we need to consider the location of the indentation. The case "indentation out" corresponds to the AFM tip not perturbing the penton (either because the AFM tip touches the substrate or avoid in the capsid without pentons). In such case we set $\alpha(t) = \alpha_0$, i.e. the spontaneous escape rate, which is related to the free energy barrier ΔG by the Kramer relation previous described above,

$$\alpha(t) = \alpha_0 = \omega_0 \exp[-\Delta G/k_B T] \quad \text{(indentation ``out'')} \quad (3)$$

Integrating the master equation Eq. (2) leads to the probability of escaping after a single indentation which is "outside" the penton domain,

$$P_f^{out}(T) = 1 - \exp(-\alpha_0 T) \quad (4)$$

where T denotes the time required for one indentation (10 ms). Second, if the indentation stimulates the penton domain (we denote this case as "in"), the tip introduces some mechanical work "W" which increases the escape rate as,

$$\alpha(t) = \omega_0 \exp\left[-\left(\Delta G - W(t)\right)/k_B T\right] = \alpha_0 \exp[W(t)/k_B T] \quad \text{(indentation ``in'')} \quad (5)$$

The "in" scenario requires a more detailed analysis. Integration of the master equation Eq. (2) using Eq. (5) leads to

$$P_f^{in}(t) = 1 - \exp\left(-\int_0^t \alpha(t)dt'\right) = 1 - \exp\left(-\alpha_0 \int_0^t \exp(W(t')/k_B T)dt'\right) \quad (6)$$

To proceed with the integration of the exponent we first examine the profile of the indentation force as a function of time (**Figure 4.5**). This profile has been measured experimentally and it has a form like a top-hat function with five different steps. In the initial step (1), the tip approaches the sample and the applied force zero; this "free-force" step has a duration t_F. Upon contact, (2)

the force increases linearly in time until it reaches the maximum (set point) force "F". The elapsed time during this "ramp" step is t_R. The force F is then held fixed for a "contact" time t_C and the rest of the process follows similarly in inverse order: force ramp back to zero (4) and tip moving away from the sample (5). The total time needed for a single indentation is thus, $T= 2t_F + 2t_R + t_C$. As a function of time the applied force, F(t), is a piecewise function,

$$\hat{F}(t) = \begin{cases} 0, & \text{if } 0 \leq t < t_F. \\ F\left(\frac{t-t_F}{t_R}\right), & \text{if } t_F \leq t < t_F + t_R. \\ F, & \text{if } t_F + t_R \leq t < t_F + t_R + t_C. \\ -F\left(\frac{t-t_F-2t_R-t_C}{t_R}\right), & \text{if } t_F + t_R + t_C \leq t < t_F + 2t_R + t_C. \\ 0, & \text{if } t_F + 2t_R + t_C \leq t < 2t_F + 2t_R + t_C. \end{cases} \quad (7)$$

where the duration of each step depends, in turn, on the maximum force F and can be determined experimentally,

$$t_{Free}^{(1)} = t_{Free}^{(2)} \equiv t_F = 0.00588 - 0.00000078F$$

$$t_{Ramp}^{(1)} = t_{Ramp}^{(2)} \equiv t_R = 0.00000088 - 0.00000041F \quad (8)$$

$$t_{Contact}^{(1)} \equiv t_C = 0.00076 - 0.000000077F$$

The next piece of information requires some relation between the applied work and the force as explained above.

We first perform the integrals appearing in the exponents of Eq. (6), for each one of the 5 time-intervals of the indentation process, (we define $\beta = 1/k_BT$),

$$I_1(t_0, t_1) = I_5(t_0, t_1) = \int_{t_0}^{t_1} \exp(0)\, dt = (t_1 - t_0)$$

$$I_2(t_0, t_1) = \int_{t_0}^{t_1} \exp\left(\frac{t - t_1}{t_R}\beta Fr\right) dt$$

$$= \frac{t_R}{\beta Fr}\left(\exp\left[\beta Fr\left(\frac{t_1 - t_F}{t_R}\right)\right] - \exp\left[\beta Fr\left(\frac{t_0 - t_F}{t_R}\right)\right]\right)$$

$$I_3(t_0, t_1) = (t_1 - t_0)\exp(\beta Fr)$$

$$I_4(t_0,t_f)=\int_{t_0}^{t_1}\exp\left(\frac{t-2t_F-2t_R-t_C}{t_R}\beta Fr\right)dt$$
$$=-\frac{t_R}{\beta Fr}\left(\exp\left[-\beta Fr\left(\frac{t_1-2t_F-2t_R-t_C}{t_R}\right)\right]\right.$$
$$\left.-\exp\left[-\beta Fr\left(\frac{t_0-2t_F-2t_R-t_C}{t_R}\right)\right]\right) \quad (9)$$

Using these integrals, the probability of encountering a free penton over time results in the following piecewise function,

$$P_f(t)=\begin{cases}1-e^{-\alpha_0 I_1(0,t)}, & \text{if } 0\le t<t_F.\\ 1-e^{-\alpha_0(I_1(0,t_F)+I_2(t_F,t))}, & \text{if } t_F\le t<t_F+t_R.\\ 1-e^{-\alpha_0(I_1(0,t_F)+I_2(t_F,t_F+t_R)+I_3(t_F+t_R,t))}, & \text{if } t_F+t_R\le t<t_F+t_R+t_C.\\ 1-e^{-\alpha_0(I_1(0,t_F)+I_2(t_F,t_F+t_R)+I_3(t_F+t_R,t_F+t_R+t_C)+I_4(t_F+t_R+t_C,t))}, & \text{if } t_F+t_R+t_C\le t<t_F+2t_R+t_C.\\ 1-e^{-\alpha_0(I_1(0,t_F)+I_2(t_F,t_F+t_R)+I_3(t_F+t_R,t_F+t_R+t_C)+I_4(t_F+t_R+t_C,t_F+2t_R+t_C)+I_5(t_F+2t_R+t_C,t))}, & \text{if } t_F+2t_R+t_C\le t<2t_F+2t_R+t_C.\end{cases}$$
(10)

We are interested in evaluating this expression at t = T =$2t_F + 2t_R + t_C$, that is, after the total time-lapse of a single indentation cycle. This yields the probability of losing a penton in a single indentation performed "in" a pentamer domain,

$$P^{in}\equiv P_f^{in}(T)=-\exp\left(-\alpha_0\left(\exp\left(\frac{Fr}{\beta}\right)t_C+\left(\frac{\beta}{Fr}\right)\left(\exp\left(\frac{Fr}{\beta}\right)-1\right)2t_R+2t_F\right)\right) \quad (11)$$

In the second model the work added to the system is given by $W(t)=\left(\frac{1}{2}\right)F^2/k$ and a similar procedure leads to

$$P^{in}\equiv P_f^{in}(T)=1-\exp\left(-\alpha_0\left(\exp\left(\frac{F^2}{2k}\frac{1}{\beta}\right)t_C+\sqrt{\frac{2\pi k}{F^2}}\beta\,\mathrm{erfi}\left(\sqrt{\frac{F^2}{2k}}\frac{1}{\beta}\right)t_R+2t_F\right)\right) \quad (12)$$

As in Eq. (1), collecting the spatial details of the indentation (AFM tip either "in" or "out") leads to the total probability for penton unbinding during a single indentation,

$$B_i\coloneqq(1-\nu)P^{out}+\left(\rho_i P^{in}+(1-\rho_i)P^{out}\right) \quad (13)$$

where $\rho_i=(4-i)/3$ is the fraction of remaining pentons in the capsid-area facing the AFM, with i=1 (intact capsid), i=2 (one penton is lost) and i=3 (two pentons are lost).

A.1.1.2 Two state Markovian discrete model for the image acquisition process

We can follow a similar procedure to model the image acquisition process under the hypothesis that we are dealing with a Markov process. In the present case we are facing a discrete case, since we are interested in the escape probability as a function of the number of pixels we are indenting, unlike the previous case, in which we were interested in the evolution of the probability as a function of time. In this case we introduce the stochastic transition matrix, of the process,

$$\begin{pmatrix} 1-B & B \\ 0 & 1 \end{pmatrix} \quad (14)$$

The evolution of the discrete process can be written in terms of this matrix,}

$$\begin{bmatrix} P^{p+1}_{bonded} & P^{p+1}_{free} \end{bmatrix} = \begin{bmatrix} P^{p}_{bonded} & P^{p}_{free} \end{bmatrix} \begin{pmatrix} 1-B & B \\ 0 & 1 \end{pmatrix} \quad (15)$$

which tell us the probability of each state after resolving the pixel number p. If the initial state is

$$\begin{bmatrix} P^{0}_{bonded} & P^{0}_{free} \end{bmatrix} = \begin{bmatrix} 1 & 0 \end{bmatrix} \quad (16)$$

the probabilities of each state after having performed m indentations will be given by

$$\begin{bmatrix} 1 & 0 \end{bmatrix} \underbrace{\begin{pmatrix} 1-B & B \\ 0 & 1 \end{pmatrix} \cdots \begin{pmatrix} 1-B & B \\ 0 & 1 \end{pmatrix}}_{\text{m times}} = \begin{bmatrix} 1 & 0 \end{bmatrix} \begin{pmatrix} 1-B & B \\ 0 & 1 \end{pmatrix}^m = \begin{bmatrix} P^m_{bonded} & P^m_{free} \end{bmatrix} \quad (17)$$

we can compute the n power of the stochastic matrix,

$$\begin{pmatrix} 1-B & B \\ 0 & 1 \end{pmatrix}^m = \begin{pmatrix} (1-B)^m & 1-(1-B)^m \\ 0 & 0 \end{pmatrix} \quad (18)$$

so the probability of losing a penton after m indentations is

$$p(m) = 1-(1-B)^m \quad (19)$$

In deriving this expression, we assume that the pixels are taken at random locations, which is not strictly true because during a single image, the pixelation follows a well-defined order. However, this point is not crucial because we are interested in the probability of having lost a penton after having passed all the pixels M of the image. The large number of pixels per image (M = 128 x 128) indicates that above expression is appropriate. Taking all into account we obtain that the probability of losing a penton after having taken one image (i.e. M pixels) is

$$C \coloneqq p(M) = 1-(1-B)^M \quad (20)$$

moreover, because of M being a large number, this expression can be approximated by,

$$C \coloneqq 1-(1-B)^M \simeq 1-\exp(-BM) \quad (21)$$

which is easier to work with. Finally, the probability of releasing the "i-th" pentamer after a single image is

$$C_i \coloneqq 1-\exp(-B_i M) \quad (22)$$

A.1.1.3 Two state Markovian discrete model for collection of images

The last step is to compute the release probability after a number n of images. This is the information we can compare with experiments. The situation is formally analogous to the previous case and following a similar approach we arrive to,

$$P_i(n) \coloneqq 1 - (1 - C_i)^n \quad (23)$$

which is the expression introduced in the main text: the probability of losing the “ith” penton after having acquired “n” images (importantly: “n” starts to be counted since the previous penton is lost).

APPENDIX 2: Supplementary information of Chapter 8

A.2.1 Determination of virucidal activity

The BS EN 14476 quantitative virucidal suspension test (BS EN 14476:2013+A2:2019) in clean condition, i.e. with sterile hard water as the only interfering substance and without organic load, was carried out against HAdV2. Briefly, 500 µl of test viruses were prepared by adding 340 µl of HAdV2 stock suspension (10^9 PFU/ml) to 160 µl of distilled water. One hundred µl of the test HAdV2 was then added to 900 µl of formulation. After 60 min, 100 µl of test viral suspension was added to a Microspin S-200 HR size-exclusion chromatography column (GE, UK) to quench the activity of the formulation activity and to reduce host cell cytotoxicity. Then, 100 µl of the mixture were serially diluted in 900 µl purified water (1:10 serial dilutions). Each dilution (100 µl) was added to wells of 24 tissue culture plates containing with 70-80% confluence HeLa cells monolayer. The infective virus concentration was determined by Spearman-Kaeber method, 6 and 7 days post-infection. Reduction in infectivity is expressed as PFU/ml which relate to the number of infectious particles.

A.2.2 Viral DNA extraction, quantification, analysis of DNA damage

The DNA analysis post viral treatment method described in Maillard et al. (Maillard et al., 1995) was adapted for HAdV2. Twenty µl of purified HAdV2 suspension (10^9 PFU/ml) was added to 80 µl of each formulation for 2 h at 25°C. Control consisted of replacing the suspension with PBS. HAdV2 DNA was

extracted and purified using a high pure viral nucleic acid kit (Roche, Switzerland). Briefly, 200 µl of binding buffer supplemented with 50 µl proteinase K and poly(A)(Roche, Switzerland) was added to the treated virus suspension and incubated at 72^{o}C for 15 min. The mixture was then added to a high pure filter column and centrifuged three times at 8,000g for 1 min, with flow-through being discarded after each centrifugation cycle. The column was then washed twice with 450 µl of wash buffer (Roche, Switzerland). Elution of HAdV2 dsDNA occurred by adding 40 µl of elution buffer and centrifugation at 13,000g for 1 min. Viral DNA was stored at -20^{o}C until analysis by electrophoresis. Then 150 ng of purified viral dsDNA was mixed with 5 µl of gel loading buffer and loaded on 1.2% (w/v) agarose gel in TBE buffer with SYBR Safe DNA gel stain (ThermoFischer, United Kingdom). The lambda DNA/HindIII marker size profile was used.

Purified HAdV2 dsDNA was digested separately by SmaI and AatII restriction enzymes (Thermo Scientific, Germany) in order to evaluate more specifically potential damage to viral nucleic acid caused by formulations. After digestion, electrophoresis was performed on a 2% (w/v) agarose gel in TBE buffer at 100 V for 1 h and 30 min. Viral dsDNA bands were visualised as described earlier.

LIST OF PUBLICATIONS

- **Martín-González, N**., Hernando-Pérez, M., Condezo, G. N., Pérez-Illana, M., Šiber, A., Reguera, D., Ostapchuk, P., Hearing, P., San Martín, C. & de Pablo, P. J. (2019). Adenovirus major core protein condenses DNA in clusters and bundles, modulating genome release and capsid internal pressure. *Nucleic Acids Research*, *47*(17), 9231-9242.

- **Martín-González, N**., Darvas, S. M. G., Durana, A., Marti, G. A., Guérin, D. M., & De Pablo, P. J. (2018). Exploring the role of genome and structural ions in preventing viral capsid collapse during dehydration. *Journal of Physics: Condensed Matter*, *30*(10), 104001.

- **Martín-González, N**., Vieira Gonçalves, L., Condezo, G., San Martín, C., Rubiano, M., Fallis, I., Rubino, J. R., Khalid Ijaz, M., Maillard, J-Y. & De Pablo, P. J. (2020). Virucidal action mechanism of alcohol and divalent cations against human adenovirus. *Frontiers in Molecular Biosciences*, *7*, 426.

- **Martín-González, N**, Ibáñez Freire P., Ortega-Esteban, A., Laguna-Castro, M., San Martín, C., Valbuena, A., Delgado Buscalioni, R. & De Pablo, P. J. Long range cooperative disassembly revealed by aging during adenovirus uncoating. Under review.

- **Martín-González, N.,** Gómez-González, A., Greber, U. F., Hemmi, S., San Martín, C. & De Pablo, P. J. Protein V helps the extrication of human adenovirus core in uncoating. In preparation.

- **Martín-González, N**., Pérez-Illana, M., Hernando-Pérez, M., Condezo, G., Gallardo, J., Menéndez, M., San Martín, C. & De Pablo, P. J. Acidification induces condensation of the adenovirus core. In preparation.

- **Martín-González, N**., Ortega-Esteban, A., Moreno-Madrid, F., Llauró, A., Hernando-Pérez, M., & de Pablo, P. J. (2018). Atomic force

microscopy of protein shells: virus capsids and beyond. In *Single Molecule Analysis* (pp. 281-296). Humana Press, New York, NY.

- Ortega-Esteban, Á., **Martín-González, N**., Moreno-Madrid, F., Llauró, A., Hernando-Pérez, M., San Martín, C., & de Pablo, P. J. (2019). Structural and Mechanical Characterization of Viruses with AFM. In *Atomic Force Microscopy* (pp. 259-278). Humana Press, New York, NY.

- Hernando-Pérez, M., **Martín-González, N**., Pérez-Illana, M., Suomalainen, M., Condezo, G. N., Ostapchuk, P., Gallardo, J., Menéndez, M., Greber, U. F., Hearing, P., de Pablo, P. J. & San Martín, C. (2020). Dynamic competition for hexon binding between core protein VII and lytic protein VI promotes adenovirus maturation and entry. *Proceedings of the National Academy of Sciences.* 117 (24) 13699-13707.

- Moreno-Madrid, F., **Martín-González, N**., Llauró, A., Ortega-Esteban, A., Hernando-Pérez, M., Douglas, T., ... & de Pablo, P. J. (2017). Atomic force microscopy of virus shells. *Biochemical Society Transactions*, *45*(2), 499-511.

- Condezo, G, **Martín-González, N.**, Pérez-Illana, M., Hernando-Pérez, M., Gallardo, J., San Martín, C. (2020) Adenoviruses and their structural relatives. *Reference Module in Life Sciences, Elsevier,* ISBN 9780128096338

In the following pages the abstract of the publications is shown for more information about the related projects of the thesis.

Adenovirus major core protein condenses DNA in clusters and bundles, modulating genome release and capsid internal pressure

Martín-González, N., *Hernando-Pérez, M., Condezo, G. N., Pérez-Illana, M., Šiber, A., Reguera, D., Ostapchuk, P., Hearing, P., San Martín, C. & de Pablo, P. J.*

Abstract

Some viruses package dsDNA together with large amounts of positively charged proteins, thought to help condense the genome inside the capsid with no evidence. Further, this role is not clear because these viruses have typically lower packing fractions than viruses encapsidating naked dsDNA. In addition, it has recently been shown that the major adenovirus condensing protein (polypeptide VII) is dispensable for genome encapsidation. Here, we study the morphology and mechanics of adenovirus particles with (Ad5-wt) and without (Ad5-VII-) protein VII. Ad5-VII- particles are stiffer than Ad5-wt, but DNAcounterions revert this difference, indicating that VII screens repulsive DNA-DNA interactions. Consequently, its absence results in increased internal pressure. The core is slightly more ordered in the absence of VII and diffuses faster out of Ad5-VII– than Ad5-wt fractured particles. In Ad5-wt unpacked cores, dsDNA associates in bundles interspersed with VII-DNA clusters. These results indicate that protein VII condenses the adenovirus genome by combining direct clustering and promotion of bridging by other core proteins. This condensation modulates the virion internal pressure and DNA release from disrupted particles, which could be crucial to keep the genome protected inside the semi-disrupted capsid while traveling to the nuclear pore.

Exploring the role of genome and structural ions in preventing viral capsid collapse during dehydration

***Martín-González, N**., Darvas, S. M. G., Durana, A., Marti, G. A., Guérin, D. M., & De Pablo, P. J.*

Abstract

Even though viruses evolve mainly in liquid milieu, their horizontal transmission routes often include episodes of dry environment. Along their life cycle, some insect viruses, such as viruses from the Dicistroviridae family, withstand dehydrated conditions with presently unknown consequences to their structural stability. Here, we use atomic force microscopy to monitor the structural changes of viral particles of Triatoma virus (TrV) after desiccation. Our results demonstrate that TrV capsids preserve their genome inside, conserving their height after exposure to dehydrating conditions, which is in stark contrast with other viruses that expel their genome when desiccated. Moreover, empty capsids (without genome) resulted in collapsed particles after desiccation. We also explored the role of structural ions in the dehydration process of the virions (capsid containing genome) by chelating the accessible cations from the external solvent milieu. We observed that ion suppression helps to keep the virus height upon desiccation. Our results show that under drying conditions, the genome of TrV prevents the capsid from collapsing during dehydration, while the structural ions are responsible for promoting solvent exchange through the virion wall.

Virucidal action mechanism of alcohol and divalent cations against human adenovirus.

***Martín-González, N**., Vieira Gonçalves, L., Condezo, G., San Martín, C., Rubiano, M., Fallis, I., Rubino, J. R., Khalid Ijaz, M., Maillard, J-Y. & De Pablo, P. J.*

Abstract

Hygiene and disinfection practices play an important role at preventing spread of viral infections in household, industrial and clinical settings. Although formulations based on >70% ethanol are virucidal, there is a currently a need to reformulate products with much lower alcohol concentrations. It has been reported that zinc can increase the virucidal activity of alcohols, although the reasons for such potentiation is unclear. One approach in developing virucidal formulations is to understand the mechanisms of action of active ingredients and formulation excipients. Here, we investigated the virucidal activity of alcohol (40% w/v) and zinc sulfate (0.1% w/v) combinations and their impact on a human adenovirus (HAdV) using, nucleic acid integrity assays, atomic force microscopy (AFM) and transmission electron microscopy (TEM). We observed no difference in virucidal activity (5 log_{10} reduction in 60 min) against between an ethanol only based formulation and a formulation combining ethanol and zinc salt. Furthermore, TEM imaging showed that the ethanol only formulation produced gross capsid damage, whilst zinc-based formulation or formulation combining both ethanol and zinc did not affect HAdV DNA. Unexpectedly, the addition of nickel salt (5 mM $NiCl_2$) to the ethanol-zinc formulation contributed to a weakening of the capsid and alteration of the capsid mechanics exemplified by AFM imaging, together with structural capsid damage. The addition of zinc sulfate to the ethanol formulation did not add the formulation efficacy, but the unexpected mechanistic synergy between $NiCl_2$ and the ethanol formulation opens an interesting perspective for the possible potentiation of an alcohol-based formulation. Furthermore, we show that AFM can be an important tool for understanding the mechanistic impact of virucidal formulation.

Long range cooperative disassembly revealed by aging during adenovirus uncoating

Martín-González, N, *Ibáñez Freire P., Ortega-Esteban, A., Laguna-Castro, M., San Martín, C., Valbuena, A., Delgado Buscalioni, R. &* *De Pablo, P. J.*

Abstract

Icosahedral virus capsids are closed shells built up with a hexagonal lattice of proteins, which incorporate pentamers at their fivefold vertices. Human adenovirus particles lose pentamers (pentons) during infection under a variety of physicochemical cues, including mechanical pulling of molecular motors and the viscous drag of the cytoplasm. By combining Atomic Force Microscopy experiments with survival analysis and Markovian transition state theory, we investigate the sequence of adenovirus penton disassembly that reveals the aging of the virus structure. We show evidence that the lifetime of pentons gradually decreases, accompanied by capsid softening as neighboring pentons are lost. This cooperative dismantling process, which involves first neighbor penton-penton distances of at least 45 nm, leads to a 50% increase in the virus disassembling rate of the virus particle. Theory and experiments fit remarkably well, allowing us to obtain the spontaneous escape rate and the energy barrier of penton disassembly (~30 k_BT). The observed increase in the penton's loss rate reveals long-ranged structural correlations within the capsid. Our estimations suggest that the mechanical cues arising from the strokes of protein-motors carrying the virus to the nucleus, could help penton disassembly and warrant the timely delivery of weak enough capsids for adenovirus infection.

Protein V helps the extrication of human adenovirus core in uncoating.

Martín-González, N., *Gómez-González, A., Greber, U. F., Hemmi, S., San Martín, C. &* *De Pablo, P. J*

Abstract

Human Adenovirus packs its genome with the help of histone-like proteins, such as V, μ and VII. Here we explore the biophysical role of protein V by studying the mechanical properties of Ad5 particles with (Ad5-wt) and without (Ad5-ΔV) core protein V with Atomic Force Microscopy. We find that Ad5-ΔV particles are softer and less brittle than Ad5-wt. After cracking the particles with both single and mechanical fatigue assays, our experiments indicate that the material of the core escapes faster from wild type than ΔV structures. In the particles lacking protein V, the core seems to be more condensed and does not readily dissociate from the virion after mechanical capsid disruption. Altogether, these results suggest that protein V reduces the condensation of the Ad5 genome inside the capsid and facilitates its release once the capsid has been disrupted.

Acidification induces condensation of the adenovirus core

***Martín-González, N**., Pérez-Illana, M., Hernando-Pérez, M., Condezo, G., Gallardo, J., Menéndez, M., San Martín, C. & De Pablo, P. J*.

Abstract

The adenovirus (AdV) icosahedral capsid encloses a nucleoprotein core formed by the dsDNA genome bound to numerous copies of virus-encoded, positively charged proteins. For an efficient delivery of its genome, AdV must undergo a cascade of dismantling events from the plasma membrane to the nuclear pore. Throughout this uncoating process, the virion moves across potentially disruptive environments whose influence in particle stability is poorly understood. In this work we analyze the effect of acidic conditions on AdV particles by exploring their mechanical properties, genome accessibility and capsid disruption. Our results show that under short term acidification the AdV virion becomes softer and its genome less accessible to an intercalating dye, even in the presence of capsid openings. The AFM tip penetrates deeper in virions at neutral pH, and mechanical properties of genome-less particles are not altered upon acidification. Altogether, these results indicate that the main effect of acidification is the compaction of the nucleoproteic core, revealing a previously unknown role for chemical cues in adenovirus uncoating.

Atomic force microscopy of protein shells: virus capsids and beyond.

***Martín-González, N**., Ortega-Esteban, A., Moreno-Madrid, F., Llauró, A., Hernando-Pérez, M., & de Pablo, P. J.*

Abstract

In Atomic Force Microscopy (AFM) the probe is a nanometric tip located at the end of a microcantilever which palpates the specimen under study as a blind person uses a white cane. In this way AFM allows obtaining nanometric resolution images of individual protein shells, such as viruses, in liquid milieu. Beyond imaging, AFM also enables the manipulation of single protein cages, and the characterization a variety physicochemical properties able of inducing any measurable mechanical perturbation to the microcantilever that holds the tip. In this chapter we start revising some recipes for adsorbing protein shells on surfaces. Then we describe several AFM approaches to study individual protein cages, ranging from imaging to spectroscopic methodologies devoted to extracting physical information, such as mechanical and electrostatic properties.

Structural and Mechanical Characterization of Viruses with AFM

*Ortega-Esteban, Á., **Martín-González, N**., Moreno-Madrid, F., Llauró, A., Hernando-Pérez, M., San Martín, C., & de Pablo, P. J.*

Abstract

Microscopes are used to characterize small objects with the help of probes that interact with the specimen, such as photons and electrons in optical and electron microscopies, respectively. In atomic force microscopy (AFM) the probe is a nanometric tip located at the end of a micro cantilever which palpates the specimen under study as a blind person manages a walking stick. In this way AFM allows obtaining nanometric resolution images of individual protein shells, such as viruses, in liquid milieu. Beyond imaging, AFM also enables not only the manipulation of single protein cages, but also the characterization of every physicochemical property able of inducing any measurable mechanical perturbation to the microcantilever that holds the tip. In this chapter we start revising some recipes for adsorbing protein shells on surfaces. Then we describe several AFM approaches to study individual protein cages, ranging from imaging to spectroscopic methodologies devoted for extracting physical information, such as mechanical and electrostatic properties. We also explain how a convenient combination of AFM and fluorescence methodologies entails monitoring genome release from individual viral shells during mechanical unpacking.

Dynamic competition for hexon binding between core protein VII and lytic protein VI promotes adenovirus maturation and entry

*Hernando-Pérez, M., **Martín-González, N**., Pérez-Illana, M., Suomalainen, M., Condezo, G. N., Ostapchuk, P., Gallardo, J., Menéndez, M., Greber, U. F., Hearing, P., de Pablo, P. J. & San Martín, C.*

Abstract

Adenovirus minor coat protein VI contains a membrane-disrupting peptide that is inactive when VI is bound to hexon trimers. Protein VI must be released during entry to ensure endosome escape. Hexon:VI stoichiometry has been uncertain, and only fragments of VI have been identified in the virion structure. Recent findings suggest an unexpected relationship between VI and the major core protein, VII. According to the high-resolution structure of the mature virion, VI and VII may compete for the same binding site in hexon; and noninfectious human adenovirus type 5 particles assembled in the absence of VII (Ad5-VII-) are deficient in proteolytic maturation of protein VI and endosome escape. Here we show that Ad5-VII- particles are trapped in the endosome because they fail to increase VI exposure during entry. This failure was not due to increased particle stability, because capsid disruption happened at lower thermal or mechanical stress in Ad5-VII- compared to wild-type (Ad5-wt) particles. Cryoelectron microscopy difference maps indicated that VII can occupy the same binding pocket as VI in all hexon monomers, strongly arguing for binding competition. In the Ad5-VII- map, density corresponding to the immature amino-terminal region of VI indicates that in the absence of VII the lytic peptide is trapped inside the hexon cavity, and clarifies the hexon:VI stoichiometry conundrum. We propose a model where dynamic competition between proteins VI and VII for hexon binding facilitates the complete maturation of VI, and is responsible for releasing the lytic protein from the hexon cavity during entry and stepwise uncoating.

Atomic force microscopy of virus shells

*Moreno-Madrid, F., **Martín-González, N**., Llauró, A., Ortega-Esteban, A., Hernando-Pérez, M., Douglas, T., ... & de Pablo, P. J.*

Abstract

Microscopes are used to characterize small objects with the help of probes that interact with the specimen, such as photons and electrons in optical and electron microscopies, respectively. In atomic force microscopy (AFM), the probe is a nanometric tip located at the end of a microcantilever which palpates the specimen under study just as a blind person manages a walking stick. In this way, AFM allows obtaining nanometric resolution images of individual protein shells, such as viruses, in a liquid milieu. Beyond imaging, AFM also enables not only the manipulation of single protein cages, but also the characterization of every physicochemical property capable of inducing any measurable mechanical perturbation to the microcantilever that holds the tip. In the present revision, we start revising some recipes for adsorbing protein shells on surfaces. Then, we describe several AFM approaches to study individual protein cages, ranging from imaging to spectroscopic methodologies devoted to extracting physical information, such as mechanical and electrostatic properties. We also explain how a convenient combination of AFM and fluorescence methodologies entails monitoring genome release from individual viral shells during mechanical unpacking.

Adenoviruses and their structural relatives

*Condezo, G, **Martín-González, N.**, Pérez-Illana, M., Hernando-Pérez, M., Gallardo, J., San Martín, C.*

Abstract

Adenoviruses have complex, non-enveloped icosahedral capsids with triangulation number pseudoT = 25. Trimers of the major coat protein (hexon) form the icosahedral facets, while the vertices are occupied by a pentamer of penton to which trimeric fibersare attached. Four types of minor coat proteins complete the shell, modulating the quasi-equivalent icosahedral interactions. The dsDNA genome, bound to a large amount of positively charged proteins, forms the non-icosahedral core. Hexon monomers fold as a double β-barrel perpendicular to the capsid surface. Viruses infecting very different organisms, from bacteria to archaea to humans, also use this fold to build their infectious particles.